Technische Universität München
Fakultät für Medizin

Synthetic lethalities to target a MYC-driven PDAC subtype

Katharina Lankes

Vollständiger Abdruck der von der Fakultät für Medizin der Technischen Universität München zur Erlangung einer

Doktorin der Naturwissenschaften (Dr. rer. nat.)

genehmigten Dissertation.

Vorsitz: Prof. Dr. Dieter Saur

Prüfer*innen der Dissertation:

1. Prof. Dr. Günter Schneider
2. Prof. Dr. Matthias Feige

Die Dissertation wurde am 21.09.2022 bei der Technischen Universität München eingereicht und durch die Fakultät für Medizin am 21.02.2023 angenommen.

I. Content

I. Content 2
II. Abstract 5
III. Zusammenfassung 6
IV. Introduction 8
1. Pancreatic ductal adenocarcinoma 8
2. Molecular subtyping of PDAC 10
3. The oncogene MYC and how to target it: Synthetic lethality 13
a. Properties and implications of MYC 13
b. Strategies to target the “undruggable” MYC 15
c. The concept of synthetic lethality 17
d. Intention and aim of this work 21
V. Material 22
1. Pancreatic cancer cell lines 22
2. Primer 23
3. Antibodies 24
4. Chemicals, reagents and media 25
5. Buffer and solutions 27
6. Consumables 28
7. Kits 29
8. Technical equipment 29
9. Software 30
10. Inhibitors 31
VI. Methods 33
1. Cell culture 33
a. Human cell lines 33
b. Murine cell lines 33
c. Storage of cell lines 33
d. Mycoplasma testing 34
2. Cell viability assays 34
a. MTT assay 34
b. CellTiter-Glo® ATP assay 35
3. Drug screening approach 35
a. FDA-approved, anti-cancer drug library 35

b. Epigenetics drug library 35
4. Clonogenic growth assay 36
5. Protein expression analysis 36
a. Seeding and harvesting 36
b. Protein concentration analysis 37
c. Western blot 37
d. Quantification 38
6. RNA expression analysis 38
a. Seeding and harvesting 38
b. RNA extraction and cDNA synthesis 38
c. qRT-PCR and quantification 39
7. Flow cytometry 40
8. Caspase 3/7 assay 40
9. Statistical analysis 40
VII. Results 41
1. Human PDAC cell lines show differential MYC protein expression 41
2. Unbiased drug screen of FDA-approved anticancer drugs identifies vulnerabilities in MYC high human PDAC cells 44
3. Human PDAC cells with active MYC are primed for Bortezomib-induced NOXA-dependent apoptosis 48
4. Response of PDAC cells to perturbants of proteostasis is heterogenous 50
5. Cellular subtype determines sensitivity for epigenetic compounds 52
6. Refined unbiased drug screen in PDAC cells identifies epigenetic MYC-associated vulnerabilities 54
7. PRMT5 is connected to MYC in PDAC 56
8. MYC controls Prmt5 inhibitor activity 57
9. PRMT5 inhibitors induce apoptosis in MYC hyperactivated PDAC cells 61
10. No synergistic effects could be detected with PRMT5i 62
11. Effect intensity of PRMT5i synthetic lethality depends on the cell model 65
VIII. Discussion 67
1. Proteasome inhibition as synthetic lethality with MYC in PDAC 67
2. Targeting a synthetic lethal interaction between MYC and PRMT5 in PDAC 71
IX. Supplementary Material 77
X. Abbreviations 85
XI. Figures 102
XII. Tables 102
XIII. References 103

XIV.Acknowledgement.. 118

II. Abstract

Pancreatic cancer (PDAC) still remains a huge challenge due to late diagnosis, early metastasis, and unsatisfying therapeutic options, which are mainly complicated by tumor heterogeneity, incomplete understanding of cellular mechanisms, upcoming resistance to treatment and a lack of patient stratification. The particularly aggressive, quasi-mesenchymal subtype of PDAC is mainly characterized by overexpression of the myelocytomatosis oncogene (MYC), a very important and so far “undruggable” signaling hub controlling cell growth and proliferation, protein synthesis, vasculogenesis and angiogenesis, metabolic reprograming, and other pathways involved in tumorigenesis. Pharmacological targeting of MYC synthetic lethal partners enables to improve therapeutic strategies specifically for this subgroup of PDAC patients. To decipher such MYC-associated vulnerabilities we first conducted two unbiased drug screens using a) a Food and Drug Administration (FDA)-approved anti-cancer drug library and b) an epigenetic drug library on well-characterized human PDAC cell lines. In the first library we detected and validated augmented sensitivity for compounds interfering with deoxyribonucleic acid (DNA) metabolism, folate metabolism, topoisomerase I and II, transcription, Histone de-acetylases (HDACs), and the proteasome in MYC high cell lines. The following analysis of the proteasome inhibitor Bortezomib showed increased apoptosis in human and genetically modified murine models of MYC overexpression. This was mainly visible in cleavage of poly- (adenosine diphosphate (ADP)-ribose) polymerase (PARP), impaired growth and a left-shift in dose response curves. In addition, the mechanism of apoptosis was clearly phorbol-12-myristate-13-acetate-induced protein 1 (PMAIP1 = NOXA)-dependent. As MYC-driven cancers feature an elevated protein level, further impairment of unfolded protein response (UPR) by disturbing the ubiquitin proteasome system (UPS) seems to be intolerable and lead to cell death. In the epigenetic library one of the particularly interesting top hits was a protein arginine methyltransferase 5 (PRMT5) inhibitor. We documented a robust connection between PRMT5 and MYC across species. A pronounced sensitivity for several PRMT5 inhibitors in MYC-hyperactivated PDAC cells could be shown in human and gain-of-function murine models, predominantly in long term assays. Phosphorylation of histone H2Ax indicating DNA damage and cell cycle arrest in the G2/M phase were always detectable after PRMT5 inhibition, but resulted in apoptotic cell death shown by monitoring PARP cleavage only in high MYC expressing cells. Although some research is still needed to unravel the exact molecular mechanism, in sum we determined two targetable MYC-associated vulnerabilities in PDAC, the ubiquitin proteasome system and protein arginine methyltransferases, that could be exploited in development of subtype-specific therapeutic approaches.

III. Zusammenfassung

Das Pankreaskarzinom (PDAC) stellt immer noch eine große Herausforderung dar, da dieser Tumor oft erst spät diagnostiziert wird, schon früh metastasiert und es noch keine zufriedenstellenden Behandlungsoptionen gibt. Diese werden zudem durch Tumorheterogenität, lückenhaftes Verständnis der molekularen Zellmechanismen, Therapieresistenz und fehlende Stratifizierung der Patienten erschwert. Der besonders aggressive, quasi-mesenchymale Subtyp des PDAC lässt sich vor allem durch eine Überexpression des Myelozytomatose Onkogens (MYC) charakterisieren, das einen unverzichtbaren und bis heute nicht angreifbaren Signalknotenpunkt in der Zelle darstellt und Zellwachstum, Zellproliferation, Proteinsynthese, Vaskulogenese und Angiogenese, metabolische Reprogrammierung und andere Signalwege kontrolliert, die für die Tumorentstehung entscheidend sind. Indem wir synthetisch letale Partner von MYC medikamentös angreifen, könnten wir Therapiestrategien speziell für diese Gruppe von Patienten mit PDAC verbessern. Um solche MYC-assoziierten Vulnerabilitäten zu finden wurden unvoreingenommen zwei Medikamenten-Screens mit gut charakterisierten humanen PDAC-Zelllinien durchgeführt. Dabei wurde a) eine Bibliothek genutzt, die von der FDA zugelassene Krebsmedikamente enthielt, und b) eine Bibliothek mit epigenetisch wirksamen Stoffen. In der ersten Bibliothek entdeckten wir Verbindungen, die den DNA- und Folat-stoffwechsel, sowie die Regulierung von Topoisomerase I und II, Transkription, HDACs und das Proteasom von Zellen mit hoher MYC-Expression beeinflussen. Die folgende Analyse des Proteasominhibitors Bortezomib zeigte durch Spaltung von PARP, eine Behinderung des Wachstums und eine Verschiebung der Dosis-Wirkungs-Kurven nach links eine gesteigerte Apoptose in humanen und genetisch modifizierten murinen Modellen mit MYC-Überexpression. Zudem war die gezeigte Apoptose eindeutig abhängig von NOXA. Da MYC-basierte Tumore ein erhöhtes Proteinlevel besitzen, scheint eine weitere Beeinträchtigung der Antwort auf ungefaltete Proteine durch Störung des Ubiquitin-Proteasom-Systems (UPS) nicht tolerierbar zu sein und zum Zelltod zu führen. In der Bibliothek mit epigenetisch wirksamen Medikamenten befand sich ein Protein-Arginin-Methyltransferase 5 (PRMT5) Inhibitor unter den interessantesten Testkandidaten. Wir konnten eine robuste Verbindung zwischen PRMT5 und MYC in verschiedenen Spezies feststellen. Auch hier waren humane Zellen und murine `gain-of-function` Modelle des MYC-aktivierten Pankreaskarzinoms deutlich sensitiver bezüglich verschiedener PRMT5 Inhibitoren, vor allem im Langzeitversuch. Die Phosphorylierung des Histons H2Ax als Nachweis für DNA-Schäden und ein Arrest des Zellzyklus in der G2/M-Phase konnten stets nach PRMT5-Inhibition nachgewiesen werden. Jedoch resultierte dies nur bei Zellen mit hoher MYC-Expression im apoptotischen Zelltod, was wieder durch Spaltung von PARP gezeigt werden konnte. Obwohl die genauen

molekularen Mechanismen noch weiter erforscht werden sollten, konnten wir zusammengefasst zwei medikamentös angreifbare MYC-assoziierte Vulnerabilitäten beim Pankreaskarzinom, nämlich das UPS und Protein-Arginin-Methyltransferasen, beschreiben. Beide könnten zukünftig in der Entwicklung Subtypen-spezifischer Therapieansätze von Nutzen sein.

IV. Introduction

1. Pancreatic ductal adenocarcinoma

Pancreatic cancer states 3.2% of all new cancer cases in the USA according to the Surveillance, Epidemiology, and End Results (SEER) database.[1] In 2020, it is estimated that 57,600 new cases and 47,050 deaths will occur, which are 7.8% of all cancer related deaths.[1] The median age at diagnosis is 70 years and a 5-year relative survival rate of 10% (2010 – 2016) shows the dismal prognosis of this cancer type.[1] Also, in the last 30 years the death rate did not change much in contrast to other cancer types. Rahib et al. projected the incidence and death rates of pancreatic cancer in the USA to the year 2030.[2] From 62,000 cases in 2020 it is calculated to rise to 88,000 in 2030, thereby becoming the second leading cause of cancer-related death in both sexes.[2] In Europe the ASR (age-standardized mortality rates using the world standard population) is predicted to be stable at 8.0 for men and increased at 5.6 for women in 2019.[3] Northern America and Europe thus have the highest incidence of pancreatic cancer in the world.[4] Factors, which are known to impact on survival are on one hand hereditary and on the other hand age, sex, quality of healthcare, co-morbidities and lifestyle including smoking, alcohol and obesity.[5] Due to surgery being the only potential cure of pancreatic cancer these days and only 20% of cases being surgically resectable, progress in treatment strategies, prevention, screening methods for early detection, patient stratification and therapeutic targets has to be made.[6] To this end, in October 2020 2,772 studies were registered worldwide at ClinicalTrials.gov.[7]

Pancreatic cancer usually presents in a late tumor stage owed also to the fact that symptoms are rather unspecific: abdominal or back pain, dyspepsia, unexpected weight loss, painless jaundice or others.[8,9] The cellular origin is still debated, but as to current knowledge about 90% of all pancreatic lesions are pancreatic ductal adenocarcinoma (PDAC), 5% are pancreatic neuroendocrine tumors (PNET), and the remaining 5% are of other exocrine origin, which is the reason why PDAC often is used as a synonym for pancreatic cancer and will be used in the following as well.[10] Precursor lesions of the carcinoma can be mucinous cystic neoplasms (MCN), intraductal papillary mucinous neoplasms (IPMN) and in most cases pancreatic intraepithelial neoplasms (PanIN), all of them converting stepwise into invasive pancreatic carcinoma acquiring different mutations based on initial mutation of Kirsten rat sarcoma viral oncogene homolog (KRAS), for example found in 90% of low grade PanINs (reviewed by Distler et al.).[11] In 2001, Hruban et al. published a scheme for classification of PanINs generally accepted today, even though these classifications underlie constant revisions.[12] Whereas IPMNs acquire mutations in Guanine nucleotide binding protein (GNAS) and/or V-Raf murine sarcoma viral oncogene homolog B (BRAF) in early stages and in Transformation related

protein 53 (p53) in later stages, PanINs exhibit mutations in Cyclin-dependent kinase inhibitor 2A (CDKN2A) / protein 16 (p16) in earlier and in Mothers against decapentaplegic homolog 4 (SMAD4) and/or p53 in later stages.[5,13-15] Of total pancreatic lesions 90% have activated KRAS and also 90% have loss of function of p16 and lately it has been published that the gene dosage of mutant KRAS in precursor lesions drives tumorigenesis and metastasis.[16-19] Although the sequence of mutations is generally known, early detection of precancerous lesions still poses a huge challenge due to lack of reliable biomarkers.[20]

As already mentioned the therapeutic options for PDAC are very limited. Only a partial or complete pancreatectomy can cure this disease and chemotherapeutic agents are often used to improve survival in an adjuvant setting. As PDAC is poorly immunogenic, novel immune checkpoint inhibitor therapies that have emerged over the past decade hold little promises. The longest known chemotherapeutics used in PDAC are Gemcitabine and 5-fluorouracil (5-FU) / folinic acid, which represent the basis for the nowadays standard of care. Patients are stratified according to their fitness which depends on age, recovery from surgery and performance status. In case of low fitness a combination of Gemcitabine and Capecitabine is used, in patients of high fitness the so called modified FOLFIRINOX (folinic acid, 5-FU, Irinotecan, and Oxaliplatin) regimen is applied.[21] After the first steps to establish these therapies mainly two studies set the cornerstone for this gold standard: In European Study Group for Pancreatic Cancer (ESPAC)-4 trial, the combination of Gemcitabine and Capecitabine performed superior to Gemcitabine monotherapy with a median overall survival (mOS) of 28.0 months compared to 25.5 months increasing only slightly the number of grade 3 or 4 adverse events (63% versus 54%).[22] In Gastrointestinal *Partenariat de Recherche en Oncologie Digestive* (GI PRODIGE) 24 trial the modified FOLFIRINOX showed a mOS of 54.4 months compared to 35 months with Gemcitabine alone.[23] Here grade 3 or 4 adverse events were detected in 75.9% versus 52.9% of patients, thus explaining the need for higher fitness for this treatment.[23] However, if the pancreatic tumor is not resectable or metastatic, the therapeutic options are mainly restricted to alleviation of symptoms and palliative care. Nevertheless, many studies have been conducted leading to a standard-of-care as well in these cases. FOLFIRINOX has been shown to be superior to Gemcitabine in metastatic PDAC for individuals with good fitness in the *Actions Concertées dans les Cancers Colorectaux et Digestifs* (ACCORD) trial and the Metastatic Pancreatic Adenocarcinoma Clinical Trial (MPACT) established nab-Paclitaxel/Gemcitabine combination therapy compared to Gemcitabine monotherapy.[24,25] Up to now most of the studies used different combinations of chemotherapies, but also radiation studies like Alliance for clinical trials in oncology study (ALLIANCE) or Preoperative chemoradiotherapy versus immediate surgery for resectable and borderline resectable pancreatic cancer (PREOPANC), immunotherapeutic trials and gene therapy attempts have been conducted, all of them without any promising results that could

improve standard-of-care in metastatic unresectable PDAC.[26-30] If the tumor is borderline resectable or the resection success can be increased, a neoadjuvant setting of therapy is used before surgery. Prep-02 / Japanese Study Group of Adjuvant Therapy for Pancreatic Cancer (JSAP)-05 showed that a combination of Gemcitabine and S-1 prolonged mOS from 36.7 months to 26.6 months compared to no treatment before resection.[31] A similar effect has been observed in the ESPAC-5F trial showing a significant survival benefit for patients undergoing surgery after neoadjuvant treatment.[32] The confirmation of the results of the ALLIANCE trial, where modified FOLFIRINOX, together with radiotherapy in some patients, was used in borderline resectable fit patients is still ongoing.[33] Knowledge of mutations or copy number variations in PDAC has had some impact on prognosis, but not yet on therapy, so targeted therapies are only marginally used for PDAC treatment. One starting point for targeted therapies so far seem to be DNA damage repair defects for example in Breast cancer gene (BRCA) 1/2, which increase the sensitivity of the pancreatic tumor to platinum agents and Olaparib.[34,35] But in contrast, studies on BRCA- or Partner and localizer of BRCA2 (PALB) 2-mutated PDAC using cisplatin, Gemcitabine or Veliparib could not be confirmed to be effective so far.[36,37] In the end, the main challenges of pancreatic cancer therapy still remain the cancer's often very late diagnosis due to unspecific symptoms, its early metastasis and the few treatment options available.

2. Molecular subtyping of PDAC

Taking all these aspects into account, research started to focus on subtype-specific therapeutic targets to improve outcome for at least a portion of PDAC patients. The basis to achieve this was to identify and characterize different subtypes and many important attempts have been made varying mainly in sample type and used techniques. The earliest study was conducted by Jones et al., where they used gene sequencing for homozygous deletions and amplifications and microarrays for single nucleotide polymorphism (SNPs).[38] The number of samples was very limited, but they already found the typical PDAC pathways (KRAS, tumor protein 53 (TP53), SMAD4 and CDKN2A) involved as well as a core set of 12 pathways in total including Wingless-related integration site (Wnt) / Neurogenic locus notch homolog protein (Notch) signaling and MYC.[38] In 2011, Collisson et al. published the results of a DNA-microarray-based gene expression profiling and the comparison to an existing dataset.[39,40] The clustering of the gene expression pattern revealed three subtypes, which they termed classical, quasi-mesenchymal and exocrine-like, ranging from a well-differentiated to a so called "digested" phenotype.[10,39] They validated these subtypes across different datasets due to the low number of samples and detected an association to patient outcome, whereby a classical subtype shows the best outcome.[39] At that time, specific targeting in vitro was limited by the few existing chemotherapeutic agents. One year later, Biankin et al. used whole-exome

sequencing and copy number variation (CNV) analysis to identify the usual but also some novel pathways altered in PDAC involved in chromatin modification, DNA repair and metastasis.[41] Similarly, Waddell et al. conducted whole-genome sequencing and CNV analysis, which resulted in the definition of four PDAC subtypes: A stable subtype with fewer variations and mutations in *KRAS*, *SMAD4* and *TP53*, a locally rearranged subtype with one to two chromosomes showing significant abnormalities, a scattered subtype with a moderate number of structural variation events and an unstable subtype exhibiting large structural variation, mutation of DNA repair genes, but responsive to platinum-based agents.[42] The main driver mutations were still not targetable, but the study again found some novel genes mutated. The same year, Moffitt et al. used ribonucleic acid (RNA) expression analysis on a lot more samples and digitally separated between tumor, stroma and normal tissue.[10,43] They identified two subtypes of tumor, termed classical and basal-like, and two types of stroma, termed normal and activated, with the latter always having the worse prognosis.[10,43] In unfavorable combination of tumor and stroma, the risk was shown to be cumulated.[43] The third important publication in this field in 2015 was of Witkiewicz and colleagues.[44] They again analyzed CNVs and conducted whole-exome sequencing and linked the results to patient outcome.[44] No subtypes were defined in this study, but rather key signaling pathways like KRAS, Transforming growth factor beta (TGF-β), Notch, retinoblastoma (RB), DNA repair with some alterations being potentially targetable, for example BRAF V600E by Vemurafenib.[44] Importantly, as the first study they found amplification of the oncogene MYC to be associated with a very poor prognosis in PDAC patients.[44] In 2016, Bailey et al. published the subtyping study with the most specimen so far using a combination of whole-genome sequencing and deep-exome sequencing.[10,45] They found ten overlapping mechanistic classifications, again including KRAS (in 92% of samples), TGF-β, Wnt / Ring finger protein 43 (RNF43), cell cycle checkpoints, RNA processing, BRCA/DNA-repair and histone modification.[45] A subsequent RNA expression analysis lead to the clustering into four PDAC subtypes.[45] The squamous subtype shows a poor prognosis, more mutations in TP53 and Lysine demethylase 6A (KDM6A) and activation of the MYC pathways, whereas the pancreatic progenitor subtype involves development genes and inactivation of TGF-β receptor 2.[45] The immunogenic subtype is characterized by immune infiltration correlating with histopathology, and activation of genes responsible for acquired immune suppression, for example Cytotoxic T-lymphocyte-associated Protein 4 (CTLA-4) and Programmed cell death protein 1 (PD-1), which in sum possibly makes it responsive to immunotherapies.[45] The aberrantly differentiated endocrine exocrine (ADEX) subtype shows alterations in the KRAS network and in genes involved in later stages of exocrine and endocrine cell development.[10,45] In conclusion, most of these studies commonly identified KRAS signaling, DNA repair, G1/S phase regulation and transition, TGF-β signaling and Wnt/Notch signaling, but also MYC (Jones et al. 2008; Witkiewicz et al. 2015; Bailey et al.

2016) as main drivers for development of molecular subtypes in PDAC.[10,38,44,45] The slight differences can be well explained by the differing tissue specimen and the methods used, but also by the fact that subtypes can coexist within one single tumor and are subject to ongoing changes in the genomic landscape.[46,47]

All this research led to a quite good genetic characterization of PDAC subtypes, but how can this be translated into responsivity for specific therapies and finally into clinical benefit? Some subtypes indicate vulnerabilities to targeted therapy, but not all identified tumor drivers are targetable yet and, in addition, some cancer genes critical for tumorigenesis and tumor maintenance remain to be identified. To address these questions, the genomic characterization has to be combined with drug sensitivity profiling. For cancers in general, large screens in hundreds of cancer cell lines with a huge variety of drugs with different targets and mechanisms have been conducted in a high-throughput manner to link genomic aberrations to drug sensitivity, usable biomarkers and prognosis.[48,49] Compared to tumor tissue the cell line approach, although being further away from the actual patient, has some advantages. The genomic alterations of cell lines are precisely known, they still reflect the diversity of the original tumor and they can be used for overexpression or knock-down experiments.[49] In 2012, Barretina et al. published The Cancer Cell Line Encyclopedia (CCLE) in Nature.[50] Gene expression data, CNV analysis and sequencing data from 479 human cancer cell lines were linked to pharmacological profiles for 24 anti-cancer drugs. Datasets like this are highly useful when generating or testing new hypotheses. Recent profiling approaches can also make use of novel techniques like patient-derived organoids (PDOs), which are genetically closer to the patients than cell lines but still manageable in a screen.[51] An important and extensive screen was conducted by Iorio et al.[52] They made use of 1,001 human cancer cell lines, mapped to data from 11,289 tumors and genomically characterized, to screen them against 265 well-known as well as experimental anti-cancer compounds. The outcome was the identification of novel treatment applications, subgroups and gene-drug-associations. 30 cell lines of PDAC were screened but left out in the later analysis. For instance, they detected driver gene amplifications of MYC in a colorectal cancer sensitive to Temozolomide. In fact, Iorio et al. were not the first to identify MYC amplification as a clinically relevant event in cancer that facilitates stratification strategies for therapy selection. This oncogene was found to be overexpressed in up to 70% of viral and alcohol-related hepatocellular carcinoma and to be associated with an aggressive phenotype.[53-55] An analysis of The Cancer Genome Atlas (TCGA) dataset for genetic alterations in 12 cancer types stated CNVs in the MYC gene locus as the third most frequent among all tumor entities.[56] And for PDAC, Schleger et al. found as early as in 2002 that 16% are characterized by high MYC expression and 13% by low levels of MYC.[57,58] Even lately, a bioinformatics-based analysis of transcriptomic, genetic and clinical data of several patient cohorts with resectable and non-resectable PDAC identified four mainly

metabolically characterized subtypes: quiescent, glycolytic, cholesterogenic, and mixed.[59] The glycolytic subtype showed the shortest median survival and amplification of *KRAS* and *MYC* correlated with higher expression of glycolytic genes.[59] This, together with the observations in molecular subtyping by Jones et al., Bailey et al. and especially Witkiewicz et al., nails down MYC and its network, as an important oncogenic driver in specific patient subpopulations in different cancer entities, being strongly associated with poor prognosis in PDAC. Most recently, several publications even demonstrated a reciprocal cross-talk between MYC and the tumor microenvironment, which contributes to immune escape of PDAC.[60-62] Finally, the feasibility of using MYC as a stratification marker in patients has already been demonstrated by use of conventional immunohistochemistry and 3D culture models such as organoids, as well as Positron Emission Tomography (PET) scans of ^{89}Zr-desferrioxamine-labeled transferrin as a tracer for MYC activity tested in preclinical models.[58,63]

3. The oncogene MYC and how to target it: Synthetic lethality

a. Properties and implications of MYC

Extensive reviews have been written about MYC and its role in tumorigenesis, for example by Dang C. in 2012, so only the most important aspects can be mentioned here.[64] The MYC family of oncogenic transcription factors consists mainly of C-MYC, N-MYC and L-MYC, which are all involved in human tumorigenesis. N-MYC expression is usually restricted to neuronal tissue, but C-MYC can be functionally replaced by N-MYC at least in murine development, cellular growth and differentiation.[65] In advanced stage human neuroblastoma, N-MYC was found to be amplified, whereas in human small cell lung cancer L-MYC was detected to be amplified and expressed.[66,67] C-MYC, the main player of the family and thus simply termed MYC in the following, has been discovered in chicken as a cellular homolog of the oncogenic v-myc in avian myelocytomatosis virus strain 29.[68,69] It is located on chromosome 8q24, which was detected due to the translocation of this chromosomal part in Burkitt's lymphoma cells.[70] Structurally, MYC is a basic-helix-loop-helix transcription factor binding for example E-box elements enriched in promoter and enhancer regions of DNA only when hetero-dimerized with its partner MYC-associated protein X (MAX).[71] MYC and MAX dimerize via a leucine-zipper dimerization motif in MYC and activate the transcription of target genes by recruiting the positive transcription elongation factor complex, which phosphorylates the RNA polymerase II thus increasing transcription.[55] Although generally activating target genes, MYC and MAX in combination with Myc interacting zinc finger protein 1 (MIZ-1) can also lead to target gene repression.[72,73] The MYC protein has a N-terminal transactivation domain (TAD) with transcriptional regulation elements called "Myc boxes" (MB), a central region with a polypeptide sequence rich in proline (P), glutamic acid (E), serine (S), and threonine (T) (PEST) domain

and the C-terminal Basic helix loop helix leucine zipper (bHLH-LZ) domain.[74] It can be subject to a variety of post-translational modifications including phosphorylation, ubiquitination and Small ubiquitin-like modifier (SUMO) -ylation, exerting numerous functions in the cell. The *MYC* gene consists of three exons with exon 1 being non-coding and has four alternative promoters, whereby promoter 2 accounts for most of total MYC in normal cells.[75] MYC not only activates transcription via RNA polymerase II, but also I and III, and it is estimated to have approximately 25,000 binding sites in the human genome.[76-78] Additionally, differences in high and low affinity DNA-binding of MYC/MAX have been described, as well as the recruitment of associated factors into complexes that change chromatin architecture by looping and bring even distant transcribed genes into close contact.[79,80] Overexpression of MYC, for instance, causes binding of MYC/MAX even to low affinity sites and enhancers and drives alterations of the transcriptome and metabolic imbalances.[80-82] Especially, because MYC also exhibits target-gene independent functions, which has been recently reviewed by Baluapuri et al., it not only regulates a significant proportion of all genes in an organism, but is involved in almost every aspect of tumor biology, some of them still being mechanistically unclear.[78,83] MYC is basically involved in proliferative and growth promoting signaling pathways and thus as well in oncogenic transformation.[84,85] It plays a role in protein synthesis, vasculogenesis and angiogenesis, metabolic reprograming, inhibition of cell differentiation and genomic instability.[86-90] The loss of MYC can lead to inhibition of cell proliferation and extensive DNA damage response.[91,92] In tumorigenesis it executes multiple roles including the promotion of metastasis and its oncogenic potential has been demonstrated in an Eμ-Myc mouse model as early as in 1985, showing the perturbation of cellular division, differentiation and apoptosis.[93,94] MYC is estimated to be elevated or deregulated in up to 70% of human cancers and an addiction to MYC has been described by showing a sustained loss of neoplastic phenotype after short inactivation of MYC.[64,95] High expression of this transcription factor has been linked to aggressive prostate cancer and triple negative breast cancer, and as described earlier to an aggressive subtype of PDAC.[44,64,96,97] In addition, it has been shown to interact with Notch signaling, Phosphoinositide 3 kinase (PI3K) signaling and MEK / Extracellular-signal-regulated kinase (ERK) signaling as an integrator of several pathways in normal and cancer cells.[98-100] Specifically in PDAC, MYC has been found to drive tumor progression and to act also downstream of oncogenic KRAS.[101,102] Deregulation of MYC in PDAC involves but is not limited to genetic aberration, transcriptional regulation, post-transcriptional regulation and post-translational protein stability.[103] Intriguingly, latest research has claimed MYC-activation to be a direct switch to transform PanINs to PDAC, which in addition seems to be completely and immediately reversible.[60] But what on one hand is promoting tumorigenesis can on the other hand be the Achilles heel of MYC-driven cancers: The cell's fail-safe mechanism of MYC-induced apoptosis can limit its tumorigenic capacity through at least two pathways.[78,104] One

way is via the induction of p14 (human) / p19 (murine) ADP ribosylation factor (ARF) and stabilization of p53.[105] The other way is the release of cytochrome c from mitochondria and the following oligomerization and effect of Bcl-2-associated X (BAX).[106,107] The latter is partly mediated by the Bcl-2 homology domain 3 (BH3)-only protein Bcl-2-interacting mediator of cell death (BIM), which has been shown by an acceleration of MYC-induced lymphomagenesis in the absence of BIM, and the repression of anti-apoptotic B-cell lymphoma-extra large (Bcl-xL) and B-cell lymphoma 2 (Bcl2).[108,109] Likewise, induction of proliferation by MYC can work in concert with alterations in the apoptotic machinery, for example in Bcl-2, and lead to enhanced tumorigenesis as documented in hematologic malignancies.[110] Besides this there are hints that overexpression or upregulation of MYC is inducing DNA damage and overriding cell cycle arrest signals, which results in genetic instability and can thus again lead to apoptosis.[92,111] So physiologically, cells have to hold tight control of their MYC level and keep the balance between proliferation and apoptosis. However, MYC-driven cancers like specific subtypes of PDAC are already “primed-for-death” due to the aforementioned MYC-induced vulnerabilities.[58]

b. Strategies to target the “undruggable” MYC

Pharmacological targeting of MYC or such vulnerabilities can help to drive these primed cancer cells into cell death.[79,112,113] MYC itself is considered “undruggable” so far due to its intrinsically disordered structure, its lack of enzymatic activity and its extremely important and non-redundant role as a signaling hub in the cell affecting many pathways and potentially causing severe side effects when targeted. Interestingly, the generation of Omomyc, a dominant-negative variant of MYC, which is able to form heterodimers with wild-type MYC, proved the existence of a therapeutic window in MYC inhibition.[112,114] Omomyc interferes with MYC/MAX dimerization and consequently inhibits E-box dependent transcription of target genes. This systemic MYC inhibition showed only mild and reversible toxicities in mice and no resistance mechanisms were detected.[115] Due to these features and the proof-of-concept, Omomyc seems a first promising candidate for targeting MYC/MAX binding directly, the most obvious strategy.[116] Screens of Kiessling et al. identified Mycro1 and Mycro2.[117] Later, Mycro3 has been shown to block proliferation and induce apoptosis and tumor shrinkage in an oncogenic Kras-driven PDAC mouse model and in xenotransplants of human PDAC cell lines with no obvious side effects.[118] Also in PDAC models, the MYC/MAX specific compounds 10058-F4 and 10074-G5 have been discovered by a yeast-two-hybrid-based assay.[119] In vitro, the F4 compound could impair proliferation and induce apoptosis in human PDAC cells, whereas in vivo apoptosis of transplanted human cells in mice could only be induced synergistically with Gemcitabine.[120] This already demonstrates the pharmacokinetic problems the small-molecule

inhibitors face in vivo and furthermore, potential escape mechanisms and off-target effects will have to be elucidated, when thinking of a clinical setting.[121]

More indirect ways to target MYC signaling are to reduce MYC protein expression, to interfere with protein turnover or to repress MYC-dependent activation of target genes. For example, to tackle MYC expression, Bromodomain and extra terminal domain (BET) inhibitors have been used in different settings. As the coactivator of transcription Bromodomain-containing protein (BRD) 4, a BET-family member, has been identified to be a main regulator of MYC expression in acute myeloid leukemia, several BET inhibitors have been developed in the following.[122] I-BET and JQ1 have subsequently been tested in different MYC-driven hematologic malignancies.[122-125] Some of them have been shown to respond only partially, others not at all, in the end being highly context-dependent. In PDAC, BET inhibitors could block cell growth in 3D collagen or patient-derived xenograft models, but effects on MYC protein expression could not be detected.[126,127] So far it was not possible to show that the effects of BET inhibitors are clearly MYC-dependent, but in 2018 Muhar et al. published at least a strong hint on that.[128] They combined Thiol (SH)-linked alkylation for the metabolic sequencing of RNA (SLAMseq), a method for RNA quantification, and pharmacological inhibition and found that BRD4 co-activates polymerase II dependent transcription, which can be inhibited by BET inhibitors in turn leading to deregulation of MYC.[128] Importantly, the group defined a core set of MYC target genes and established the BRD4-MYC-axis in gene regulation.[128] Subsequently, Bian et al. substantiated the dependency of BET inhibitor sensitivity on MYC expression in pancreatic cancer cell lines, xenografts and organoids.[129,130] Another indirect strategy is to target MYC protein turnover. In normal cells, MYC is a short-lived protein with a half-life of 20 – 30 minutes, but in cancer the turnover is often deregulated.[112,131] Although there is also calpain-dependent cleavage of MYC, which doesn't degrade the complete protein but produces MYC-nick, a 298-amino-acid amino-terminal fragment involved in microtubule regulation, the main route for MYC processing is the UPS, an adenosine triphosphate (ATP)-dependent enzymatic mechanism.[132] MYC, like other proteins, is tagged for degradation by addition of ubiquitin molecules and subsequently degraded by the 26S proteasome. This ubiquitination as well as SUMOylation are tightly regulating MYC proteostasis. The crucial event for stabilization of MYC is the phosphorylation at the serine 62 (S62) residue of the N-terminal MYC homology box I by ERK for example.[112] Glycogen synthase kinase 3 beta (GSK3β) then can phosphorylate threonine 58 (T58) to enable MYC signaling.[112,133] Additionally, several other proteins are involved in MYC protein stability like F-box and WD repeat domain-containing 7 (FBW7), Ubiquitin specific peptidase 28 (USP28), NF-kappa-B essential modulator (NEMO), and HECT, UBA and WWE domain containing E3 ubiquitin protein ligase 1 (HUWE1), all possible targets and reviewed in Farrell & Sears 2014.[131] To accelerate the degradation of MYC one strategy can be to use Protein phosphatase 2A (PP2A). This protein can

dephosphorylate S62 and thus initiate ubiquitination by recruiting E3 ubiquitin ligase Skp, Cullin, F-box containing (SCF) complex containing FBW7. Endogenous PP2A inhibitors have been found to be overexpressed in PDAC.[134] And blocking USP28, the first deubiquitinating enzyme connected to MYC stability, leads to decreased MYC expression and tumor cell proliferation.[135] A quite recent technology to recruit target proteins to E3 ligases and feed them into UPS-dependent degradation is the PROTAC technology. In 2015, a phthalimide-conjugated BET inhibitor has been described as proteolysis targeting chimera (PROTAC), the starting point of this field of research.[136] PROTACs consist of a binding-domain to the protein of interest, a linker, and a binding-domain to an E3 ligase.[137] dBET1 has been shown to recruit cereblon to ubiquitinate and degrade BRD2, BRD3 and BRD4 in a murine xenograft model of leukemia.[136] This deregulation of BRD4 also lead to a reduction of MYC expression being consistent with the publication of Muhar et al.[128] In addition, currently research is ongoing to develop PROTACs against MYC itself. HUWE1, an E3 ligase involved in MYC stability, can be exploited through a different mechanism. This protein leads to ubiquitination at K63 thus not degrading MYC but acting downstream on the transactivation of MYC target genes.[138] HUWE1 inhibitors can consequently deactivate part of the MYC-dependent oncogenic network, even recently demonstrated for multiple myeloma.[139,140] Other ways to target MYC as a general amplifier of oncogenic signaling can work via multi-protein complexes containing epigenetic writers and readers or via the basal transcription machinery.

c. The concept of synthetic lethality

The probably most elegant strategy to target MYC signaling in cancer is the concept of “synthetic lethality” that was followed in this work. There are many reviews covering this topic with the main aspects being summarized in the following.[141,142] Synthetic lethality (SL) means in general that a cancer-associated vulnerability due to mutation or overexpression of an oncogene can be used together with pharmacological inhibition of another not necessarily related gene, protein or pathway to drive the cancer cell into cell death and meanwhile spare normal cells (Fig.1; adapted from Wirth et al. and O’Neil et al.[112,141]). Tumor- or even subgroup-specific mechanisms may exist in this context. First in 1997, it has been proposed that SL interactions could help to identify new anti-cancer drug targets and maybe even reuse existing inhibitors for new purposes.[143]

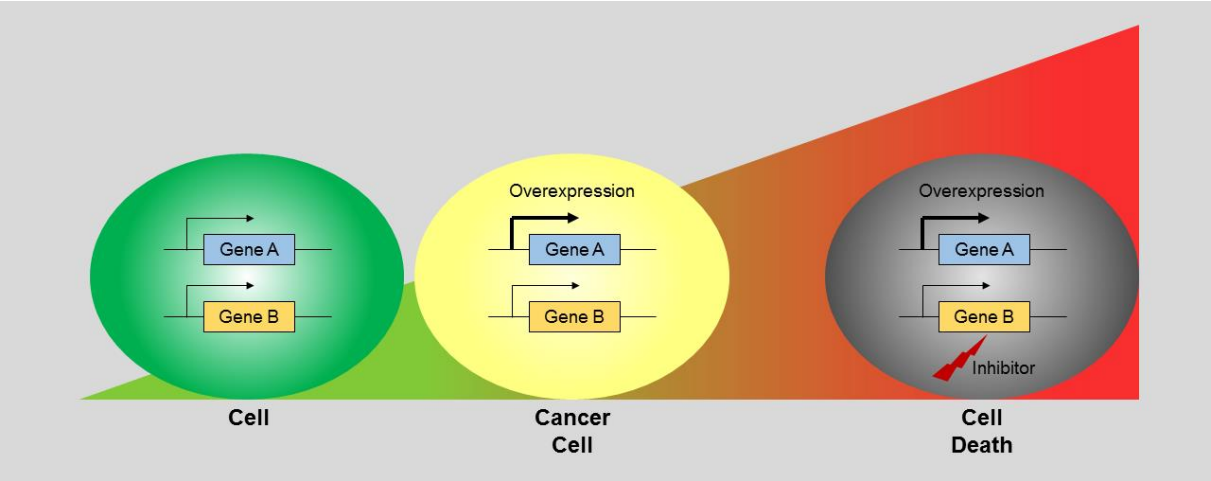

Fig. 1 Concept of synthetic lethality
A cancer-associated trait like overexpression of gene A works in concert with pharmacological inhibition of gene B to drive cancer cells into cell death.

Different screening techniques like RNAi or Clustered regularly interspaced short palindromic repeats (CRISPR) have been used since then to detect SL in cancer in general and in a MYC-driven setting. In a variety of them, the so called synthetic dosage lethality (SDL) caused by overexpression has been described. SDL has been discovered in yeast and has been established in a screen for SL interaction genes of overexpressed Centromere DNA-binding protein complex CBF3 subunit C (CTF13), or Origin recognition complex subunit 6 (ORC6), a replication origin.[144,145] SL can not only be dependent on the cancer type, but also on the metabolic state or microenvironment and thus be specific for certain cell lines proving heterogeneity of tumors. And importantly, it can implicate three or more genes until it results in a phenotype and background mutations like loss of p53 can suppress SL interactions for example between PARP and BRCA1.[146] This interaction involving inhibition of PARP and BRCA1/2 mutation, which is common in breast cancer, was the first that made it to the clinic. In 2005, it has been spotted in a hypothesis-driven approach and in 2009 the first clinical trial with PARP inhibitors in BRCA1/2 germline mutated tumors has been published.[147,148] Subsequently, this strategy has been approved for cancer patients and thus is a good example for overcoming challenges like resistance mechanisms, off-target effects and cytotoxicity on the way to clinical benefit. Large-scale SL screens have been carried out in yeast using conserved genes or orthologs producing a global genetic interaction network we can make use of.[141,149] Of course, there were doubts as to whether screenings in model organisms could be extrapolated to humans, but these concerns have also been successfully addressed. Srivas et al. identified 1420 SL interactions in yeast orthologs and found the strongest ones to be conserved in human cell culture.[150] In the context of MYC overexpression some targeted approaches on kinases important for cell cycle maintenance and cell proliferation brought up the following: siRNA against GSK3β reduced phosphorylation of T58 in MYC leading to increased MYC levels and apoptosis.[151] So called small-molecule MYC pathway response

agents (MYRA-A and MYRA-B) could inhibit growth and induce apoptosis selectively in MYC overexpressing cells, although targeting different mechanisms.[152] And the CDK1 inhibitor Purvalanol together with MYC overexpression caused apoptosis in vitro and prolonged survival of tumor cell transplanted mice.[153] To obtain a global picture of MYC-dependent SL interactions, unbiased high-throughput screens followed these hypotheses-driven approaches. Frenzel et al. published a screen in human B-cell and lymphoma cell lines with conditional MYC expression treated with a library of 80 conventional cytotoxic agents.[154] 25% of these drugs induced apoptosis or inhibited cell proliferation in a MYC-dependent manner, targeting different cellular mechanisms like microtubules, topoisomerases, DNA-, RNA- and protein synthesis and turnover.[154] Kessler and colleagues did a genome-wide RNAi screen in human mammary epithelial cells (HMECs) using a gain-of-function model with a tamoxifen-inducible MYC-estrogen-receptor fusion transgene (MYC-ER) published earlier and a retroviral library of short hairpin RNAs (shRNAs).[155,156] They discovered that the loss of SAE1/2 (SUMO-activating enzyme) inhibits SUMOylation and is synthetic lethal with MYC overexpression, working via mitotic catastrophe and MYC hyperactivation. The survival benefit of patients with MYC high breast cancer even correlates with low SAE1/2 levels.[155] Importantly, this finding was recently corroborated by Biederstädt et al., who could demonstrate that a MYC-driven subtype of PDAC is susceptible to pharmacologic SUMO inhibition.[157] Another high-throughput small interfering RNA (siRNA) screen of approx. 3,300 druggable genes in human foreskin fibroblasts (HFFs) overexpressing MYC via a retroviral vector showed that targeting of one third of them induces accumulation of DNA damage.[158] Also histone acetylation and transcriptional elongation genes (Transformation/Transcription domain associated protein (TRRAP) and BRD4) were identified to be synthetic lethal with MYC. After the screen they validated one hit, the Casein kinase 1 epsilon (CSNK1e), in vivo. CSNK1e expression correlates with N-MYC amplification in neuroblastoma and C-MYC in other cancer entities and its inhibition stopped growth of N-MYC-amplified neuroblastoma xenografts.[158] Liu et al. carried out a siRNA screen of the human kinome in a MYC-ER osteosarcoma cell line using automated microscopy of PARP cleavage indicating apoptosis.[159] Their hits were mainly AMPK-related protein kinase (ARK) 5 and 5' adenosine monophosphate-activated protein kinase (AMPK), involved in Mechanistic target of rapamycin kinase complex (mTORC) 1 pathway and glutamine metabolism and responsible for maintaining energy levels in the cell. In MYC-overexpressing cells inhibition of ARK5 collapses cellular ATP levels and subsequently induces apoptosis. Two of five PDAC cell lines also responded to ARK5 inhibition and the depletion of this protein in a mouse model of MYC-driven hepatocellular carcinoma prolonged survival.[58,159] Cermelli and colleagues integrated three of the aforementioned screening outputs for MYC SL genes by network analysis using information from several human databases.[160] The only single SL gene in common between the Kessler and Toyoshima

screens was BRD4, but they also identified three prominent functional signaling hubs in all screens: Initiation and elongation of transcription, positive and negative regulation of MYC/MAX interaction, and cell cycle checkpoint and DNA repair pathways including ubiquitination and SUMOylation.[160] Some additional information was added by the genome-wide siRNA screen of Topham et al.[161] They found that MYC sensitizes cells of lung, breast, ovarian and colon cancer to mitotic blockers and accelerators of mitotic progression, for example Taxol.[161] MYC is up-regulating pro-apoptotic BH3-only proteins and suppressing anti-apoptotic Bcl-xL. Thus, response to Taxane in breast cancer correlates positively with MYC levels but negatively with Bcl-xL levels, which could be induced pharmacologically.[161] Especially for PDAC, Beglyarova et al. developed new physiological models, the patient-derived xenografts (PDXs), where they could test a large panel of clinical compounds.[162] In vitro, the most effective ones were interfering with protein turnover or transcription. Interestingly, in PDX models the Excision repair cross-complementation group 3 (ERCC3) inhibitor Triptolide caused complete regression, which was even superior in MYC-amplified PDXs where it resulted in depletion of MYC. The expression of ERCC3, a component of the TFIIH transcription complex, correlates with poor prognosis and resistance to Triptolide was found to be mediated by elevated ERCC3 and MYC levels.[162] Nevertheless, there was still some meaningful targeted hypothesis-driven research in the last years, bringing even more SL interaction into light. MYC regulates the UPR via binding to the promoter and enhancer of Inositol-requiring enzyme 1 (IRE1), increasing its transcriptional activity by forming a complex with X-box binding protein 1 (XBP1). In breast cancer and others, silencing or inhibiting XBP1 or IRE1 RNase activity pharmacologically, for instance using a small-molecule inhibitor, blocks growth of MYC-overexpressing cells and PDXs in vivo.[163,164] In MYC-driven tumors, a synergistic effect between “8866” and Docetaxel chemotherapy could be shown.[163] Also in prostate cancer models the same UPR pathway could be targeted by a RNase domain-specific inhibitor of IRE1α, which again linked UPR to MYC activation.[165] The UPR, extensively reviewed by Walter & Ron and Zhang et al., is triggered by endoplasmic reticulum (ER) stress following accumulation of unfolded or misfolded proteins as a result of disrupted proteostasis.[55,166] The UPR then increases expression of chaperones, clears proteins via ER-associated degradation (ERAD) or autophagy and attenuates protein translation to rescue the cell. In case of irreversible damage it also induces apoptosis.[55] And the UPR possesses three main sensor proteins in the ER membrane, IRE1, Protein kinase R-like endoplasmic reticulum kinase (PERK) and Activating transcription factor 6 (ATF6), to detect ER stress. From prostate cancer mouse models and others it is known that MYC activation is causing ER stress, proving the interconnectivity of MYC and UPR.[80,167] In addition, direct MYC targets are regulating UPR elements, MYC itself is able to repress or enhance autophagy and the IRE1 and PERK pathways are targeted directly.[168] Vice versa, MYC is regulated by UPR components like

XBP1. Keeping these points in mind it is not surprising that deregulated UPR helps MYC in its oncogenic functions and that MYC SL targets can be found in these pathways. A last example is the work of Genovese et al.[169] They investigated a conditional $Kras^{G12D}$ mouse model of PDAC and discovered Kras-independent escaper cell populations that are more de-differentiated and aggressive and are characterized by SWI/SNF-related matrix-associated actin-dependent regulator of chromatin subfamily B member 1 (SMARCB1)-MYC-driven mesenchymal reprogramming. Herein, the depletion of Smarcb1 activates MYC signaling increasing protein metabolism and ER-stress mediated UPR. The genetic and pharmacological inhibition of IRE1 signaling or combined regimen targeting UPR can now impair the development of these aggressive mesenchymal MYC-driven PDAC subpopulations in mice and patient-derived models.[169] A different way to trigger ER-stress mediated apoptosis is to interfere with the UPS disturbing proteostasis. As mentioned earlier, the tight regulation of MYC proteostasis is essential for the cell, thus inhibition of the UPS will lead to accumulation of MYC, but also UPR-related and pro-apoptotic proteins, in either case causing apoptosis. An inhibitor of the ubiquitin-activating enzyme (UAE) called TAK-243 was shown to induce ER-stress and UPR in diffuse large B-cell lymphoma (DLBCL) cells.[170] MYC sensitizes these cells even more to UAE inhibition, also in xenografts and primary patient-derived cells. In this setting, TAK-243 even proved increased potency compared to the classical proteasome inhibitor Bortezomib.[170]

d. Intention and aim of this work

As there are several different drugs and corresponding mechanisms that potentially lead to SL with MYC overexpression, a limited screen in PDAC cell lines with a FDA-approved drug library was performed in a completely unbiased manner to decipher promising candidates. In addition to pharmacological targeting of the genetic landscape in PDAC, recent studies are emerging on epigenetic traits that characterize this cancer type.[171] One promising example is the combined inhibition of BET family proteins and HDACs.[172] The epigenetic footprint of a given cell type is mainly formed by post-translational modifications that determine the conformation, localization, interaction capacity, stability and activity of proteins. These modifications can be among others phosphorylation, hydroxylation, ubiquitination, SUMO-ylation, acetylation or methylation, usually being reversible by corresponding enzymes. To take this into account as well, PDAC cell lines will be also screened for SL interactions between MYC and epigenetic compounds.

Both screening approaches enable to further explore the concept of synthetic lethality with MYC in pancreatic cancer and thereby use it to detect novel mechanisms and therapeutic areas for already existing drugs. This will increase the chance to see a clinical benefit soon.

V. Material

1. Pancreatic cancer cell lines

Name	**Species**	**Mutations**[173]	**RRID number**
BxPC3	human	Heterozygous for *BRAF* p.Val487_Pro492delinsAla (c.1460_1474delGTGTAGGTGCTGTCA) Homozygous for *CDKN2A* deletion Homozygous for *SMAD4* deletion Homozygous for *TP53* p.Tyr220Cys (c.659A>G)	CVCL_0186
DanG	human	Heterozygous or homozygous for *KRAS* p.Gly12Val (c.35G>T) Homozygous for *TP53* c.972_993+16del38	CVCL_0243
F2612 PPT Caput	murine	*Hdac2* lox/lox, *Pdx*-Flp, *Kras* FSF-G12D/+, *Trp53* del/+, *R26* FSF-CreERT2/FSF-CreERT2	-
F2800 PPT1	murine	*Hdac2* lox/lox, *Pdx*-Flp, *Kras* FSF-G12D/+, *Trp53* del/+, *R26* FSF-CreERT2/LSL-Tva	-
HPAC	human	*CDKN2A* p.Glu120Ter (c.358G>T) *KRAS* p.Gly12Asp (c.35G>A)	CVCL_3517
huPDAC3[#]	human (primary)	*KRAS*^{G12D} mutation	-
HupT3	human	Heterozygous for *KRAS* p.Gly12Arg (c.34G>C) Heterozygous for *MSH6* p.Lys1358fs*2 (c.4071_4072insGATT) Homozygous for *TP53* p.Arg282Trp (c.844C>T)	CVCL_1299
HupT4	human	Heterozygous for *KRAS* p.Gly12Val (c.35G>T) (ClinVar=VCV000012583) Homozygous for *TP53* p.Ile255Thr (c.764T>C) (ClinVar=VCV000376623)	CVCL_1300
IMIM-PC1	human	*KRAS* p.Gly12Asp (c.35G>A) (ClinVar=VCV000012582) *TP53* p.Leu130Val (c.388C>G) (ClinVar=VCV000458543)	CVCL_4061
huPDAC17[#]	human (primary)	*KRAS*^{G12D} mutation	-
MiaPaCa2	human	Homozygous for *CDKN2A* deletion (PubMed=11787853). Homozygous for *KRAS* p.Gly12Cys (c.34G>T) (ClinVar=VCV000012578) Homozygous for *TP53* p.Arg248Trp (c.742C>T) (ClinVar=VCV000012347)	CVCL_0428

Panc0504	human	Heterozygous for *KRAS* p.Gly12Asp (c.35G>A)	CVCL_1637
Panc1	human	Homozygous for *CDKN2A* deletion Heterozygous for *KRAS* p.Gly12Asp (c.35G>A) Homozygous for *TP53* p.Arg273His (c.818G>A)	CVCL_0480
PaTu-8988S	human	Homozygous for *KRAS* p.Gly12Val (c.35G>T) Homozygous for *TP53* p.Arg282Trp (c.844C>T)	CVCL_1846
PaTu-8988T	human	Homozygous for *EP300* Ex17-19del (c.4342del448) Homozygous for *KRAS* p.Gly12Val (c.35G>T) Homozygous for *SMAD4* deletion Homozygous for *TP53* p.Arg282Trp (c.844C>T)	CVCL_1847
PPT-9091*	murine	*p48*-Cre +/-, LSL-*Kras* +/-, Tva del +/-	-
PSN1	human	Homozygous for *CDKN2A* deletion Heterozygous for *KRAS* p.Gly12Arg (c.34G>C) Homozygous for *SMAD4* deletion Homozygous for *TP53* p.Lys132Gln (c.394A>C) Amplification of *c-MYC*	CVCL_1644
huPDAC7[#]	human (primary)	*KRAS*^{G12D} mutation	-

[#] Primary-dispersed human PDAC cell lines (HuPDAC3, HuPDAC7, HuPDAC17) were isolated from surgically-resected (HuPDAC3, HuPDAC17) or PdX-derived (HuPDAC7) human PDAC as described.[157,174] They were established and analyzed in accordance with the Declaration of Helsinki and were approved by the local ethics committee (Project 207/15, 1946/07 and 330/19).

* The murine cell line PPT-9091 was transduced with the pBabepuro-myc-ER construct, which was a gift from Wafik El-Deiry (Addgene plasmid # 19128 http://n2t.net/addgene:19128; RRID:Addgene_19128). The transduction, carried out by Christian Schneeweis and Zonera Hassan, and the line is described elsewhere.[157,175]

2. Primer

Real-Time Quantitative Reverse Transcription Polymerase Chain Reaction (qRT-PCR)		
Gene	**Species**	**Sequence 5`- 3`**
Gapdh fwd	murine	GGG TTC CTA TAA ATA CGG ACT GC
Gapdh rev	murine	TAC GGC CAA ATC CGT TCA CA
Prmt5 fwd	murine	CTG TCT TCC ATC CGC GTT TCA
Prmt5 rev	murine	GCA GTA GGT CTG ATC GTG TCT G

Mycoplasma PCR	
Primer	**Sequence 5`- 3`**
5`Primer 1	CGC CTG AGT AGT ACG TTC GC
5`Primer 2	CGC CTG AGT AGT ACG TAC GC
5`Primer 3	TGC CTG GGT AGT ACA TTC GC
5`Primer 4	TGC CTG AGT AGT ACA TTC GC
5`Primer 5	CGC CTG AGT AGT ATG CTC GC
5`Primer 6	CAC CTG AGT AGT ATG CTC GC
5`Primer 7	CGC CTG GGT AGT ACA TTC GC
3`Primer 1	GCG GTG TGT ACA AGA CCC GA
3`Primer 2	GCG GTG TGT ACA AAA CCC GA
3`Primer 3	GCG GTG TGT ACA AAC CCC GA

3. Antibodies

Primary Antibodies				
Protein	**Host**	**Dilution**	**Manufacturer**	**RRID number**
β-Actin (#A5316)	mouse	1:5,000	Sigma-Aldrich, Merck, Darmstadt	AB_476743
Cleaved Parp (Asp214) (#51 90000017)	mouse	1:1,000	BD Pharmingen, Franklin Lakes, NJ, USA	-
c-myc (#9402S)	rabbit	1:1,000	Cell Signaling Technology, Inc., Danvers, MA, USA	AB_2151827
E-Cadherin (#sc-7870)	rabbit	1:1,000	Santa Cruz Biotechnology, Dallas, TX, USA	AB_2076666
γH2AX (#05-636)	mouse	1:1,000	Merck Millipore, Burlington, MA, USA	AB_2755003
GAPDH (#ACR001P)	mouse	1:10,000	Acris GmbH, Herford	AB_1616730
H4R3me2 (#A-3718-050)	rabbit	1:1,000	EpiGentek Group Inc., Farmingdale, NY, USA	-
Noxa (#ALX-804-408-C100)	mouse	1:1,000	Enzo Life Science, Farmingdale, NY, USA	AB_2052079
Prmt5 (#79998S)	rabbit	1:1,000	Cell Signaling Technology, Inc., Danvers, MA, USA	AB_2799945
Vimentin (#5741)	rabbit	1:1,000	Cell Signaling Technology, Inc., Danvers, MA, USA	AB_10695459

Secondary Antibodies			
Antibody	**Dilution**	**Manufacturer**	**RRID number**
Anti-mouse IgG (H+L) (DyLight® 680 Conjugate) (#5470)	1:10,000	Cell Signaling Technology, Inc., Danvers, MA, USA	AB_10696895
Anti-mouse IgG (H+L) (DyLight® 800 4x PEG Conjugate) (#5257)	1:10,000	Cell Signaling Technology, Inc., Danvers, MA, USA	AB_10693543
Anti-rabbit IgG (H+L) (DyLight® 680 Conjugate) (#5366)	1:10,000	Cell Signaling Technology, Inc., Danvers, MA, USA	AB_10693812
Anti-rabbit IgG (H+L) (DyLight® 800 4x PEG Conjugate) (#5151)	1:10,000	Cell Signaling Technology, Inc., Danvers, MA, USA	AB_10697505
Chemiluminescence: Licor WesternSure® HRP goat anti-mouse IgG (#926-80010)	1:10,000	Licor Biosciences, Bad Homburg	-
Substrate: Thermo Scientific SuperSignal™ West Pico PLUS Chemiluminescent Substrate (#34579)	-	Thermo Fisher Scientific, Inc., Waltham, MA, USA	-

4. Chemicals, reagents and media

Name	**Manufacturer**
2-Mercaptoethanol (#M6250)	Sigma-Aldrich, Merck, Darmstadt
(3-(4,5 Dimethylthiazol-2-yl)-2,5 diphenyltetrazolium bromide) MTT Reagent (#M2128)	Sigma-Aldrich, Merck, Darmstadt
10x TaqMan RT Buffer (#4486220)	Applied Biosystems, Thermo Fisher Scientific, Inc., Waltham, MA, USA
4-hydroxytamoxifen (≥70% Z isomer) (4-OHT) (#H6278)	Sigma-Aldrich, Merck, Darmstadt
Agarose (#A9539)	Sigma-Aldrich, Merck, Darmstadt
Ammonium persulfate (APS) (#A3678)	Sigma-Aldrich, Merck, Darmstadt
Aqua B. Braun 1,000ml (#0082479E)	B. Braun, Melsungen
Blotting grade non-fat powdered milk (#T145.3)	Carl Roth GmbH + Co. KG, Karlsruhe
Bovine serum albumin (BSA), fraction V (#11930.03)	Serva Electrophoresis GmbH, Heidelberg

Bradford reagent, 5x (#39222.03)	Serva Electrophoresis GmbH, Heidelberg
Bromophenol blue (#B8026)	Sigma-Aldrich, Merck, Darmstadt
Cell Lysis Buffer (#9803)	Cell Signaling Technology, Inc., Danvers, MA, USA
Complete, EDTA-free, protease inhibitor cocktail tablets (#11873580001)	F. Hoffmann-LaRoche AG, Basel, Switzerland
Crystal Violet (#C6158)	Sigma-Aldrich, Merck, Darmstadt
Dimethyl sulfoxide (DMSO) (#7029.2)	Carl Roth GmbH + Co. KG, Karlsruhe
Dimethyl sulfoxide for cell culture (#A3672,0250)	PanReac AppliChem ITW Reagents, Darmstadt
dNTP Mix 25mM (#331550)	Biozym Scientific GmbH, Hessisch Oldendorf
Dodecylsulfate Na-salt in pellets (SDS) (#20765.03)	Serva Electrophoresis GmbH, Heidelberg
Dulbecco`s Modified Eagle`s Medium (DMEM) – high glucose (#D5796)	Sigma-Aldrich, Merck, Darmstadt
Dulbecco's phosphate buffered saline (PBS) (#D8537)	Sigma-Aldrich, Merck, Darmstadt
Dulbecco's phosphate buffered saline, powder (#56064C)	Sigma-Aldrich, Merck, Darmstadt
Ethylenediaminetetraacetic acid (EDTA) (Versen) 1% (w/v) in PBS w/o Ca^{2+} w/o Mg^{2+} (#L2113)	Biochrom, Merck, Darmstadt
Ethanol (EtOH) (100%)	Merck KGaA, Darmstadt
Ethanol (80%) Alkopharm 80	BrüggemannAlcohol Heilbronn GmbH, Heilbronn
Ethidium bromide (#E1510)	Sigma-Aldrich, Merck, Darmstadt
Fetal Calf Serum (#TMS-013-B)	Merck Millipore, Darmstadt
GeneRuler™ 100bp DNA ladder (#SM0241)	Fermentas GmbH, St. Leon-Rot
Glycerol (#3783.1)	Carl Roth GmbH + Co. KG, Karlsruhe
Glycine (#3187.4)	Carl Roth GmbH + Co. KG, Karlsruhe
Methanol (#4627.5)	Carl Roth GmbH + Co. KG, Karlsruhe
$MgCl_2$ 25mM (#PEQL01-1599)	Peqlab, VWR International , Llc., West Chester, PA, USA
MultiScribe Reverse Transcriptase (#4308228)	Applied Biosystems, Thermo Fisher Scientific, Inc., Waltham, MA, USA
Penicillin (10000 units/ml) / Streptomycin (10000 µg/ml) solution (#15140122)	Gibco by life technologies, Thermo Fisher Scientific, Inc., Waltham, MA, USA
Phosphatase inhibitor mix I (#39050)	Serva Electrophoresis GmbH, Heidelberg
Prestained protein ladder PageRuler™ (#26617)	Thermo Fisher Scientific, Inc., Waltham, MA, USA
Propidium iodide (PI) (#P4170)	Sigma-Aldrich, Merck, Darmstadt
Random hexamers $p(dN)_6$ (#11034731001)	F. Hoffmann-LaRoche AG, Basel, Switzerland
REDTaq® ReadyMix™ (#P4600)	Sigma-Aldrich, Merck, Darmstadt
RNase A (#12691)	Invitrogen, Thermo Fisher Scientific, Inc., Waltham, MA, USA
RNase inhibitor (#N8080119)	Applied Biosystems, Thermo Fisher Scientific, Inc., Waltham, MA, USA

ROTIPHORESE®NF-Acrylamid/Bis-Lösung 30 % (#3029.1)	Carl Roth GmbH + Co. KG, Karlsruhe
Roswell Park Memorial Institute (RPMI) Medium 1640 (1x) + GlutaMAX™ (#61870036)	Gibco by life technologies, Thermo Fisher Scientific, Inc., Waltham, MA, USA
N,N,N',N'-Tetramethylethylenediamine (TEMED) (#2367.1)	Carl Roth GmbH + Co. KG, Karlsruhe
Tris(hydroxymethyl)-aminomethane (Tris) (#2449.3)	Carl Roth GmbH + Co. KG, Karlsruhe
Trypan blue 0.4%, 0.85% NaCl (#17-942E)	BioWhittaker®, Lonza Group AG, Basel, Switzerland
Trypsin – EDTA Solution 10x (#59418C)	Sigma-Aldrich, Merck, Darmstadt
Tween® 20 (#9127.2)	Carl Roth GmbH + Co. KG, Karlsruhe

5. Buffer and solutions

Buffer/Solution	**Components**
5% Protein loading buffer (Laemmli)	10% SDS 50% Glycerol 228 mM Tris hydrochloride 0.75 mM Bromophenol blue 5% 2-Mercaptoethanol adjusted to pH 6.8
50x Tris acetate EDTA (TAE) buffer	2 M Tris 50 mM EDTA 5.71 % Acetic acid adjusted to pH 8.5
Blocking buffer and antibody solution	5% skim milk powder in PBS or Tris buffered saline (TBS)
Crystal Violet solution	2.5% EtOH 4% Crystal Violet in H_2O
Freezing Medium	70% DMEM 20% Fetal calf serum (FCS) 10% DMSO
Running buffer, 1x	25 mM Tris 192 mM Glycine 0.1% SDS in H_2O
Separating gel buffer	1.5 M Tris adjusted to pH 8.8 with HCl
Stacking gel buffer	0.5 M Tris adjusted to pH 6.8 with HCl
TBS 10x	100 mM Tris 1.5 M NaCl in H_2O adjusted to pH 7.4 (washing buffer) / pH 8.0 (blocking buffer)
Transfer buffer, 1x	25 mM Tris 192 mM Glycine 20% Methanol

	in H_2O adjusted to pH 8.3
Washing buffer	0.1% Tween20 in PBS or TBS

6. Consumables

Consumable	**Manufacturer**
24-well plate (#353047)	Falcon™, Corning, Inc., Corning, NY, USA
6-well plate (#353224)	Falcon™, Corning, Inc., Corning, NY, USA
96-well plate, clear (#353072)	Falcon™, Corning, Inc., Corning, NY, USA
96-well plate, white with clear bottom (#3610)	Falcon™, Corning, Inc., Corning, NY, USA
Arm protector Raucodrape® (#33103)	Lohmann & Rauscher, Rengsdorf
Cell culture flask CELLSTAR® 50ml, 250ml, 500ml (#690175; #658175; #660175)	Greiner bio-one, Greiner AG, Kremsmünster, Austria
Cell scraper 25cm (#83.3951)	Sarstedt AG & Co. KG, Nümbrecht
ClearLine® filter tips 10µl, 100µl, 200µl, 1000µl (#713130; #713116; #713117; #713118)	ClearLine®, Dutscher Group, Brumath, France
Combitips advanced® 0.5ml, 1ml, 2.5ml, 5ml, 10ml (#0030089421; #0030089430; #0030089448; #0030089456; #0030089464)	Eppendorf AG, Hamburg
CryoPure tube (#72.380)	Sarstedt AG & Co. KG, Nümbrecht
Falcon™ 15ml Conical Centrifuge Tube (#188271)	Falcon™, Corning, Inc., Corning, NY, USA
Falcon™ 50ml Conical Centrifuge Tube (#227261)	Falcon™, Corning, Inc., Corning, NY, USA
Nitrile Powder-free examination gloves Abena® classic (#290419)	Abena® GmbH, Zörbig
Pasteur pipette (#9260101)	Hirschmann Laborgeräte GmbH & Co. KG, Eberstadt
PCR reaction tube (#72.991.002)	Sarstedt AG & Co. KG, Nümbrecht
Pipette tips 200µl, 1000µl (#70.760.002; #70.3050)	Sarstedt AG & Co. KG, Nümbrecht
Protran® 0.2µm NC Nitrocellulose membrane (#10600001)	Amersham, GE Healthcare, Amersham, England
qPCR 96-well microplate (#PCR-96-LP-AB-C)	Axygen®, Corning, Inc., Corning, NY, USA
Reaction tube 0.5ml, 1.5ml and 2ml (#72.704; #72.706; # 72.695.200)	Sarstedt AG & Co. KG, Nümbrecht
Sealing Film Platemax CyclerSeal (#UC-500)	Axygen®, Corning, Inc., Corning, NY, USA
Serological pipette CELLSTAR® 5ml, 10ml, 25ml, 50ml (#606180; #607180; #760180; #768180)	Greiner bio-one, Greiner AG, Kremsmünster, Austria
Tissue culture dish 100x20mm (#353003)	Falcon™, Corning, Inc., Corning, NY, USA
Wipes Professional Strong 100V	Lucart, Porcari, Italia

7. Kits

Kit	Manufacturer
Caspase-Glo® 3/7 Assay System (#G8091)	Promega Corporation, Fitchburg, WI, USA
CellTiter-Glo® Luminescent Cell Viability Assay (#G7573)	Promega Corporation, Fitchburg, WI, USA
GoTaq® qPCR master mix (#A6001)	Promega Corporation, Fitchburg, WI, USA
Maxwell® LEV simplyRNA Purification Kit (#AS1280)	Promega Corporation, Fitchburg, WI, USA
QuantiFast SYBR green PCR Kit (#204054)	Qiagen N.V., Venlo, Netherlands

8. Technical equipment

Device	Manufacturer
Analytical balance A 120 S	Sartorius AG, Göttingen
Analytical balance BP 610	Sartorius AG, Göttingen
Autoclave 2540 EL	Tuttnauer Europe B.V., Breda, Netherlands
AxioCam HRc	Carl Zeiss AG, Oberkochen
Bag sealer Folio FS 3602	Severin Elektrogeräte GmbH, Sundern
Centrifuge Galaxy Mini	Eurolab, Merck KGaA, Darmstadt
Centrifuge Mikro 220R	Andreas Hettich GmbH & Co. KG, Tuttlingen
Centrifuge Rotina 380	Andreas Hettich GmbH & Co. KG, Tuttlingen
Centrifuge Rotina 46R	Andreas Hettich GmbH & Co. KG, Tuttlingen
CO_2 incubator HERAcell®	Heraeus Holding GmbH, Hanau
CO_2 incubator MCO 5AC 17AI	Sanyo Denki K.K., Panasonic, Moriguchi, Osaka, Japan
CO_2 incubator NB-203XL	N-Biotek, Bucheon-si, Gyeonggi-do, South Korea
Electrophoresis power supply Power Pac 200	Bio-Rad Laboratories, Inc., Hercules, CA, USA
Flatbed scanner Perfection V370 Photo	Seiko Epson K.K., Suwa, Nagano, Japan
Gallios flow cytometer	Beckman Coulter, Brea, CA, USA
Gel electrophoresis chamber Compact L/XL	Biometra, Analytik Jena AG, Jena
Glass ware, Schott Duran®	Schott AG, Mainz
Horizontal gel electrophoresis system	Biozym Scientific GmbH, Hessisch Oldenburg
Horizontal shaker Biometra® WT17	Biometra, Analytik Jena AG, Jena
Horizontal shaker Titramax 100	Heidolph Instruments GmbH & Co. KG, Schwabach
Laminar flow HERAsafe®	Heraeus Holding GmbH, Hanau
Magnetic stirrer, Ikamag® RCT	IKA® Werke GmbH & Co. KG, Staufen
Maxwell® RNA purification	Promega Corporation, Fitchburg, WI, USA
Microcentrifuge 5415 D	Eppendorf AG, Hamburg

Microcentrifuge 5417 R	Eppendorf AG, Hamburg
Microplate reader (CLARIOstar)	BMG Labtech GmbH, Ortenberg
Microplate reader (FLUOstar OPTIMA)	BMG Labtech GmbH, Ortenberg
Microscope Axiovert 25	Carl Zeiss AG, Oberkochen
Microwave	Siemens AG, Munich
Mini centrifuge MCF-2360	LMS Consult GmbH & Co. KG, Brigachtal
Mini Trans-Blot® Cell	Bio-Rad Laboratories, Inc., Hercules, CA, USA
Mini-PROTEAN® Tetra Vertical Electrophoresis Cell	Bio-Rad Laboratories, Inc., Hercules, CA, USA
Multipette® E3x	Eppendorf AG, Hamburg
Multipette® M4	Eppendorf AG, Hamburg
Multiskan FC Microplate Reader	Thermo Fisher Scientific, Inc., Waltham, MA, USA
Multiskan RC Microplate Reader	Thermo Fisher Scientific, Inc., Waltham, MA, USA
NanoDrop ND-1000 spectrophotometer	Peqlab, VWR International , Llc., West Chester, PA, USA
Neubauer hemocytometer, improved	LO-Laboroptik GmbH, Bad Homburg
Odyssey® infrared imaging system	Licor Biosciences, Bad Homburg
pH meter 521	WTW Wissenschaftlich Technische Werkstätten GmbH, Weilheim
Pipettes Research plus®	Eppendorf AG, Hamburg
Power supplies E844, E822, EV243	Peqlab, VWR International , Llc., West Chester, PA, USA
Stripettor® Ultra	Corning, Inc., Corning, NY, USA
TaqMan, PE StepOnePlus™ Real Time PCR System	Applied Biosystems, Thermo Fisher Scientific, Inc., Waltham, MA, USA
Thermal Cycler T100™	Bio-Rad Laboratories, Inc., Hercules, CA, USA
Thermocycler T1	Biometra, Analytik Jena AG, Jena
Thermomixer compact	Eppendorf AG, Hamburg
Tube racks	TPP® Techno Plastic Products AG, Trasadingen, Switzerland
UVsolo TS Imaging System	Biometra, Analytik Jena AG, Jena
Vortex Genius 3	IKA® Werke GmbH & Co. KG, Staufen
Water bath 1083	GFL Gesellschaft für Labortechnik mbH, Burgwedel

9. Software

Software	**Source**	**RRID number**
Ascent Software for Multiskan	Thermo Fisher Scientific, Inc., Waltham, MA, USA	-
AxioVision 4.3	Carl Zeiss AG, Oberkochen	-
ClustVis	Metsalu, T., Vilo, J., 2015. ClustVis: a web tool for visualizing clustering of multivariate data using Principal	-

	Component Analysis and heatmap. Nucleic Acids Research. https://biit.cs.ut.ee/clustvis/[176]	
Epson Scan Software	Seiko Epson K.K., Suwa, Nagano, Japan	-
Flowjo Software	FlowJo, LLC, Ashland, OR, USA	SCR_008520
GraphPad Prism 5	La Jolla, CA, USA	SCR_002798
Image Studio Lite Ver 5.2	Licor Biosciences, Bad Homburg	SCR_013715
Microsoft Office	Microsoft Corporation, Redmont, WA, USA	-
NanoDrop ND-1000 V.3.1.0	Peqlab, VWR International , Llc., West Chester, PA, USA	SCR_016517
SkanIt RE 5.0	Thermo Fisher Scientific, Inc., Waltham, MA, USA	-
StepOne™ Software v2.3	Applied Biosystems, Thermo Fisher Scientific, Inc., Waltham, MA, USA	SCR_014281
SynergyFinder 2.0	Ianevski, A., Giri, K. A., Aittokallio, T., 2020. SynergyFinder 2.0: visual analytics of multi-drug combination synergies. Nucleic Acids Research. gkaa216, https://doi.org/10.1093/nar/gkaa216[177]	-

10. Inhibitors

Inhibitor/Drugs	**Manufacturer**	**Developer**
5-FU (#S1209)	Selleck Chemicals Llc, Houston, TX, USA	-
AZD7762 (#S1532)	Selleck Chemicals Llc, Houston, TX, USA	-
Bortezomib (#B-1408)	LC-Laboratories, Woburn, MA, USA	-
Epigenetics Compound Library (#L1900)	Selleck Chemicals Llc, Houston, TX, USA	-
EPZ004777 (#S7353)	Selleck Chemicals Llc, Houston, TX, USA	-
FDA-approved Compound Library	NCI/DTP Open Chemicals Repository, MD,USA	-
Gemcitabine (#S1714)	Selleck Chemicals Llc, Houston, TX, USA	-
GSK3326595 (#S8664)	Selleck Chemicals Llc, Houston, TX, USA	GlaxoSmithKline, Brentford, UK
GSK591 (#18354)	Cayman Chemical, Biomol GmbH Hamburg	GlaxoSmithKline, Brentford, UK
INK-128 (#I-3344)	LC-Laboratories, Woburn, MA, USA	-
JNJ-64619178 (#S8624)	Selleck Chemicals Llc, Houston, TX, USA	Johnson & Johnson, New Brunswick, NJ, USA

ML-93[157]	Millennium Pharmaceuticals/Takeda, Cambridge, MA, USA	-
MT-DADMe-ImmA (#HY-101496)	MedChemExpress, Monmouth Junction, NJ, USA	-
Navitoclax (#S1001)	Selleck Chemicals Llc, Houston, TX, USA	-
Panobinostat (#S1030)	Selleck Chemicals Llc, Houston, TX, USA	-
RI-1 (#S8077)	Selleck Chemicals Llc, Houston, TX, USA	-
S63845 (#A8737)	APExBIO Technology LLC, Houston, TX, USA	-
SN-38 (#S4908)	Selleck Chemicals Llc, Houston, TX, USA	-
TAK-243 (#S8341)	Selleck Chemicals Llc, Houston, TX, USA	Takeda Pharmaceutical, Tokio, Japan
Taxol (#S1150)	Selleck Chemicals Llc, Houston, TX, USA	-
Veliparib (#S1004)	Selleck Chemicals Llc, Houston, TX, USA	-
Vorinostat (=Suberanilohydroxamic acid / SAHA) (#V-8477)	LC-Laboratories, Woburn, MA, USA	-

VI. Methods

1. Cell culture

a. Human cell lines

Human pancreatic cancer cell lines were cultured in DMEM - high glucose or RPMI GlutaMAX® medium with 10% (v/v) FCS and 1% (v/v) Penicillin/Streptomycin, depending on the cell line (DMEM: Panc1, Patu-8988S, Patu-8988T, MiaPaCa2; RPMI: DanG, PSN1, HPAC, IMIM-PC1, BxPC3, HupT3, HupT4, Panc0504, huPDAC3, huPDAC7, huPDAC17). For splitting they were washed with PBS and detached using EDTA (1:20 in PBS). They were authenticated regularly (last authentication October 2019) by Multiplexion (Multiplexion GmbH, Heidelberg, Germany) or Microsynth (Microsynth AG, Balgach, Switzerland) and tested for mycoplasma contamination.

b. Murine cell lines

All murine pancreatic cancer cell lines were established from $Kras^{G12D}$-driven mouse models of pancreatic cancer and cultivated as described.[178] Identity of these cell lines was verified by genotyping PCR. Murine cell lines were cultured in DMEM - high glucose with 10% (v/v) FCS and 1% (v/v) Penicillin/Streptomycin. For splitting they were washed with PBS and detached using EDTA (1:20 in PBS).

To generate mesenchymal and epithelial fractions of PDAC cell lines, the cells were washed with PBS and detached with Trypsin from the flask. The first fraction detaching was taken into a new flask and recultured, containing the more mesenchymal cells. Again, Trypsin was added to the flask and a mixed fraction detaching now was discarded. The cells remaining in the flasks were considered the most epithelial cells and recultured. This procedure was repeated 3 – 5 times depending on the cell line to stabilize the fractions.

c. Storage of cell lines

Cells were washed with PBS and detached using EDTA. Afterwards, they were resuspended in PBS and centrifuged at 1,000xg for 5min at 4°C. PBS was aspirated and cells were resuspended in freezing medium. They were stored in 2ml freezing vials for short term at -80°C and for long term in liquid nitrogen. To thaw them, they were washed with PBS by centrifuging them at 1,000xg for 5min at room temperature (RT) to remove DMSO and taken into their respective medium.

d. Mycoplasma testing

All used cell lines were tested regularly after thawing for mycoplasma contamination by PCR as described.[179] Briefly, cells were seeded in 6-well plates in 3ml of their respective medium without antibiotics and with 10% FCS for one week. 2ml of the medium was taken and centrifuged at RT at 250xg for 2min. The supernatant was pipetted into a fresh tube and centrifuged again for 10min at RT at 20,000xg. The supernatant was removed, the pellet was resuspended in the remaining liquid and heat inactivated at 95°C for 3min. 2µl of this was used as a template in the following PCR:

PCR mix (1x)	15µl	REDTaq ReadyMix
	2µl	5`Primer dilution (10µl of each 5`Primer + 30µl H_2O)
	2µl	3`Primer dilution (10µl of each 3`Primer + 70µl H_2O)
	9µl	H_2O

Cycler conditions	95°C	15min	
	94°C	1min	x40
	60°C	1min	
	74°C	1min	
	72°C	10min	
	25°C	∞	

The PCR product was then loaded onto a 2% agarose gel, separated via gel electrophoresis for 1h at 100V and visualized using an UV imaging system.

2. Cell viability assays

a. MTT assay

3,000 cells per well were seeded in 100µl medium in clear 96-well plates. Drugs were added in 20µl medium the next day in technical triplicates, and after three days incubation time, 10µl MTT reagent (dilution 5mg/ml) was added to each well for measurement of cell viability. Plates were incubated for 4h at 37°C, medium was removed and the formazan crystals were dissolved in 200µl DMSO:EtOH (v/v) (1:1) per well on a shaker for 10min at RT. Absorbance was measured at 595nm on a Multiskan RC microplate reader. The half-maximal growth inhibitory (GI_{50}) concentration (non-linear regression model) and the area-under-the-curve (AUC) were calculated with GraphPad Prism 5.

b. CellTiter-Glo® ATP assay

1,000 cells per well for 6-day treatments or 2,000 cells per well for 3-day treatments were seeded in 100µl medium in white, clear-bottom 96-well plates. Drugs were added in 20µl medium the next day and after three or six day incubation time, the plate was put out of the incubator to equilibrate to RT. Then, 25µl CellTiter-Glo® reagent (buffer and substrate mixed 1:1) from Promega was added to each well. After 10min of gentle shaking at 300rpm and 20min of incubation at RT protected from light, luminescence was measured on a FLUOstar OPTIMA microplate reader with a gain of 1,500. The half-maximal growth inhibitory (GI_{50}) concentration values (non-linear regression model) and the area-under-the-curve (AUC) were calculated with GraphPad Prism 5.

3. Drug screening approach

a. FDA-approved, anti-cancer drug library

The anti-cancer drug library with 129 compounds was obtained as a plated set from the NCI/DTP Open Chemicals Repository (NCI/DTP, MD, USA). In this screen a recently published approach was adapted.[180] To select for drugs highly active in the nanomolar range, two human cell lines with high MYC expression (DanG, PSN1) and two with low MYC expression (Panc1, PaTu-8988S) were screened with a single dose of 600nM of each drug in the 96-well format. For this screening, MTT assay was used as a readout for cell viability, 3,000 cells per well were seeded and it was performed as biological triplicates conducted in technical triplicates. The mean response in the MYC high cell lines was divided by the mean response in the MYC low cell lines and drugs were ranked according to the ratio. A ratio >2 was defined as a hit. The screening results were visualized using ClustVis software.[176]

b. Epigenetics drug library

The epigenetics compound library was purchased from Selleckchem (L1900; Selleck Chemicals Llc, Houston, Texas, USA). For this screening, three human cell lines with high MYC expression and network activity (DanG, PSN1, PaTu-8988T) and three with low MYC expression/activity (Panc1, PaTu-8988S, HPAC) were used. In addition, two murine HDAC cell lines split into a mesenchymal and an epithelial fraction each were also tested. 2,000 cells per well of a 96-well plate were seeded and treated with the drugs after 24h. The following dilutions were used for all drugs to obtain dose-response curves: 10µM, 5µM, 2µM, 0.5 µM, 0.2 µM, 0.05µM, 0.02 µM. A treatment period of three days was used in the screening experiment. The screening was conducted as one biological replicate performed as technical triplicate. ATP was measured as a surrogate for the dose response using

CellTiter-Glo® assay. The area under the dose response curves (AUC) for each drug and cell line were determined with GraphPad Prism 5 using a non-linear regression model. The difference (ΔAUC) between the mean AUC of three MYC high cell lines and three MYC low cell lines or two mesenchymal and two epithelial fractions, respectively, was calculated and drugs were ranked according to the p-value of the ΔAUC. Drugs with a p-value < 0.05 were defined as a hit. The screening results were visualized using ClustVis software.[176]

4. Clonogenic growth assay

1,000 – 4,000 cells were seeded in 500µl medium in 24-well plates, depending on the cell line (1,000 for PSN1, PaTu-8988T and PPT-9091 MYC-ER, 4,000 for PaTu-8988S and Panc0504, 2,000 for MiaPaCa2 WT/Noxa KO, and 3,000 for all others). After 24h, drugs in different concentrations were added in 50µl of medium followed by culturing for one week, or two weeks for MiaPaCa2 WT/Noxa KO. Afterwards the medium was removed and cells were washed with PBS. The cell colonies were stained with 0.2% (w/v) Crystal Violet solution for 30min on a shaker at RT. Then the wells were washed three times with tap water, dried at least overnight and subsequently visualized using a flatbed scanner. For quantification 600µl of 1% (w/v) SDS were added to each well and the plates were shaken over night at RT. Absorbance of the dissolved Crystal Violet was measured at 595nm on a CLARIOstar microplate reader. Values were normalized on each DMSO control and means were calculated out of three biological replicates. In the synergy screen, only one biological replicate was used and "*the expected drug combination responses were calculated based on ZIP reference model using SynergyFinder2.0. Deviations between observed and expected responses with positive and negative values denote synergy and antagonism respectively".*[177]

5. Protein expression analysis

a. Seeding and harvesting

Cells were seeded in 5ml of their respective medium (plus EtOH or 600nM 4-OHT in PPT-9091-MYC-ER cells) in 10cm cell culture dishes and treated the next day. For determination of basal protein expression they were harvested at 80% confluency and for time kinetics according to the experiment. For preparing the whole cell lysates, dishes were put on ice, medium was removed and they were washed with PBS. After removal of most PBS, 100µl of Cell Signaling Lysis Buffer supplemented with Protease Inhibitor and Phosphatase Inhibitor was pipetted onto the dishes, cells were collected using a cell scraper, lysed by incubation for ten minutes on ice, and subsequently frozen at -80°C. For cleaved PARP analysis the supernatant of cells was collected in a tube as well as the 5ml PBS used for washing the dish. The tube was centrifuged at 1,000xg for 5min at 4°C and

after removing the supernatant the pellet was resuspended in the lysis buffer after scraping the dish.

b. Protein concentration analysis

Protein samples were thawed on ice and centrifuged for 10min at maximum speed and 4°C. Bradford reagent was diluted 1:5 with H_2O and 300µl were pipetted into each well of a clear 96-well plate. As a standard dilution series BSA (1µg/µl) was used in concentrations of 1.5ng/µl, 3ng/µl, 6ng/µl, 12ng/µl and 24ng/µl. Then 1µl of each sample was pipetted into each well in triplicates. Afterwards, absorbance was measured on a Multiskan FC microplate reader at 595nm and protein concentrations were calculated using the standard curve and the mean of the triplicates. Finally, samples were diluted with H_2O and protein loading buffer to equalize protein concentration and heated at 95°C for 5min before freezing them at -20°C.

c. Western blot

Protein samples were loaded onto 10% (cleaved PARP, MYC, and PRMT5) or 15% (γH2Ax and H4R3me2s) polyacrylamide gels (for preparation, see following tables) with a marker (Prestained protein ladder PageRuler™) and separated using SDS-page gel electrophoresis at 80 – 100V for 2 – 3 hours in running buffer. Then the proteins were transferred onto a nitrocellulose membrane using a wet blot system with transfer buffer at 350mA for 2h. The membranes were blocked for 45min in blocking buffer (PBS or TBS respective to the antibody dilution) on a shaker at RT and incubated over night at 4°C with a primary antibody according to the experiment diluted in 5% (w/v) skim milk in PBS (E-cadherin, vimentin, cleaved PARP, MYC, PRMT5, NOXA, and Glyceraldehyde 3-phosphate dehydrogenase (GAPDH)) or TBS (γH2Ax and H4R3me2s). The next day, the membranes were washed three times 5min with washing buffer (PBS or TBS respective to the antibody dilution), a corresponding secondary antibody diluted in 5% (w/v) skim milk in PBS or TBS was incubated with the membranes for 1h at RT and the western blots were visualized using an Odyssey Infrared Imaging System. This procedure was repeated for every antibody used on the membrane. NOXA and GAPDH blots have been performed by chemiluminescence.

Stacking gel (1x)

ddH_2O	1,500µl
Stacking gel buffer	650µl
30% Acrylamide	375µl
10% SDS	25µl
10% APS	12.5µl
TEMED	5µl

Separation gel (1x)

	10% gel	**15% gel**
ddH_2O	2,050µl	1,250µl
Separation gel buffer	1,300µl	1,300µl
30% Acrylamide	1,650µl	2,500µl
10% SDS	50µl	50µl
10% APS	25µl	25µl
TEMED	7.5µl	7.5µl

d. Quantification

Protein bands were quantified using the Image Studio Lite Software. Protein expression values were normalized on expression of a housekeeping protein (β-Actin) and final expression values were calculated out of three biological replicates.

6. RNA expression analysis

a. Seeding and harvesting

Cells were seeded in 5ml of their respective medium (plus EtOH or 600 nM 4-OHT in PPT-9091 MYC-ER cells) in 10cm cell culture dishes. For basal messenger RNA (mRNA) measurements the plates were harvested at 80% confluency, which was after 48h. For harvest, dishes were put on ice, medium was removed and they were washed with PBS. After removal of most PBS, 100µl of RNA Solution supplemented with thioglycerol (Promega Maxwell® 16 LEV simplyRNA Tissue Kit) was pipetted onto the dishes, cells were collected using a cell scraper and frozen immediately at -80°C.

b. RNA extraction and cDNA synthesis

Samples were thawed on ice and RNA was isolated using the Promega Maxwell® 16 LEV simplyRNA Tissue Kit and instrument following the manufacturer's instructions. In the final step, RNA was eluted into RNAse-free water and subsequently concentration was measured on the NanoDrop. After that, RNA was diluted to equalize concentration to approx. 0.05µg/µl (2µg RNA in 38.5µl H_2O). cDNA was synthesized using a Thermocycler with the following master mix and program:

RT-PCR mix (1x)	10µl	10x TaqMan RT Buffer
	22µl	MgCl2 (25mM)
	20µl	dNTP-Mix 2.5mM
	5µl	Random Hexamers
	2µl	RNase Inhibitor
	2.5µl	Multiscribe Reverse Transcriptase (50 U/µl)

	38.5µl	RNA dilution

Cycler conditions	25°C	10min
	48°C	60min
	95°C	5min
	4°C	∞

c. qRT-PCR and quantification

Primers were tested for efficiency before use in an experiment. Briefly, a test sample expressing the targeted mRNA was used for a 5-point dilution series in the expected concentration range. qPCR was performed with the new primers using also housekeeping gene and water control. The mean CT value for the primers over three replicates was correlated with the log(concentration) for each dilution point and the slope was calculated for this graph. The slope value was checked at the ThermoFisher website[181] and should show an efficiency between 90 – 110% to deem the primers suitable for experiments.

cDNA was diluted 1:5 and efficient primers were diluted 1:10 with H_2O. The following master mix was prepared and 10µl of it were pipetted on top of 2.5µl diluted cDNA into each well of a qPCR microplate:

qPCR master mix (1x)	6.25µl	2 x SYBR MM Buffer
	0.125µl	FWD Primer
	0.125µl	REV Primer
	0.1µl	CXR
	3.4µl	H_2O

Each sample was pipetted in triplicates, H_2O was used as a quality control and *Gapdh* was used as a housekeeping gene. The microplate was sealed, centrifuged at 1,000rpm for 1min and measured in the StepOne Plus device using Quantitation – Comparative CT (ΔΔ CT) program:

Cycler conditions	95°C	10min	
	95°C	15sec	⎫
	60°C	1min	⎭ x40
	95°C	15sec	
	60°C	1min	
	95°C	15sec	

Values were normalized to the housekeeping gene and values over three biological replicates were calculated.

7. Flow cytometry

Cells were seeded in 5ml of their respective medium in a 10cm cell culture dish, treated the next day and harvested at the indicated time points. For harvest, medium was collected in a tube as well as PBS for washing. Cells were detached by trypsinization and added to their supernatant. The tube was centrifuged at 1,000xg for 5min at 4°C, the supernatant was removed and the pellet was resuspended in 1ml 70% Ethanol (-20°C). Until further analysis these samples were stored at 4°C. Then, 1ml ice cold PBS was added and after centrifugation the pellet was resuspended in 1ml PBS. 2.5µl of RNase (stock concentration 20mg/ml) were added and the samples were incubated for 60min at 37°C protected from light. For cell cycle analysis 50µl of PI (stock concentration 2mg/ml) were added, samples were incubated for at least 5min, filtrated and measured at the Gallios flow cytometer. Results were analyzed with FlowJo™ Software and calculated over three biological replicates.

8. Caspase 3/7 assay

The cells were seeded and treated like described for the cell viability assays in technical triplicates on white, clear-bottom 96-well plates. At the indicated time points, the Caspase-Glo® 3/7 Assay System from Promega was used to determine executioner caspase activity. Briefly, 70µl of liquid were taken from each well and discarded. Buffer and substrate from the Promega kit were mixed and 50µl of this solution was pipetted into each well, resulting in a 1:1 ratio of medium and solution. The plates were shaken for 30sec at 300rpm and incubated for 30min at RT protected from light. Finally, luminescence was measured on a FLUOstar OPTIMA microplate reader with a gain of 4,095. Results were calculated over three biological replicates conducted as technical triplicates.

9. Statistical analysis

All experiments were conducted in biological and technical triplicates and error bars are calculated using standard deviation unless otherwise stated in the figure legends. Two-sided Student`s paired or unpaired t-test was used to investigate statistical significance, as indicated. p-values were calculated with GraphPad Prism 5 and are stated in the figure legends including significance.

VII. Results

1. Human PDAC cell lines show differential MYC protein expression

To identify MYC-associated vulnerabilities in pancreatic cancer we performed two unbiased drug screens. Prior to the screen we selected commercially available human PDAC cell lines and assessed their MYC protein level (Fig.2A). Based on this quantification, we divided them into two groups: “MYC high” (DanG, PSN1, PaTu-8988T, MiaPaCa2, and HupT3) with a mean relative MYC expression over three independent experiments above 0.07 and “MYC low” (Panc1, PaTu-8988S, HPAC, BxPC3, IMIM-PC1, HupT4 and Panc0504) below 0.07 (Fig.2B). The FDA-approved library screen was carried out in a two versus two setting using the cell lines Panc1, PaTu-8988S, DanG and PSN1, for the epigenetic screen PaTu-8988T and HPAC were added. These six cell lines differ not only in MYC expression but also in morphology with Panc1, PaTu-8988S, DanG and HPAC being rather epithelial and PSN1 and PaTu-8988T more mesenchymal (Fig.2C). To determine the number of cells to seed for each screen, we previously analyzed growth curves of the human cell lines. As in the FDA-screen MTT assay was used to assess viability and in the epigenetic screen CellTiter-Glo (CTG) assay, we tested the suitable cell number in both (Fig.3A and 3B, Tab.1A and 1B). Measurement was done on day 4 during the screens, so we decided for 3,000 cells to seed in the FDA-drugs MTT screen and 2,000 cells in the epigenetic CTG screen, assuring a still growing cell population at the time point of measurement on one hand and avoiding problems with clonality or impaired growth on the other hand. The selection of cell lines for the screens was also supported by analysis of publicly available transcriptional datasets (CCLE) and Gene Set Enrichment Analysis (GSEA) showing activation of the MYC network in the MYC high cell lines.[175]

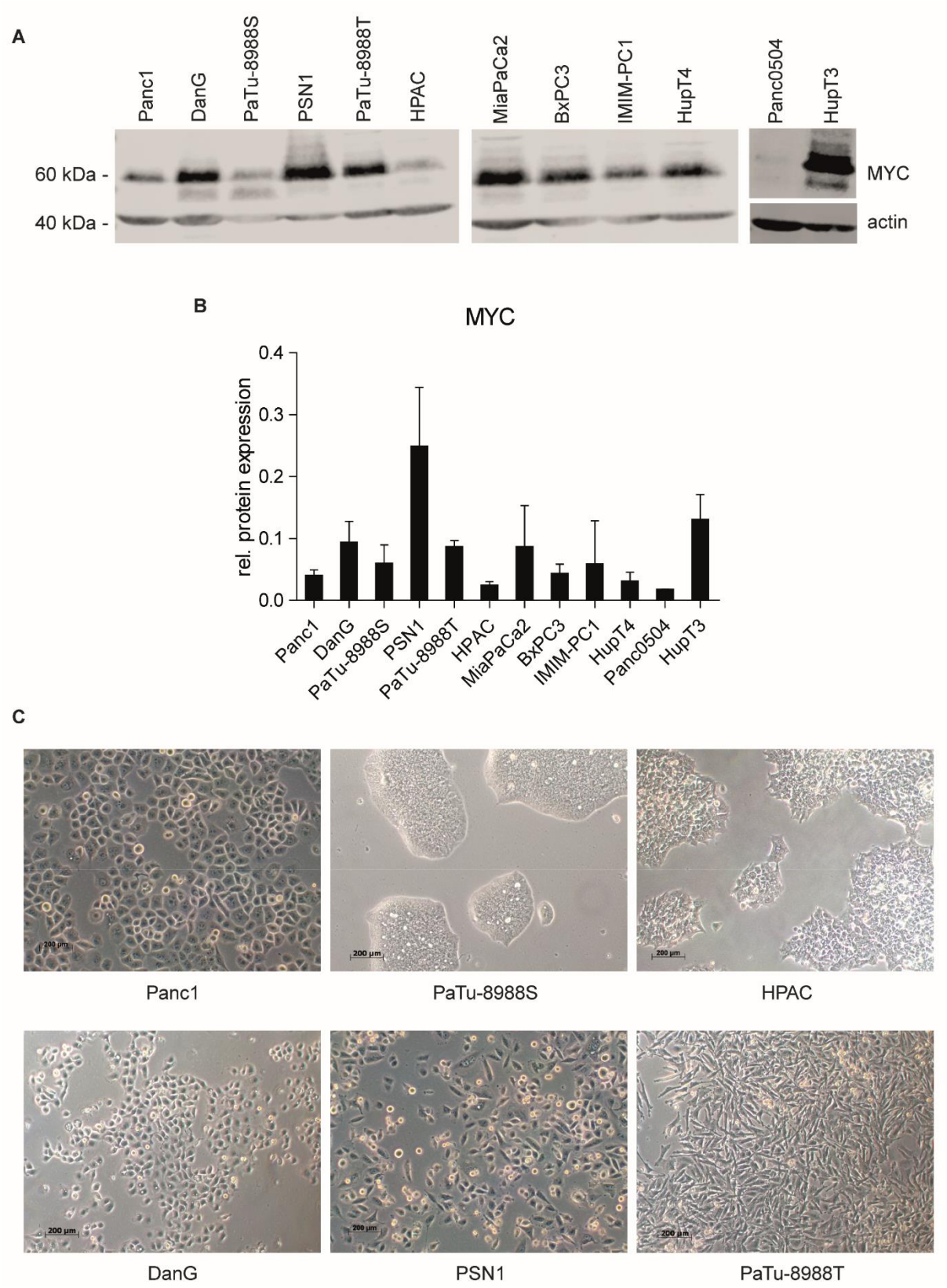

Fig. 2 MYC protein expression and morphology of human PDAC cell lines
A) One representative western blot assessing MYC protein expression in ten human PDAC cell lines. β-Actin (actin) was used as a housekeeping protein. **B)** Quantification of three independent biological replicates like in A). MYC expression was calculated relative to β-Actin expression. **C)** Morphology of cell lines as seen via light microscopy (magnification 10x0.25; scale bar shows 200µm).

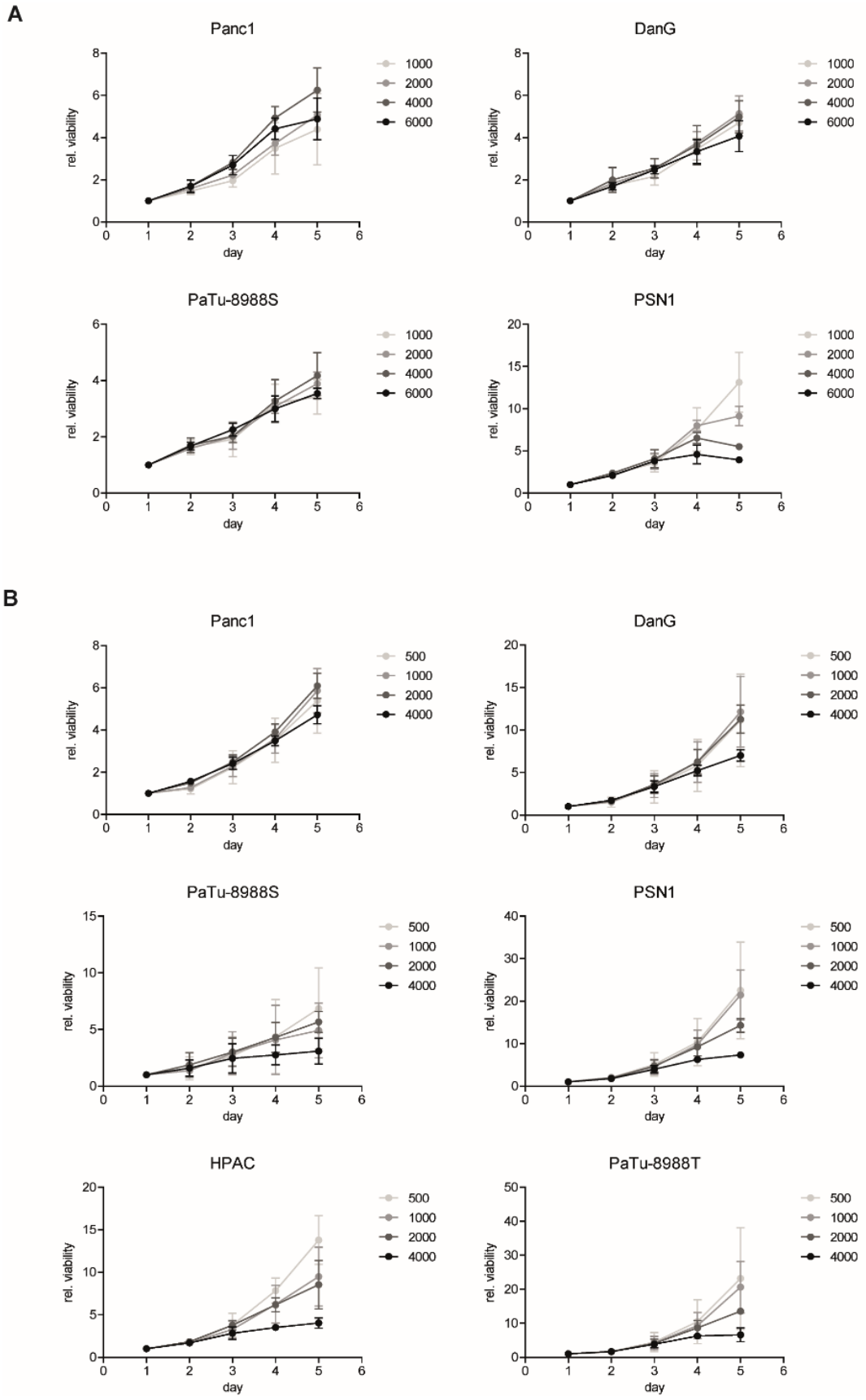

Fig. 3 Growth curves of human PDAC cell lines used for screening

A) Growth curves of depicted cell lines measured via MTT assay. Indicated cell numbers were seeded in 96-well plates and viability was measured each day and normalized to day 1. Graphs were calculated out of three independent biological replicates. **B)** Similar to A), using CTG assay instead of MTT assay for viability measurement.

Tab. 1 Doubling Times of human PDAC cell lines

A) Doubling times of indicated human PDAC cell lines calculated from the MTT growth curves described in Fig.3A via linear correlation of cell number and optical density. **B)** Similar to A), using the CTG growth curves described in Fig.3B.

A

Cell Line	Doubling Time (h)
Panc1	45
PaTu-8988S	49
DanG	46
PSN1	27

B

Cell Line	Doubling Time (h)
Panc1	47
PaTu-8988S	34
HPAC	29
PaTu-8988T	28
DanG	31
PSN1	23

2. Unbiased drug screen of FDA-approved anticancer drugs identifies vulnerabilities in MYC high human PDAC cells

Panc1, PaTu-8988S as MYC low and DanG, PSN1 as MYC high human PDAC cell lines were used in a screening with a FDA-approved anticancer drug library containing 129 drugs that cover various pathways. The workflow of this screen is outlined in Fig.4A. Compounds showing a twofold difference in the responsiveness of the MYC high cell lines were defined as hits. The eleven hit candidates represented different drug classes like HDAC inhibitors, DNA antimetabolites, proteasome inhibitors, topoisomerase I and II inhibitors, inhibitors of transcription and of folate metabolism (Fig.4B and Tab.S1).

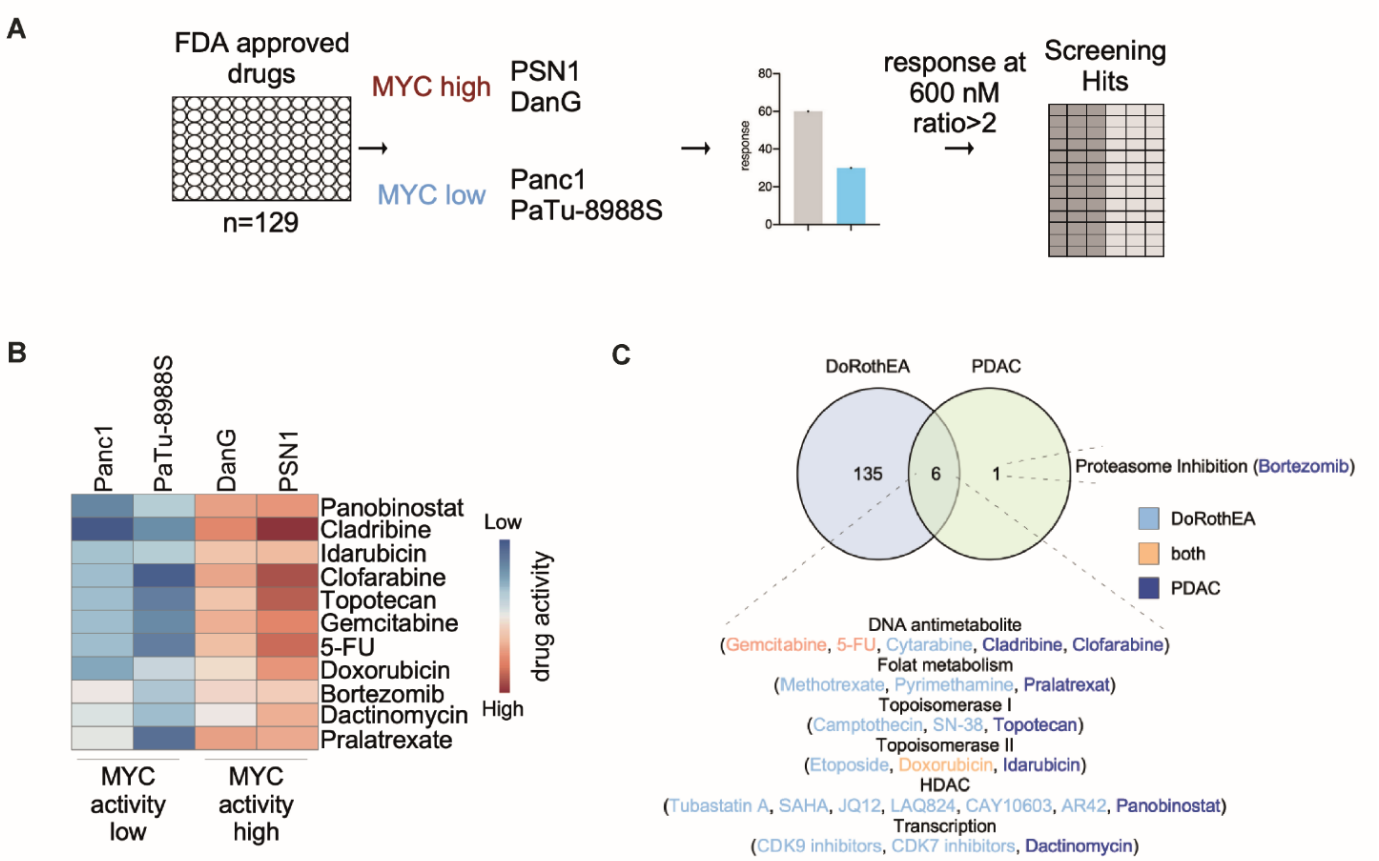

Fig. 4 Unbiased FDA-approved anticancer drug screen in human PDAC cell lines with differential MYC expression

A) Strategy for drug screening experiments with n = 129 FDA-approved anticancer drugs. Cells were treated for 72h with 600nM of each compound and viability was measured by MTT assay. Hits were determined as a twofold difference in responsiveness. **B)** Top eleven hits from the drug screen of 129 FDA-approved compounds depicted as a variance scaled heatmap. **C)** Venn diagram comparing significant (FDRq < 0.05) drug–MYC interactions of the DoRothEA database to the hits of our drug screen (PDAC). Drugs hits were summarized into drug classes.

To substantiate the screening hits, we accessed the Discriminant Regulon Expression Analysis (DoRothEA) database. Therein, drug sensitivity is linked to the transcriptional activity of 127 transcription factors.[182] We found significant drug hits (FDRq < 0.05) in the drug-MYC interaction data, featuring sensitivity especially in MYC active cells. These database hits were assigned to drug classes and compared with our experimental drug screening hits. Six drug classes overlapped significantly with our results, pointing to the robustness of the screen (Fig.4C). As only a single dose was used in the initial drug screen, we validated the top eleven hits again separately using different doses and we calculated dose–response curves. Thereby, four additional PDAC cell lines, two with high MYC protein expression (MiaPaCa, PaTu-8988T) and two with low MYC expression (HPAC, HupT4) were tested. MYC protein expression of the analyzed cell lines is significantly different (Fig.5A). In MYC activated cell lines, we saw a left shift of most dose–response curves (Fig.5B). As only exemption, HPAC cells cluster into the batch with increased sensitivity to the validated drugs despite their low MYC protein level. However, the HPAC cell line is expressing functional wild-type p53, which could provide an explanation for this outcome. MYC high cell lines in general show a lower mean area under the dose-response curves (AUC) for all screening hits, although we observed a high variance (data not shown).[175]

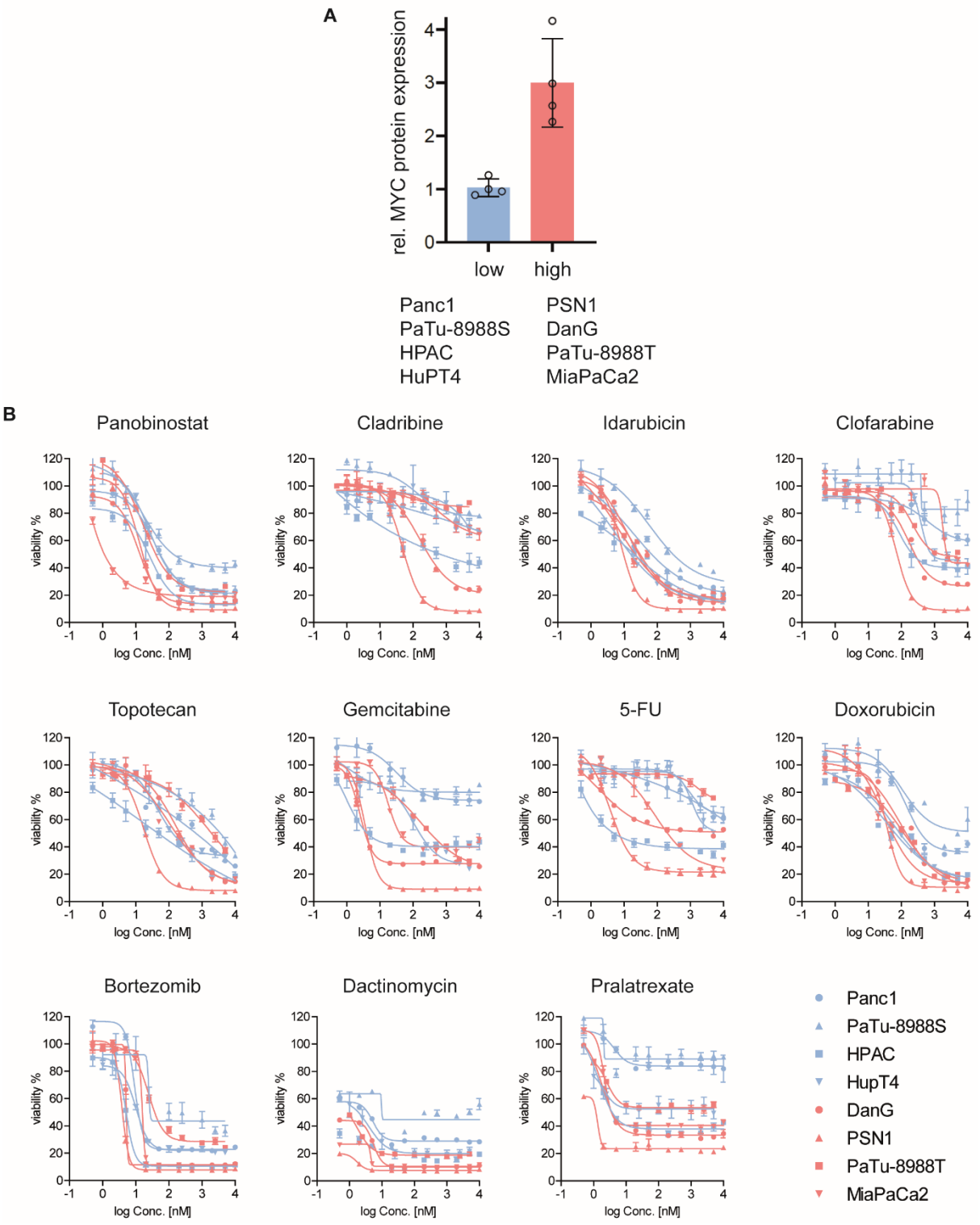

Fig. 5 Validation of FDA-approved anticancer drug screen

A) Quantification of MYC expression of the indicated cell lines. MYC expression was determined in three independent lysates via Western Blot and the mean with SD of MYC expression per cell lines is shown. p-value of an unpaired two-tailed t-test < 0.05. **B)** Viability of MYC high (red) and MYC low (blue) cells for multi-dose treatment with displayed compounds. Cells were treated for 72h and viability was measured by MTT. All experiments were conducted in n = 3 technical replicates in a dosage range of 0.5nM–10µM. Except for HPAC (n = 1), three independent biological replicates have been performed in the depicted cell lines, SEM is used for error bars here.

3. Human PDAC cells with active MYC are primed for Bortezomib-induced NOXA-dependent apoptosis

Human PDAC mRNA expression datasets were searched to define MYC-associated pathways connected with reduced survival and a squamous subtype of PDAC to prioritize the screening hits.[175] We detected overlapping MYC-connected signatures in a model of MYC estrogen receptor fusion protein (MYC-ER) in human PDAC IMIM-PC1 cells after activation of MYC.[157,175] All these signatures pointed towards increased translational activity, and indeed signatures of the UPR and UPR-activated signaling were amongst them as well. This connection of MYC to the UPR and, in accordance to our latest findings, MYC being mechanistically involved in the induction of apoptosis following proteasome inhibition in PDAC cells, called for a more detailed investigation of the screening hit Bortezomib.[183] Further database analysis and a multi-dose proteasome inhibitor screening approach on murine cell lines supported the conclusion that MYC-hyperactivated PDACs are more sensitive to perturbants of the protein homeostasis.[175] To validate our findings across species, we used a conditional gain-of-function model based on MYC estrogen receptor fusion (MYC-ER). For transduction a murine PDAC cell line with low MYC expression was used. Treatment with 4-hydoxytamoxifen (4-OHT) and shuttling of MYC-ER into the nucleus induced the MYC targets Ornithine decarboxylase 1 (Odc1) and Carbamoyl-phosphate synthetase 2, aspartate

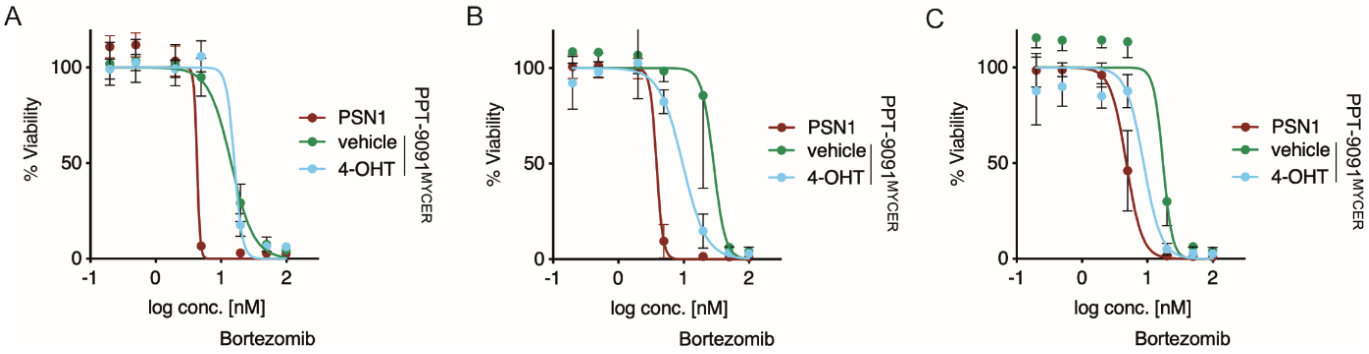

Fig. 6 Proteasome inhibitor sensitivity in MYC genetic gain-of-function
A) Viability test by CTG of PSN1 and PPT-9091-MYC-ER cell lines. Two thousand cells were seeded and after 24h treated with 600nM 4-OHT (MYC-ER shuttles into nucleus) or EtOH (vehicle) and seven increasing concentrations of Bortezomib for three days; highest conc.: 100nM. **B)** 24h pretreatment with 600nM of 4-OHT and 6-day treatment with Bortezomib 24h after seeding of 1000 cells/well similar to A). **C)** Seeding of 1000 cells/well, treatment for four days with 600nM 4-OHT and subsequent 3-day treatment with Bortezomib without 4-OHT treatment according to A). For A)–C), the SD was used for error bars and three independent biological replicates were conducted as technical triplicates.

transcarbamylase, and dihydroorotase (Cad) in this cell line and endogenous Myc is repressed by its negative autoregulation (model characterized by Zonera Hassan and Christian Schneeweis).[175]

Bortezomib-sensitive MYC-amplified PSN1 cells were included into this experiment as a control. When PDAC cells were seeded in 4-OHT for 24h and treated with Bortezomib for the following three days, sensitivity to proteasome inhibition did not change (Fig.6A). Taking into account that the cellular system needs time for adaptation to altered MYC, we chose two different strategies. The first was to pretreat the cells with 4-OHT for 24h prior to a 6-day treatment with Bortezomib, which demonstrated enhanced sensitivity in the MYC active cells (Fig.6B). Secondly, we pretreated the cells with 4-OHT for 96h and proceeded with Bortezomib treatment for 72h. This approach sensitized the cells to Bortezomib as well (Fig.6C). Next, we took a closer look at the specific cellular effects of Bortezomib in human PDAC lines with differential MYC expression. Previously, our group described that Bortezomib-induced

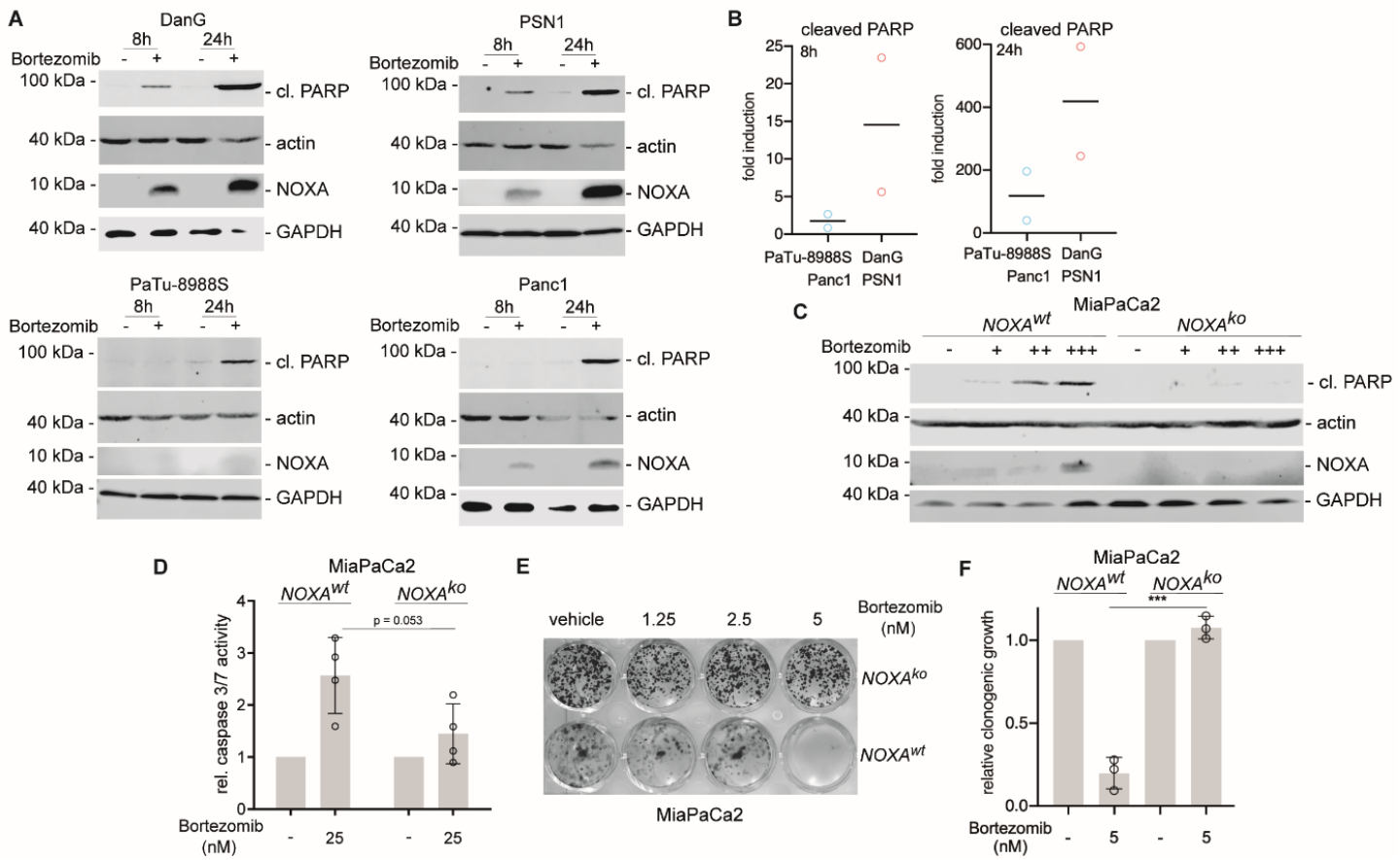

Fig. 7 Priming of PDAC cells with MYC overexpression for proteasome inhibitor-induced apoptosis
A) Lysates of indicated cell lines were blotted (western blot) to different membranes to determine expression of cleaved PARP, NOXA and β-actin (actin) or GAPDH as loading controls, after 8h and 24h treatment with 50nM Bortezomib or DMSO (vehicle control). Shown is one representative experiment of three biological replicates. NOXA blots were performed and kindly provided to us by our cooperation partner PD Dr. Matthias Wirth. **B)** The cleaved PARP band was quantified in three independent experiments and the mean fold induction of cleaved PARP expression in MYC low (Panc1, PaTu-8988S) and MYC high (DanG, PSN1) cell lines is depicted. **C)** Western blot analysis for expression of NOXA and cleaved PARP of MiaPaCa2 cells harboring either NOXA wild-type expression or a NOXA knockout. β-Actin (actin) and GAPDH served as loading controls. Cells were treated for 24h with Bortezomib (+ 50nM, ++ 100nM, +++ 200nM) or DMSO as vehicle control (-).These blots were performed and kindly provided to us by our cooperation partner PD Dr. Matthias Wirth. **D)** Relative caspase 3/7 activity (mean with SD) of MiaPaCa2 NOXA wild-type versus NOXA knockout cells. Cells were treated for 24h with Bortezomib (25nM) or DMSO as vehicle control (-).p-value of an unpaired two-tailed t-test is p=0.053. **E)** Clonogenic growth assay of MiaPaCa2 NOXA knockout and wild-type cells treated with the indicated concentrations of Bortezomib. One representative experiment out of three is depicted. **F)** Quantification of three independent clonogenic growth assays (mean with SD) according to E). p-value of an unpaired two-tailed t-test < 0.001 (***).

apoptosis of PDAC cell lines is mediated by MYC-dependent activation of pro-death BCL2 family members, including NOXA.[183] To find out whether increased apoptosis induction is the main cause of the pronounced proteasome inhibitor sensitivity in MYC active PDAC cell lines, cleavage of the caspase substrate PARP and NOXA protein expression were assessed over time. The MYC high cell lines demonstrated significant induction of NOXA and subsequently, levels of cleaved PARP rised eight hours after the treatment (Fig.7A). Twenty-four hours after treatment, MYC low cell lines expressed NOXA protein and activated caspase-mediated PARP cleavage as well (Fig.7A), but these Bortezomib-induced effects were always more prominent in MYC high cell lines (Fig.7B). Since NOXA was only recently shown to contribute to Bortezomib-induced apoptosis in PDAC cell lines, we knocked out the *NOXA* gene in MiaPaCa2 cells using CRISPR-Cas9 system (model characterized by Zonera Hassan and Christian Schneeweis).[175] The therapeutic response toward Bortezomib, visible by PARP cleavage, induction of caspases 3/7 and cell growth, is clearly reduced in NOXA-deficient MiaPaCa2 cells (Fig.7C-7F), highlighting the relevance of this protein for Bortezomib-induced apoptosis.

4. Response of PDAC cells to perturbants of proteostasis is heterogenous

To determine if MYC overexpression also sensitizes PDAC cells for other perturbants of protein homeostasis, we used TAK-243, an inhibitor of the UAE, on our human screening cell lines and on our murine gain-of-function model. Interestingly, the dose-response curves of MYC low cell lines were left-shifted after TAK-243 treatment compared to the MYC high cell lines, indicating an opposite effect compared to Bortezomib (Fig.8A). Also, a TAK-243 treatment of PPT-9091 MYC-ER cells with and without MYC activation similar to Fig.6 showed no difference in response (Fig.8B-8D). This demonstrates a certain heterogeneity between perturbants of proteostasis.

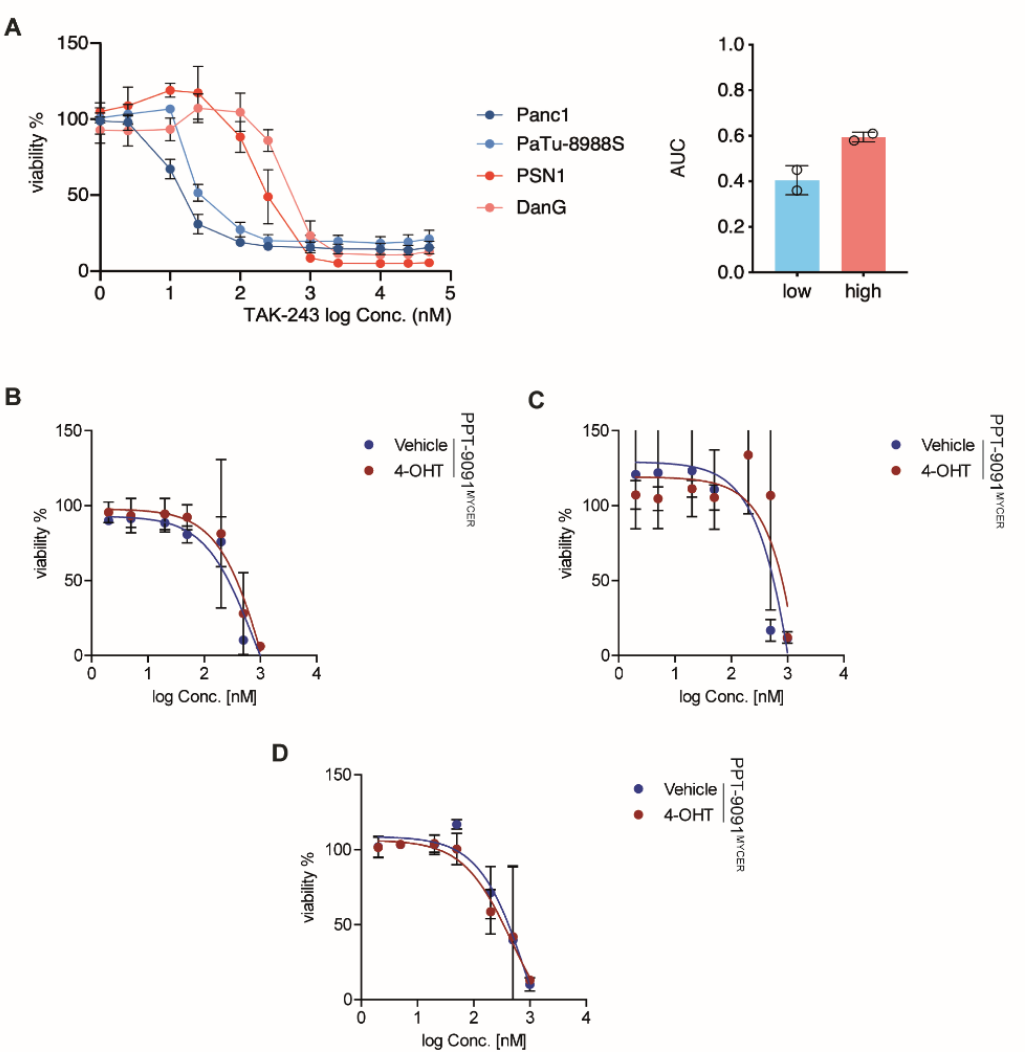

Fig. 8 UEA-inhibitor sensitivity in human PDAC cell lines and MYC genetic gain-of-function
A) Viability measured by MTT for multi-dose (max. 50µM) TAK-243 treatment of MYC high (red) and MYC low (blue) cell lines. 3000 cells/well were seeded and treated 24h later for 72h. The mean (with SD) area under the dose-response curves (AUC) in both groups is depicted. **B)** Viability of PPT-9091 MYC-ER cells measured by CTG. Two thousand cells were seeded and after 24h treated with 600nM 4-OHT (MYC activation) or EtOH (vehicle) and increasing concentrations of TAK-243 for three days; highest conc.: 1 µM. **C)** 24h pretreatment with 600nM of 4-OHT and 6-day treatment with TAK-243 24h after seeding similar to B). **D)** Treatment for four days with 600nM 4-OHT and subsequent 3-day treatment with TAK-243 without 4-OHT treatment according to B). All experiments with TAK-243 were conducted in technical triplicates and three independent biological replicates have been performed.

5. Cellular subtype determines sensitivity for epigenetic compounds

In our refined unbiased drug screen approach we focused on epigenetic compounds. As it is not only MYC that determines sensitivity for all type of drugs, we decided to screen models of different morphological subtypes as well. It is known that a mesenchymal subtype of PDAC in patients is associated with a worse prognosis and that this phenotype in turn reflects the metabolic subtype. The mesenchymal (or quasi-mesenchymal) subtype concurrently seems to be more glycolytic, whereas the epithelial (or classical) subtype seems to be rather lipogenic.[184] To address this question, we used two murine PDAC cell lines for testing the epigenetic library with 181 drugs in addition to our six well-characterized human PDAC cell lines. Before screening, the two cell lines F2612 and F2800 were each split into two fractions, in which we enriched epithelial or mesenchymal cells (Fig.9A). To characterize the fractions on protein level we used E-cadherin as an epithelial marker and vimentin as a mesenchymal marker. In both cell lines, the markers basically substantiated our subtyping, being more pronounced in F2612 (Fig.9B). Likewise, MYC could be excluded as a determinant in these lines. The workflow for the epigenetic screen of these models is outlined in Fig.9C. Compared to the FDA-approved drug screen, we used different drug doses, performed CTG to assess viability and hits were defined using delta AUC between the compared groups and a significant p-value < 0.05. The screen top hits showed a higher sensitivity of mesenchymal fractions for some HDAC inhibitors, aurora kinase inhibitors, and histone demethylase inhibitors (Fig.9D). A Proviral integration of Moloney virus kinase family (PIM) inhibitor, one antibiotic and a histone methyltransferase inhibitor was also among them. As well, we obtained results for inhibitors mainly of histone or DNA methyltransferases, but also histone acetyltransferase and histone demethylase, that were significantly more effective in epithelial fractions (Fig.9D). Examples for dose-response curves of the two top hit HDAC

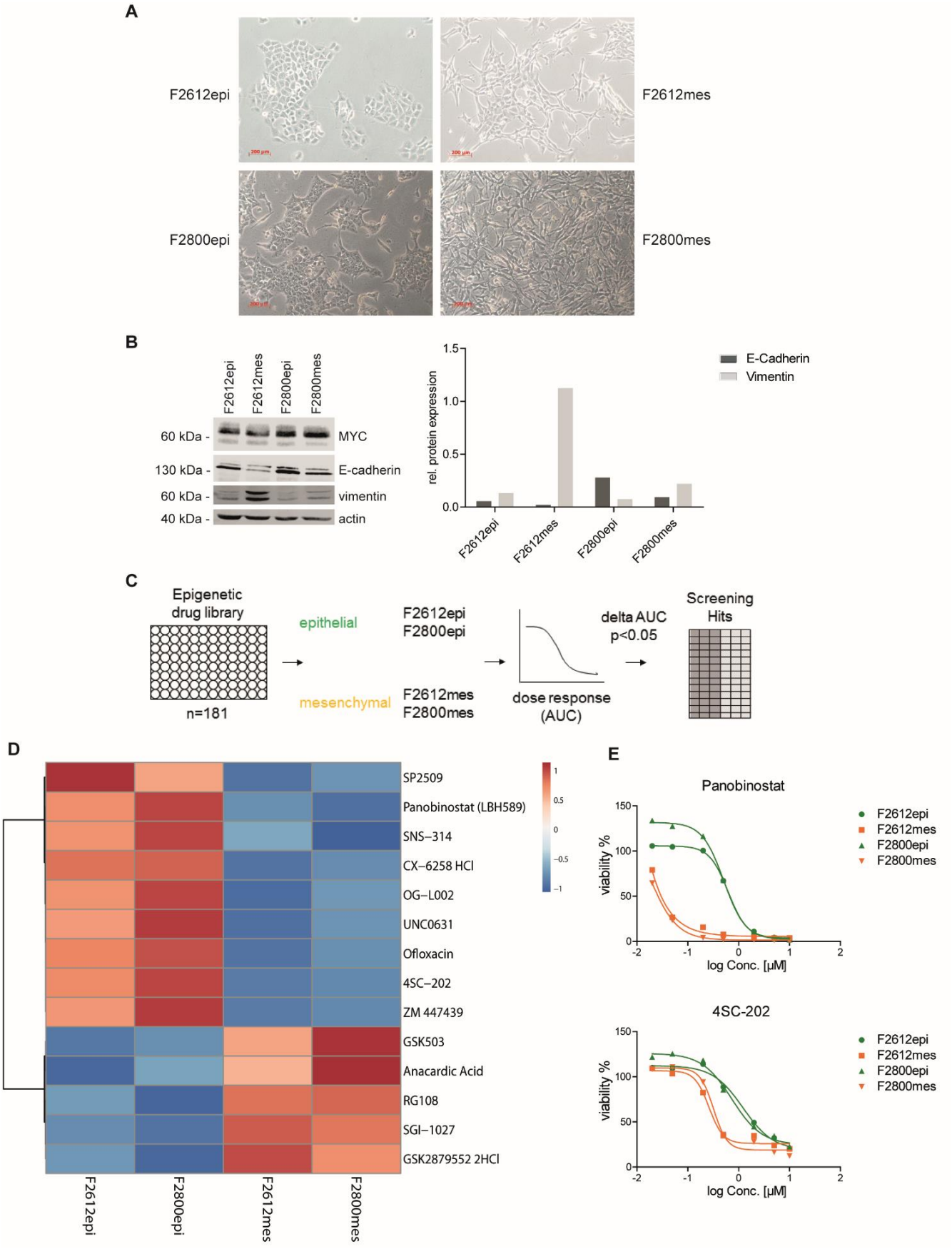
A
F2612epi
F2612mes
F2800epi
F2800mes
B
F2612epi
F2612mes
F2800epi
F2800mes
60 kDa -
MYC
130 kDa -
E-cadherin
60 kDa -
vimentin
40 kDa -
actin
rel. protein expression
1.5
1.0
0.5
0.0
E-Cadherin
Vimentin
C
Epigenetic drug library
n=181
epithelial
mesenchymal
F2612epi
F2800epi
F2612mes
F2800mes
dose response (AUC)
delta AUC p<0.05
Screening Hits
D
SP2509
Panobinostat (LBH589)
SNS−314
CX−6258 HCl
OG−L002
UNC0631
Ofloxacin
4SC−202
ZM 447439
GSK503
Anacardic Acid
RG108
SGI−1027
GSK2879552 2HCl
F2612epi
F2800epi
F2612mes
F2800mes
E
Panobinostat
viability %
log Conc. [µM]
F2612epi
F2612mes
F2800epi
F2800mes
4SC-202
viability %
log Conc. [µM]
F2612epi
F2612mes
F2800epi
F2800mes

Fig. 9 Unbiased epigenetic drug screen in epithelial and mesenchymal fractions of murine PDAC cell lines **A)** Morphology of cell line fractions as seen via light microscopy (magnification 10x0.25). **B)** Western blot for MYC, E-cadherin and vimentin protein expression in the indicated cell lines with β-Actin (actin) used as a housekeeping protein, and its quantification. Shown is one representative example of four biological replicates. **C)** Strategy for drug screening experiments with n = 181 epigenetic compounds. Cells were treated for 72h with seven concentrations of each compound (max. 10µM) and ATP as a marker of cell viability was measured by CTG assay. Hits were determined as difference in the mean area under the dose-response curve (AUC) between epithelial and mesenchymal fractions with p-value < 0.05. The screen was conducted as one biological replicate in technical triplicates. **D)** Top 14 hits of the drug screen in C) depicted as a variance scaled heatmap using AUC values as an input. **E)** Examples of dose-response curves showing two HDAC inhibitors more effective in mesenchymal fractions obtained in the screening outlined in C).

inhibitors are depicted in Fig.9E. On the underlying molecular mechanisms of these results is being worked in another project of our group.[185] To qualify for further research, the candidates will be evaluated for unambiguity regarding their curves, which will exclude, for example, Ofloxacin.

6. Refined unbiased drug screen in PDAC cells identifies epigenetic MYC-associated vulnerabilities

To further determine MYC-associated vulnerabilities in an epigenetic context we screened six already characterized human PDAC cell lines having different MYC activation status with an epigenetic drug library containing 181 drugs. The screening approach is outlined in Fig.10A. We used DanG, PSN1, and PaTu-8988T cells as models for MYC high PDAC and Panc1, HPAC, and PaTu-8988S cells as models with low MYC activity. A seven-point drug dilution was used in the screening and the experiment was conducted as three technical replicates. Several histone deacetylase (HDAC) inhibitors showed enhanced activity in PDAC with MYC overexpression (Fig.10B and Tab.S2). Moreover, the activity of the chemotherapeutics Mitomycin and Gemcitabine was linked to MYC. Like in the FDA-approved drug screen, Gemcitabine was again found to prompt MYC-associated vulnerability. Interestingly, the Janus kinase 2 (JAK2) inhibitor XL019, the PIM kinase inhibitor AZD1208, and the PRMT5 inhibitor GSK591 could also be defined as hits in this screen (Fig.10B and 10C).

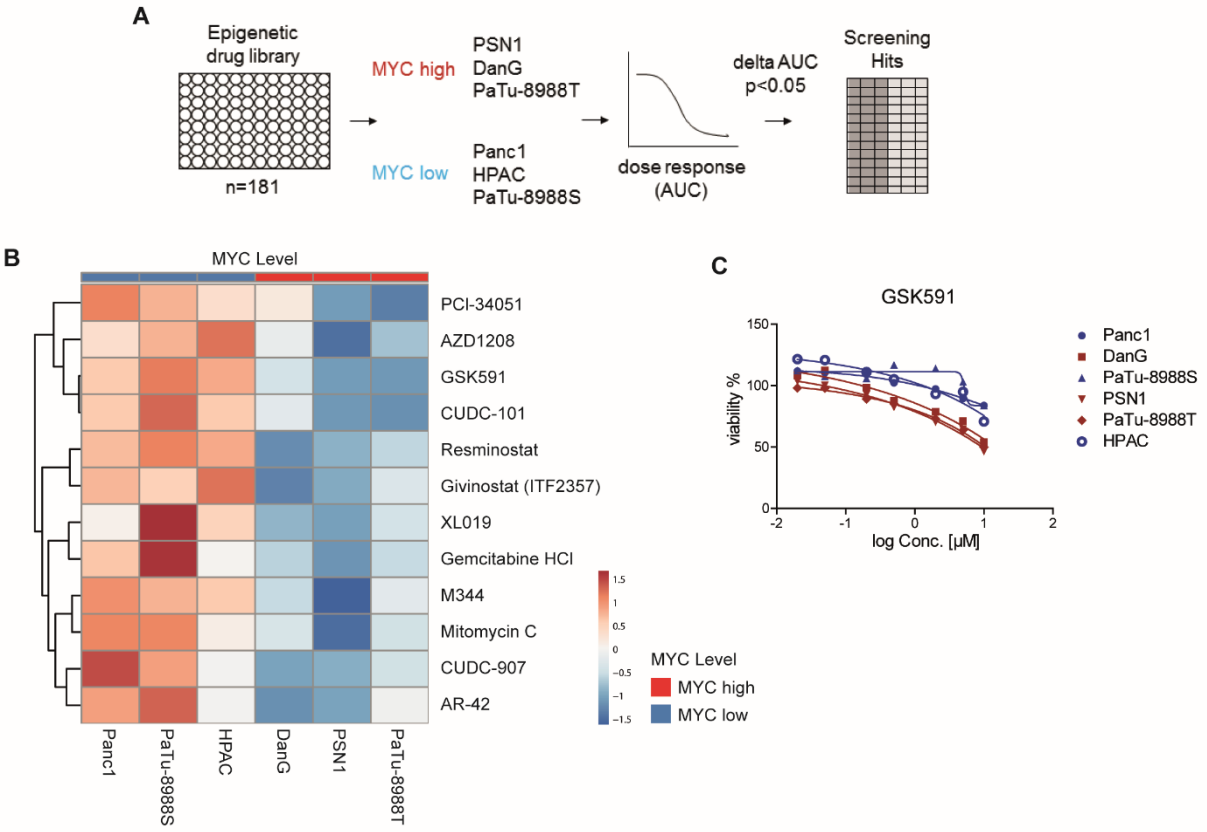

Fig. 10 Unbiased epigenetic drug screen in human PDAC cell lines with differential MYC expression
A) Strategy for drug screening experiments using a library of n=181 epigenetic drugs. Cells were treated for 72h with seven concentrations (max. 10µM) of each compound and ATP as a marker of cell viability was measured by CTG assay. Hits were determined as difference in the mean area under the dose-response curve (AUC) between MYC high and MYC low cell lines with p-value < 0.05. The screen was conducted as one biological replicate in technical triplicates. **B)** Top ten hits of the drug screen outlined in A) depicted as a variance scaled heatmap using AUC values as an input. **C)** Dose-response curve for the PRMT5 inhibitor GSK591 obtained in the screen in A).

7. PRMT5 is connected to MYC in PDAC

Since our goal is to identify and characterize a novel epigenetic MYC-associated vulnerability in the context of PDAC, we focused on our screening hit PRMT5. PRMT5 is a type II protein arginine methyltransferase catalyzing symmetrical dimethylation of arginines of histones and other proteins.[186] In addition, high PRMT5 expression was recently linked to worse survival of PDAC patients, which was the reason why we further investigated this screening top hit.[187,188] Analysis of mRNA expression datasets via GSEA gave first hints on PDAC with high expression of PRMT5 activating the MYC network.[189] To corroborate these findings on the protein level, we determined MYC and PRMT5 expression by western blotting in the human

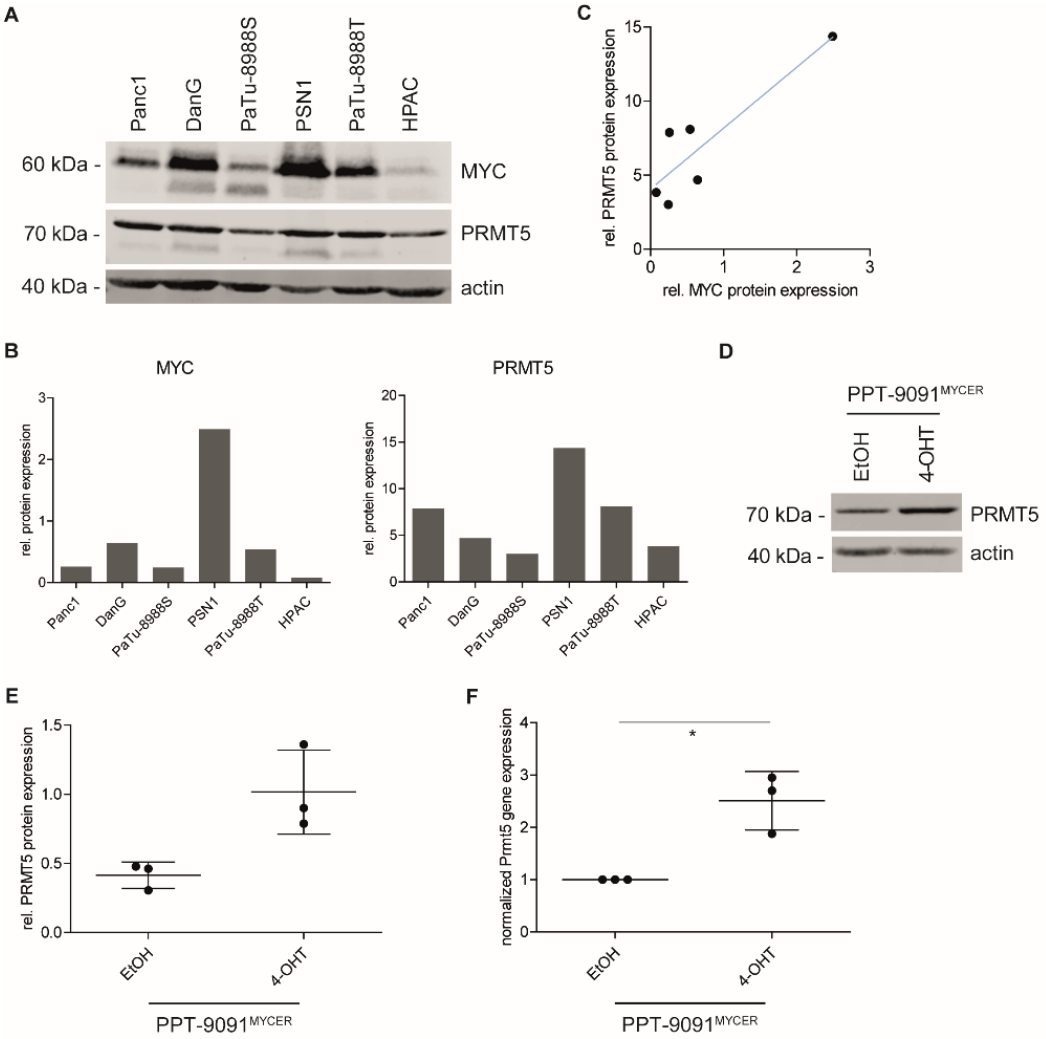

Fig. 11 Connection between MYC and PRMT5 in PDAC
A) MYC and PRMT5 protein expression of the six indicated human PDAC cell lines determined by western blotting. B-Actin (actin) served as a loading control. One representative experiment out of three is shown. **B)** Quantification of the western blot shown in A). **C)** Depicted is the linear regression (in blue) between MYC and PRMT5 protein expression assessed in A). The Pearson correlation coefficient is r = 0.88 with a p-value = 0.02. **D)** Western blot showing protein expression of PRMT5 and β-Actin (loading control) in murine PPT-9091 MYC-ER PDAC cells treated with 4-OHT (48h, 600nM) to activate MYC or EtOH as vehicle control. One representative experiment out of three is shown. **E)** Quantification of three independent experiments from D). p-value of a paired two-tailed t-test is 0.06. **F)** Quantification of *Prmt5* mRNA expression of murine PPT-9091 MYC-ER PDAC cells treated with 4-OHT (48h, 600nM) or EtOH (control) determined out of three biological replicates performed as technical triplicates by qPCR. *Gapdh* was used to normalize gene expression. Significant p-value of a paired two-tailed t-test is 0.02 (*).

PDAC cell lines used for the screen and observed a positive correlation (Fig.11A – 11C). To establish the direct link of MYC to PRMT5 cross species, we used our murine PDAC cell line with low endogenous MYC expression and MYC-ER expression vector transduction, PPT-9091 MYC-ER. In these cells, 4-OHT treatment induces MYC activity and simultaneously, PRMT5 expression at the protein (Fig.11D and 11E) and the mRNA level (Fig.11F). Together, these data argue for a robust and dynamic connection of MYC and PRMT5.

8. MYC controls Prmt5 inhibitor activity

To robustly validate the screening result, we used four MYC high (DanG, PSN1, PaTu-8988T, and HupT3) and four MYC low (Panc1, PaTu-8988S, HPAC, and Panc0504) PDAC cell lines and investigated the response to three different PRMT5 inhibitors: GSK591, GSK3326595, and JNJ-64619178.[190-192] We recapitulated the screen and found that for all PRMT5i, the dose-response curves were left-shifted and the mean AUC was significantly lower in MYC hyperactivated cell lines (Fig.12), further validating the screening hit.

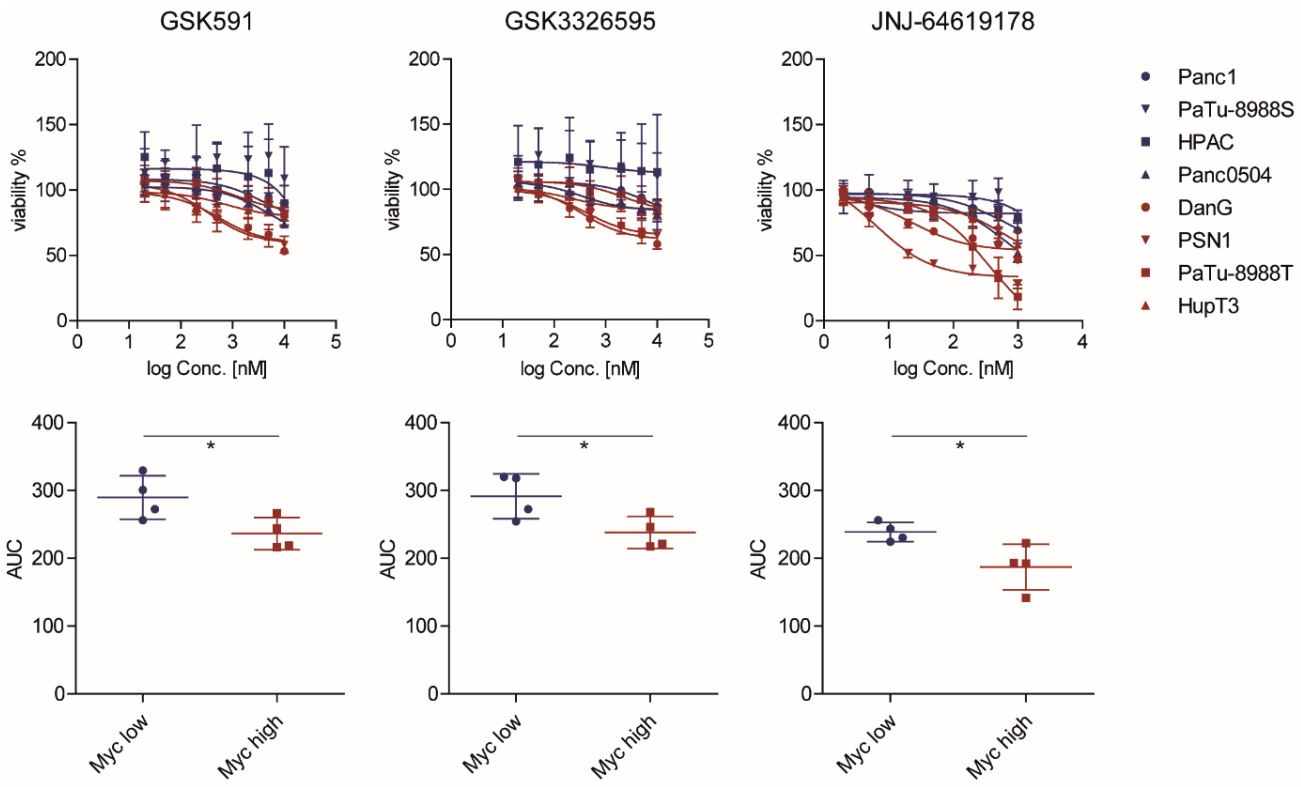

Fig. 12 Dose response of human PDAC lines with different MYC status to PRMT5 inhibitors
Viability for multi-dose treatment of MYC high (DanG, PSN1, PaTu-8988T, HupT3) and MYC low (Panc1, PaTu-8988S, HPAC, Panc0504) cell lines was measured by CTG assay. Cells were treated for 72h with the indicated compounds. All experiments were conducted in three independent biological replicates conducted as technical triplicates in a dosage range of 2nM – 10µM. The AUC in both groups is depicted for each drug. p-values of unpaired two-tailed t-tests are significant: p=0.04 (*), p=0.04 (*), and p=0.03 (*), respectively.

To assess this effect after long-term drug treatment, we repeated the validation for all three compounds and eight cell lines using a clonogenic growth assay in a larger well format to cope with the heterogenous growth rates of MYC hyperactivated cell lines (Fig.13). We quantified the assays and detected a significant impairment of growth in MYC hyperactivated lines compared to the four MYC low lines (Fig.14A and 14B). As drug responses can be heterogenous between tumors and to corroborate regulation of PRMT5i sensitivity by MYC, we tested the inhibitors in our described murine conditional overexpression model. MYC was activated in PPT-9091 MYC-ER cells via treatment with 4-OHT, which indeed shifted the dose-response curves of all three PRMT5 inhibitors to the left (Fig.15A). Consequently, clonogenic growth inhibition by PRMT5i was distinctly increased by MYC activation in this cell model (Fig.15B and 15C).

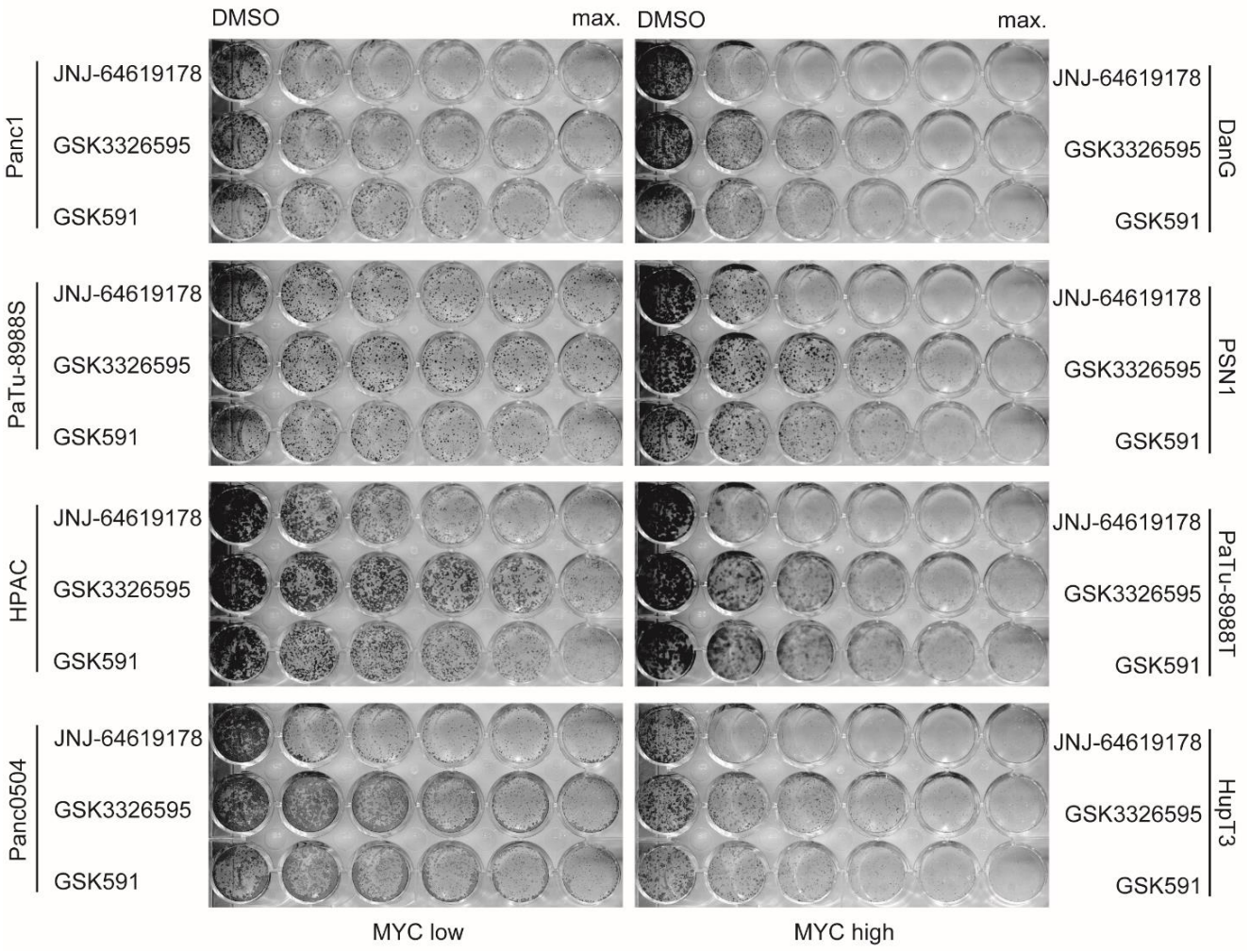

Fig. 13 Clonogenic growth assays of human PDAC lines with different MYC status treated with PRMT5 inhibitors

Clonogenic growth assays of eight depicted human PDAC cell lines treated for 7 days with indicated PRMT5 inhibitors. The drug concentrations used were a two-fold dilution from 1µM on for both GSK and from 100nM on for JNJ. One representative experiment out of three is shown. DMSO was used as vehicle control.

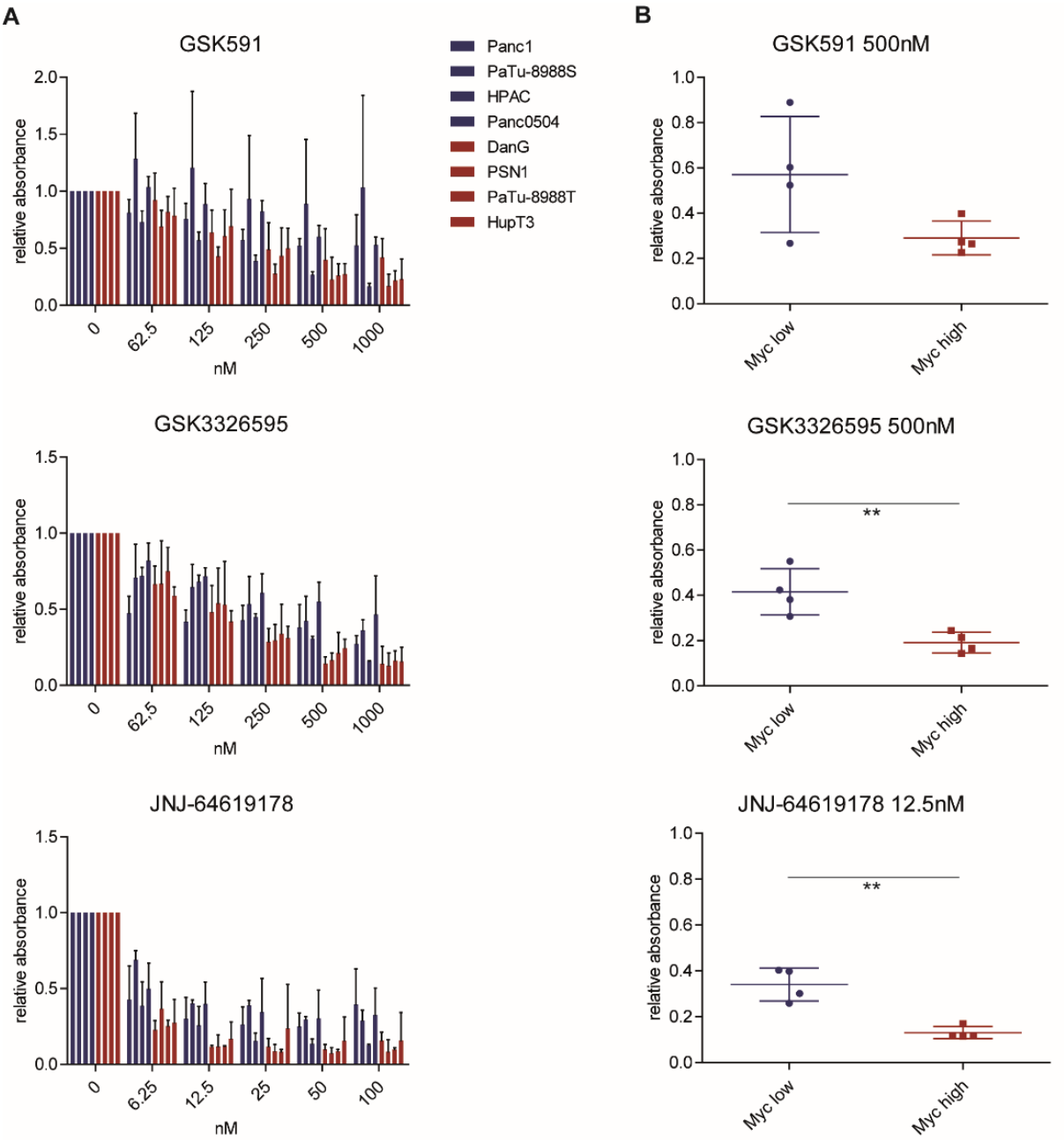

Fig. 14 Clonogenic growth in human PDAC lines with different MYC levels after treatment with PRMT5 inhibitors

A) Quantification of clonogenic growth assays of indicated cell lines (MYC low in blue, MYC high in red) with depicted PRMT5 inhibitors in depicted concentrations. Results were calculated from three independent biological replicates. **B)** Quantification of MYC high versus MYC low cell lines for the indicated concentrations, extracted from A). Values of unpaired two-tailed t-tests for GSK591, GSK3326595, and JNJ-64619178 are p=0.0809, p=0.007 (**), and p=0.0015 (**), respectively.

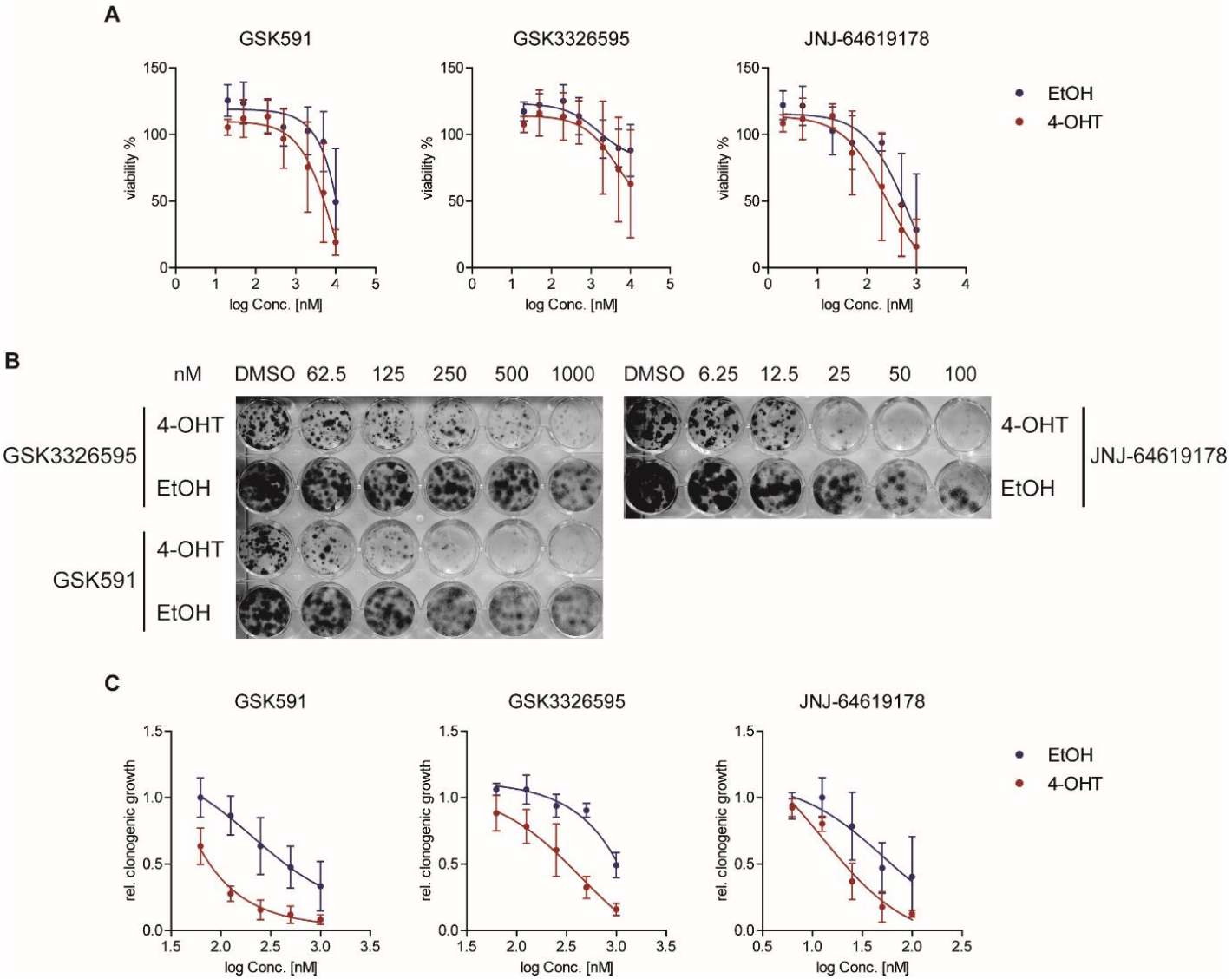

Fig. 15 Sensitivity for PRMT5 inhibitors in a murine model with MYC activation
A) Dose-response curves (max. concentration of 10µM for GSKs and 1µM for JNJ inhibitors) of PPT-9091 MYC-ER cells with (4-OHT, 600nM) or without (EtOH, control) MYC-ER activation after six day treatment with the indicated PRMT5 inhibitors measured by CTG assay in three independent biological replicates. **B)** Clonogenic growth assays of PPT-9091 MYC-ER cells with (4-OHT, 600nM) or without (EtOH, control) MYC-ER activation after seven days treatment with depicted PRMT5 inhibitors in the indicated concentrations with DMSO as control. One representative experiment out of three is depicted. **C)** Quantification of three independent biological replicates of the clonogenic growth assays as described in B).

9. PRMT5 inhibitors induce apoptosis in MYC hyperactivated PDAC cells

After confirming that PRMT5 inhibitors trigger a MYC-associated vulnerability, we worked on the underlying mechanism and selected the most efficient PRMT5i (JNJ-64619178) for further investigation. First, we analyzed growth curves of two MYC high and two MYC low human PDAC cell lines with different concentrations of PRMT5 inhibitor to specify the best time point to measure inhibitor effects. For three of four lines curves were spreading after day 3, so we decided to focus on this (Fig.16A). MYC high and MYC low cell lines both arrest in the G2/M-phase of the cell cycle after inhibitor treatment, whereas activity of executioner caspases 3/7 was connected to cells with deregulated MYC (Fig.16C and 16B). From day 3 on, JNJ-64619178 reduced distinctly the symmetrical di-methylation of histone H4R3 (Fig.17). Over a time course of five days, no significant regulation of PRMT5 and MYC expression was observed (Fig.17). It was demonstrated recently that the DNA-damage response can be induced by PRMT5 inhibition in PDAC cells.[193] Selecting an established marker for DNA-damage response, we assessed phosphorylation of H2AX. Although cells are responding to PRMT5 inhibition with phosphorylation of H2AX, it does not seem to be connected to the MYC level (Fig.17). However, induction of apoptosis, which was displayed by monitoring caspase-mediated cleavage of PARP, was again limited to MYC hyperactivated cell lines, further supporting the synthetic lethal interaction between MYC and PRMT5 (Fig.17). Overall, we could show with these data that the cellular response to PRMT5 inhibition is shifted towards apoptosis in PDAC cells with deregulated MYC expression.

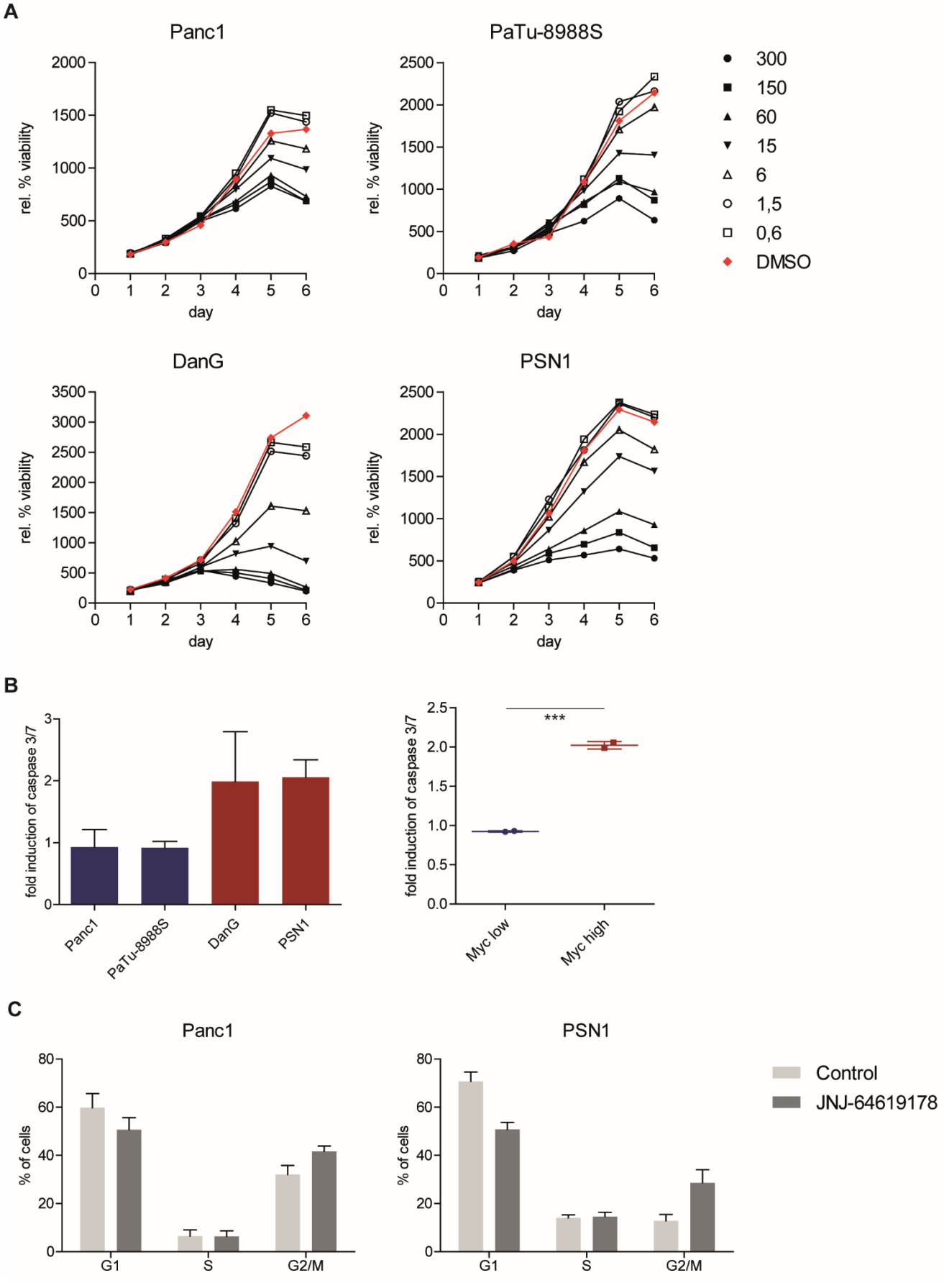
A
Panc1
PaTu-8988S
DanG
PSN1
rel. % viability
day
300
150
60
15
6
1,5
0,6
DMSO
B
fold induction of caspase 3/7
Panc1
PaTu-8988S
DanG
PSN1
***
Myc low
Myc high
C
Panc1
PSN1
% of cells
G1
S
G2/M
Control
JNJ-64619178

Fig. 16 Apoptosis and cell cycle measurement in PDAC cells after PRMT5 inhibitor treatment
A) Growth curves of depicted human PDAC cell lines (upper line MYC low, bottom line MYC high) measured by CTG assay each day after treatment with JNJ-64619178 in indicated concentrations in a 96-well format. DMSO control is shown in red. One biological replicate in technical triplicates was performed. **B)** Activity of caspases 3 and 7 determined by Caspase-Glo® 3/7 assay in three independent biological replicates in two MYC high (DanG, PSN1; red) and two MYC low (Panc1, PaTu-8988S; blue) cell lines after treatment with 40nM JNJ-64619178 for 3 days. p-value of an unpaired two-tailed t-test is p<0.001 (***). **C)** Quantification of cell cycle distribution of the indicated cell lines (Panc1 MYC low, PSN1 MYC high). Cell cycle distribution was determined by FACS of propidium iodide stained cells. Before, cells were treated with 20nM JNJ-64619178 or DMSO as vehicle control for four days. Results of three biological replicates are shown. p-value of a paired two-tailed t-test for the G2/M population is p=0.007 (**) for Panc1 and p=0.08 for PSN1, respectively.

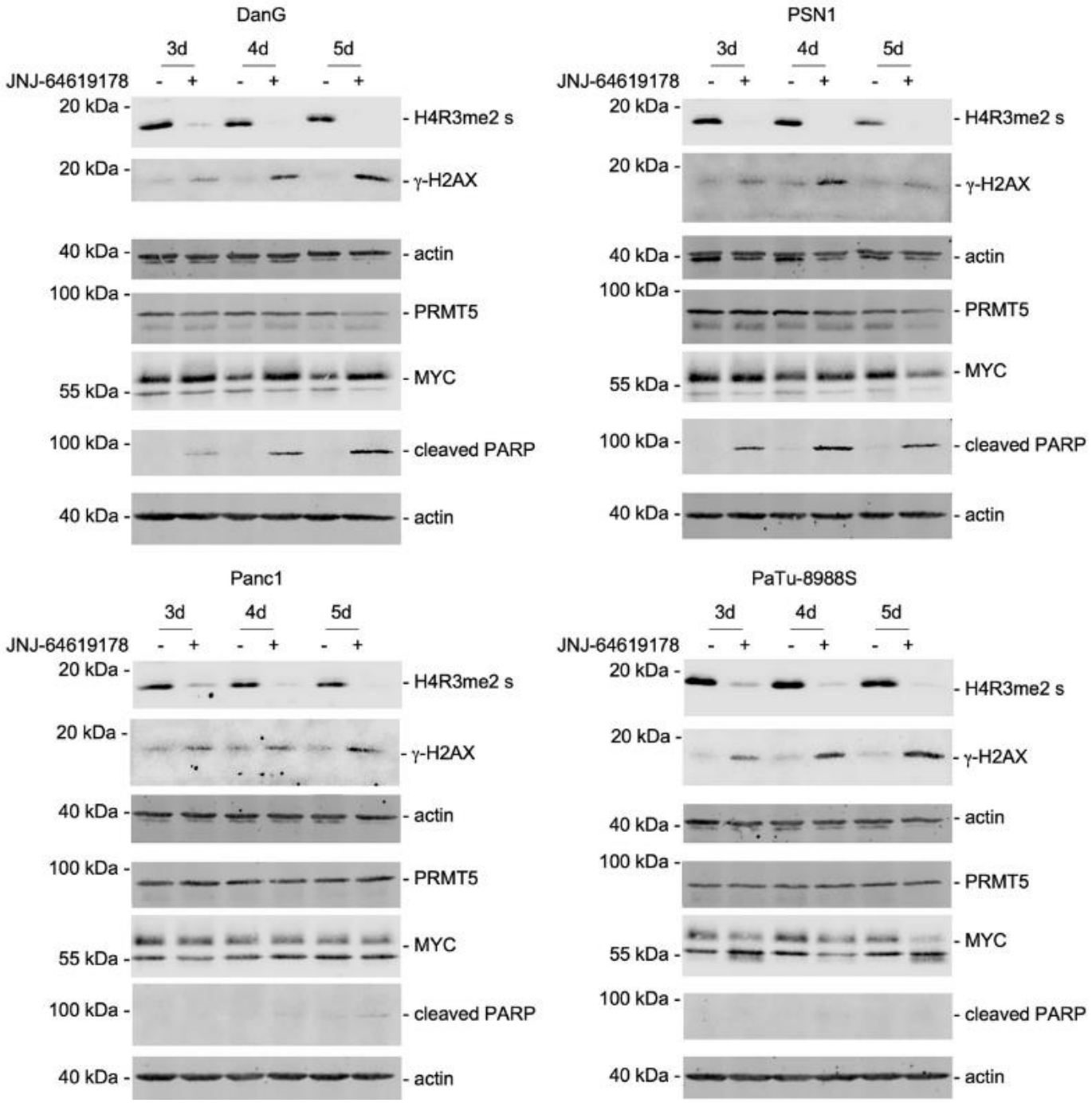

Fig. 17 Protein expression of human PDAC cell lines after PRMT5 inhibition
Western blot analysis of indicated proteins in two MYC high (DanG, PSN1) and two MYC low (Panc1, PaTu-8988S) cell lines with and without 20nM JNJ-64619178 treatment after indicated time points. B-Actin (actin) served as a loading control, DMSO was used as control treatment. One representative experiment out of three biological replicates is depicted.

10. No synergistic effects could be detected with PRMT5i

To define potential synergistic interactions between PRMT5 inhibition and inhibition of other pathways in MYC deregulated cell lines, we screened MYC-amplified PSN1 cells using JNJ-64619178 and various inhibitors in a concentration matrix in clonogenic assays. Concentrations of the test partners have been chosen according to the expected dose range of these inhibitors and were adapted if required. After quantification of one biological replicate per drug combination, we applied the SynergyFinder software tool to calculate the Zero Interaction Potency (ZIP) score indicating synergy.[194] Unexpectedly, the overall ZIP score was lower than 10 for all tested inhibitors, showing no synergism with JNJ-64619178 in PSN1 cells (Tab.1). A further screening in additional cell lines with a change in experimental setup was out of scope for this project.

Tab. 2 ZIP scores of various inhibitors with PRMT5i
MYC-amplified PSN1 cells were tested with JNJ-64619178 and the listed inhibitors using an adapted concentration matrix in clonogenic assays. Screen was performed in one biological replicate. Assays were quantified and ZIP scores were calculated using SynergyFinder software.

Drug combined with JNJ-64619178	**ZIP-Score (overall)**	**ZIP-Score (most synergistic area)**
Proteasome inhibitor (Bortezomib)	4,17	6,11
mTAPi (MT-DADMe-ImmA)	3,07	3,26
HDACi (Panobinostat)	-10,18	0,48
HDACi (SAHA)	-0,45	2,8
SUMOi (ML-93)	4,25	8,18
UAEi (TAK243)	4,6	6,83
Chemotherapy (Gemcitabine)	-2,93	-1,44
Chemotherapy (SN-38)	4,41	8,03
Chemotherapy (5-FU)	-4,17	-0,35
Chemotherapy (Taxol)	1,58	2,24
TORC1/2i (INK-128)	-4,12	0,85
Chk1i (AZD7762)	-4,49	-0,81
DOT1Li (EPZ004777)	1,28	3,2
Mcl-1i (S63845)	-1,58	1,16
RAD51i (RI-1)	6,76	9,37
PARPi (Veliparib)	6,8	10,52
Bcl-xL/Bcl-2i (Navitoclax)	6,27	11,31

11. Effect intensity of PRMT5i synthetic lethality depends on the cell model

Finally, in addition to established human PDAC cell lines, we aimed to verify the MYC-associated PRMT5i-induced vulnerability in primary human PDAC cell lines. We characterized huPDAC7, huPDAC17 and huPDAC3 regarding their MYC and PRMT5 protein status (Fig.18A and 18B), defining huPDAC7 as MYC high and huPDAC3 as MYC low. Results for huPDAC17 were inconsistent across three replicates, but tended to low MYC levels. Treatment of these cell lines with three PRMT5 inhibitors could not show a significantly reduced viability in the dose-response of huPDAC7 compared to the other two lines, which was thus not recapitulating our previous findings (Fig.18C).

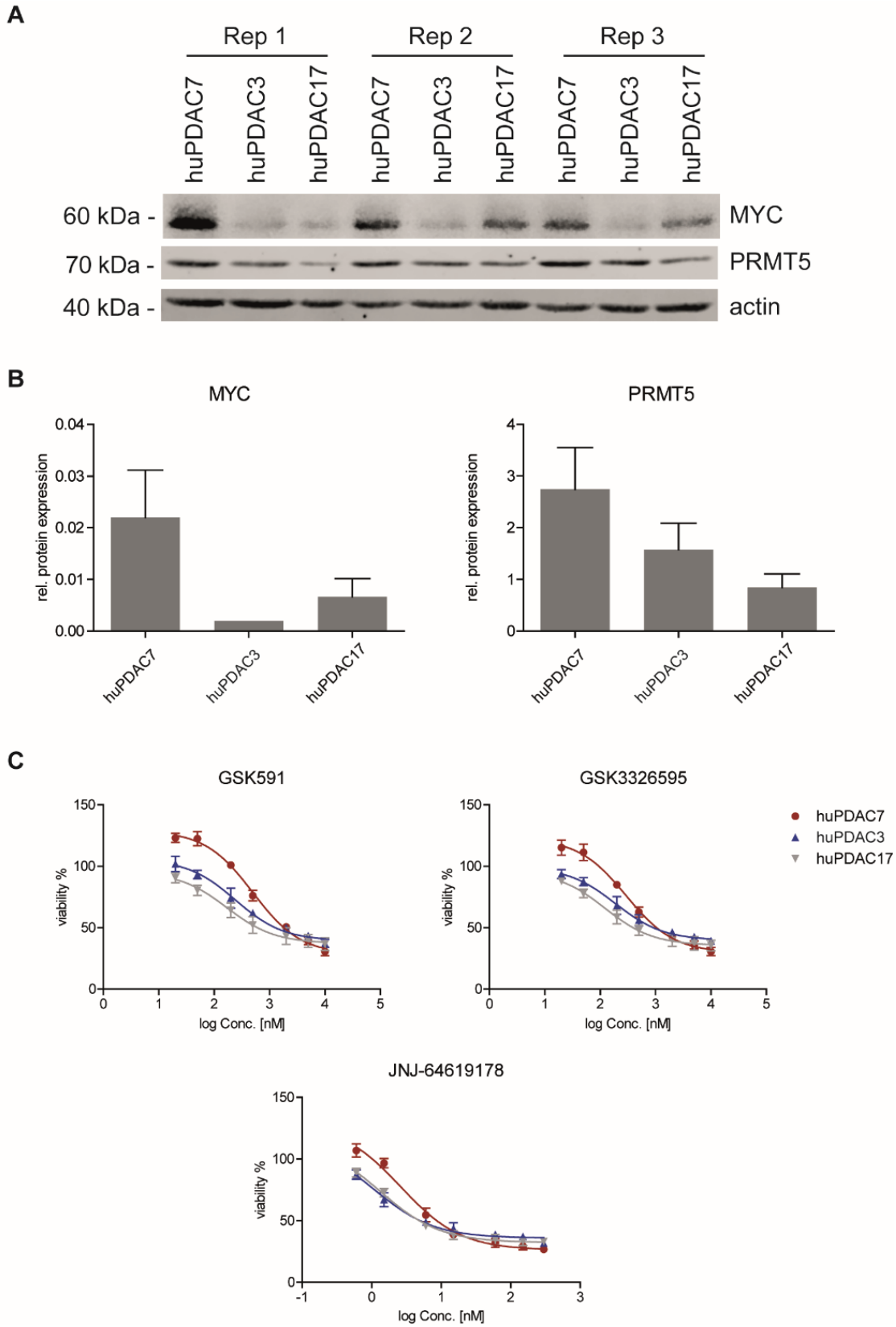

Fig. 18 PRMT5 inhibition in primary human PDAC cell lines

A) Western blot analysis of MYC and PRMT5 protein expression in indicated primary human PDAC cell lines. Three replicates are shown and β-Actin (actin) was used as a housekeeping protein. **B)** Quantification of all three replicates shown in A. **C)** Viability for multi-dose treatment of primary human PDAC cell lines was measured by CTG assay. Cells were treated for six days with the indicated compounds (PRMT5i). All experiments were conducted in three independent biological replicates conducted as technical triplicates in a dosage range of 0.6nM – 10µM.

VIII. Discussion

1. Proteasome inhibition as synthetic lethality with MYC in PDAC

The therapy of PDAC still remains a major challenge due to late diagnosis, early metastasis, and unsatisfying therapeutic options, which are mainly complicated by tumor heterogeneity, incomplete understanding of cellular mechanisms, upcoming resistance to treatment and a lack of patient stratification. A particularly aggressive subtype of PDAC is characterized by overexpression of the oncogene MYC, which seems to be sufficient to induce tumorigenesis in mice.[44,45,60] Targeting MYC-associated vulnerabilities in these cancers can enable new therapeutic strategies for this subgroup of patients.[129,130,157] To determine such vulnerabilities, we first conducted a limited unbiased drug screen using a FDA-approved drug library on PDAC cell lines. The eleven top hit drugs covered interferences with DNA metabolism, folate metabolism, topoisomerase I and II, transcription, HDACs, and the proteasome. Almost all of these pathways are also found to be linked to MYC in the DoRothEA database, which couples the activity of transcription factors to sensitivity to 265 drugs in 1,000 cell lines.[182] In fact, MYC has the highest number of transcription factor – drug interactions analyzed in that database, with all of them being sensitizing.[182] In addition, our data are supported by already published results for some of the top hits in other tumor entities. N-MYC-amplified neuroblastoma cells are more sensitive to Topotecan treatment than N-MYC negative cells.[195] And in medulloblastoma, where MYC amplification also correlates with poor survival rates, inhibition of HDACs, in this case HDAC2, is more effective in this subtype.[196] A correlation between MYC and HDAC inhibition is also described for acute myeloid leukemia (AML).[197] Another significant overlap of pathways with ours can be found in the similar screening approach of Frenzel et al. using among others neuroblastoma and Burkitt's lymphoma B cell lines with conditional MYC overexpression; a proteasome inhibitor was also detected therein to be more sensitive in MYC high cells.[154] Finally, a high-throughput screen using 938 FDA-approved drugs in MYC-driven neuroblastoma cells documented SL interactions with Pralatrexate, Gemcitabine, Carfilzomib, Bortezomib, and others, exactly matching our findings.[198] This shows that our screening approach is valid to investigate synthetic lethality and that these MYC-associated vulnerabilities are conserved across cancer entities and the MYC protein family. However, it is important to note, that there are also cases where MYC is associated with drug resistance in PDAC. It has been demonstrated by Farrell et al. that MYC is involved in a ductal-neuroendocrine lineage switch generating a Gemcitabine-resistant neuroendocrine lineage.[199] Similarly, in Paclitaxel-resistant primary PDAC cell culture a persisting induction of MYC has been discovered.[200] In these cell cultures the anti-apoptotic BCL-2 family member MCL-1 is

co-upregulated with MYC, which fits to the described role of BCL-2 family proteins as relevant modulators of MYC-triggered mitotic vulnerabilities.[161,200] Further analysis is needed to assess if BCL-2 family proteins determine MYC-mediated sensitivity or resistance in PDAC.

The previously described connection of MYC with the UPR and its mechanistic involvement in Bortezomib-induced cell death rendered our hit in disruption of proteostasis particularly interesting.[183] It is known that targeting protein homeostasis in PDAC leads to UPR induction and cell death.[201] A discovered subtype expressing cornified/squamous related genes was found to be sensitive to the proteasome inhibitor Carfilzomib and even if no relation to MYC has been described here, the observations are in line with our results.[202] MYC is mainly responsible for the accumulation of biomass in rapidly dividing cancer cells beyond KRAS dependency, thus in MYC high cells the protein folding capacity can be exceeded and the UPR has to protect them from cell death.[203] We were also able to show this by connecting MYC activity to UPR signatures in PDAC data sets and conditional MYC expression models.[175] Tumor cells have been reported to use an adapted ER-stress-induced survival pathway, but they are obviously less tolerant to any additional protein load.[204] Another observation fitting to this model is that human PDAC cell lines sensitive to the Valosin-containing protein (VCP) / p97 inhibitor NMS-873, which triggers the UPR, enrich for MYC signatures.[205,206] Although it needs further clinical validation in PDAC, available data for multiple myeloma underlines the importance of proteasome inhibitor treatment for advances in survival time of MYC-driven cancer subtype patients.[207,208] However, interference with proteostasis usually leads to variable results. The induction of the UPR can of course be MYC-independent as well involving additional pathways. For example, the 78-kDa glucose regulated protein (GRP78) / PERK / Nuclear factor erythroid 2-related factor 2 (NRF2) axis keeps low levels of cellular reactive oxygen species (ROS) and prevents them from causing apoptosis via the UPR.[209] In PDAC, NRF2 is associated with cap-dependent mRNA translation and thus supports tumor maintenance.[210] If there is a connection of the ROS-NRF2 pathway to proteasome inhibitor sensitivity remains unclear. Other factors that could play a role are the aneuploidy of cancer cells, the mutational status of the tumor suppressor p53, Epidermal growth factor receptor (EGFR) signaling, and Nuclear factor 'kappa-light-chain-enhancer' of activated B-cells (NFκB) signaling regulating anti-apoptotic proteins like X-linked inhibitor of apoptosis protein (XIAP) or BCL-2, just to mention a few.[211-215] These may be some reasons why xenograft in vivo models or PDX react controversially to proteasome inhibition, in one case being sensitive only with MYC amplification.[162,213,216,217] This lacking knowledge about mechanisms even beyond MYC-hyperactivation and a lack of patient stratification may have led to the negative outcome of a phase II PDAC trial using Bortezomib or the combination of Bortezomib and Gemcitabine.[218] Other drawbacks of proteasome inhibitor treatment may exist due to inherent characteristics of Bortezomib. Bortezomib is a dipeptide boronic acid derivate first synthesized in 1995 and

inhibiting the 26S proteasome reversibly (reviewed by Chen et al. 2011).[219] The 26S proteasome, responsible for degradation of unfolded proteins, is a multi-subunit protease located in the nucleus and cytosol. It contains two regulatory 19S subunits, which are responsible for recognition, deubiquitination, unfolding, and entry of target proteins.[219,220] The 20S proteasome unit is a cylindrical structure and the catalytic core of the proteasome, again consisting of further subunits. Among them, the α-subunits control the access of only unfolded proteins and the β-subunits are responsible for the proteolytic activities.[219] The boronic acid group of Bortezomib is able to bind to and build a complex with the active site of the threonine hydroxylation group in the β5 subunit.[219] Thereby, it inhibits its chymotrypsin-like activity and thus the induction of cell death.[219,221] Apoptosis caused by Bortezomib has been shown to be p53-independent and mediated by the pro-apoptotic protein NOXA for example in melanoma and myeloma.[222] Especially in several tumor cells, NOXA seems to be regulated directly by the transcription factor MYC mediating apoptosis upon proteasome inhibition.[198,223] MYC binding sites were identified at the NOXA promoter and the pathway seems independent of p53, Hypoxia-inducible factor 1-alpha (HIF-1α) and E2F transcription factor 1 (E2F-1).[223] Also in PDAC cell lines, Bortezomib causes apoptosis via activation of the Bcl-2 family members NOXA and BIM and increases MYC protein levels.[183] MYC binds to the promoters of these proteins dependent on the zinc-finger transcription factor Early growth response 1 (EGR1) and enhances transcription. And again, cell death occurs independently of p53 or ARF.[183] Bortezomib was the first proteasome inhibitor approved by the FDA for treatment of multiple myeloma.[224] The results which led to this accelerated approval were striking. Preclinically, Bortezomib induced growth inhibition and apoptosis in multiple myeloma and was also effective and well-tolerated in a murine model of Burkitt's lymphoma.[225,226] The same effects could be detected in models of PDAC, in addition to a sensitization to chemotherapeutics.[227,228] In phase I clinical trials an acceptable toxicity and clinical benefit in hematologic malignancies could be demonstrated, leading to phase II clinical trials in these entities.[229-231] However, in phase I clinical trials for solid tumors the success of Bortezomib was only moderate.[232,233] The problems were mainly the toxic side effects indicating a very narrow therapeutic range of Bortezomib, only minimal effects alone and also in combination not superior to current standard therapies, and upcoming resistance. For hematologic malignancies phase III clinical trials tested management and profile of possible adverse events and combination therapies and finally led to FDA-approval.[234,235] Bortezomib treatment has so far shown clear benefits in lymphoma and myeloma, even beyond its high efficacy. These cancer cells are far more dependent on elevated proteasome activity than normal cells, which renders Bortezomib highly selective.[225,236] It has several ways to exert its function, as mentioned via the UPR, NOXA-dependent apoptosis or also angiogenesis.[237,238] And it can sensitize several tumor cells to radiation or different chemotherapeutics like Gemcitabine.[225,227,228,239] In solid tumor entities like

renal cell carcinoma or non-small cell lung cancer (NSCLC) the results remained unsatisfying.[240,241] In addition to the aforementioned narrow therapeutic window, which may exist partly due to delivery problems of Bortezomib in the human body, resistance mechanisms, inhibition of Bortezomib by natural substances like ascorbic acid or flavonoids, and the reversibility of proteasome inhibition are probably responsible for the failures.[230,231,242,243] One strategy to solve this in the following was to develop novel proteasome inhibitors.[244] Carfilzomib has been approved in 2012 for multiple myeloma and works in an irreversible manner.[245] Second generation Oprozomib is structurally related to Carfilzomib, but orally bioavailable in addition and studied in multiple myeloma too.[246] Ixazomib is an oral and reversible proteasome inhibitor approved 2015 for multiple myeloma.[247] Another irreversible proteasome inhibitor is Marizomib, a natural marine bacteria-derived compound.[248] It is also being investigated in multiple myeloma, has been tested in a phase I combinatorial trial together with the HDAC inhibitor Vorinostat and is currently under investigation in a phase III clinical study for glioblastoma.[249,250] In the phase I trial, the combination had a strong synergistic antitumor activity with tolerable toxicity resulting in disease stability in 61% of the patients.[250] Other strategies are to improve Bortezomib formulations to overcome the pharmacokinetic problems and to use synergistic combinations with Bortezomib, for instance also HDAC inhibition.[251,252] Treatment with Bortezomib and SAHA seems to trigger the same MYC- and NOXA-dependent apoptotic cell death in multiple myeloma like single treatment, but could lower the necessary doses in the clinic.[252] And of course still other strategies targeting the UPS are investigated. As the UAE inhibitor TAK-243 works in concert with MYC overexpression to induce UPR and cell death in DLBCL, we tested this compound in four of our human PDAC screening cell lines as well.[170] Interestingly, we saw the opposite effect in our cell lines: MYC high cells were less sensitive than MYC low cells. Even if the number of cell lines should be increased to consolidate this effect in PDAC, a possible explanation could be an ubiquitination-independent way to degrade MYC via the proteasome. Bortezomib is working through a direct block of the proteasome, the last step in the degradation chain without a possible circumvention, whereas TAK-243 is inhibiting the first step in ubiquitination. Given the fact that for example the polyamine regulatory protein antizyme 2 has been shown already to interact with MYC and the MYC-target ODC, and accelerate their proteasomal degradation without ubiquitination, there are scenarios in which UAE inhibition is not enough to pass the threshold to apoptotic cell death due to MYC accumulation.[253,254] Proliferation and cell growth induced by a high MYC level may then lead to what we observed in our cell lines.

In sum, we show very strong hints that a MYC-driven subtype of PDAC is already primed-for-death and thus susceptible to a synthetic lethal interaction with proteasome inhibitors triggering

the UPR and apoptotic pathways. Advances of this concept in the future may help to identify subgroups of patients who will benefit from next generation proteostasis interference.

2. Targeting a synthetic lethal interaction between MYC and PRMT5 in PDAC

In the second part of the unbiased screening approach epigenetic compounds were tested for SL interactions with MYC overexpression in PDAC. In concordance with the FDA-approved drug screening results, we determined HDAC inhibitors and the chemotherapeutics Mitomycin and again Gemcitabine as top hits, indicating the robustness of our screening efforts.[189] Efficacy of Mitomycin and Gemcitabine is also connected to MYC in the DoRothEA database.[182] One particularly interesting top hit was PRMT5, a protein arginine methyltransferase. Only in the last few years much has been learned about the dysregulation of PRMT5 in several cancer types, its prognostic value and "druggability", which are some of the reasons for focusing on this candidate.[255,256] The methylation of arginine residues was already described in 1968.[257] However, the first member of the protein arginine methyltransferase family exerting this function, PRMT1, was only identified in 1996, followed by the others.[258,259] Nowadays, the PRMTs are assigned to groups termed type I, II and III. Type I are PRMT1, 2, 3, 6, 8 and Coactivator-associated arginine methyltransferase 1 (CARM1), also called PRMT4, type II are PRMT5, 9, and type III is PRMT7. All groups are able to monomethylate arginines, type I additionally asymmetrically dimethylate arginines and type II symmetrically dimethylate arginines. The primary type II PRMT is PRMT5, lately being known to play a crucial role in cancer.[186,259,260] It was discovered as a 72-kDa pICln binding protein (IBP72) and JAK-binding protein 1 (JBP1) and later identified as the mammalian protein arginine N-methyltransferase.[261-263] Interestingly, the Janus kinase 2 (JAK2) inhibitor XL019 was also identified as a hit in our epigenetic screen, probably targeting similar pathways compared to PRMT5 inhibition. PRMT5 possesses a N-terminal Triose-phosphate isomerase (TIM) barrel structure, which is responsible for building an octameric complex with its obligate partner Methylosome protein 50 (MEP50), and a C-terminal catalytic structure consisting of the Rossam fold domain, which is binding the co-factor and methyl donor S-adenosyl methionine (SAM), and the β-barrel domain binding the substrate.[264] The embryonic knockout of PRMT5 in mice is lethal, showing an important role in development as well, and it is a key regulator of alternative splicing impacting on the p53 pathway.[265,266] Arginine methylation is involved in stem cell activity, development, neurodegeneration and tumorigenesis, the latter specifically due to control of translation, growth factor signaling, tumor immunity, RNA splicing, DNA damage response and gene expression via methylation of, for instance, histone tails.[186,260] PRMT5 catalyzes the methylation of four arginines in histone tails: H4R3, H2AR3,

H3R8, and H3R2.[259,262,263] H4R3me2s and H3R8me2s usually cause transcriptional repression, which is particularly important in oncogenesis. PRMT5, together with PRMT1 and CARM1, is most highly expressed in cancer and correlates with tumor progression and a worse prognosis in different entities like lung cancer or multiple myeloma (MM).[259,267,268] In hepatocellular carcinoma (HCC), high expression of PRMT5 results in a poorer overall survival in patients too and appears to act via β-catenin.[269] PRMT1 was identified as potential therapeutic target in PDAC in recently published work.[270] But whenever PRMT1 inhibitors were used in combination with chemotherapeutics, like gemcitabine, the need for stratification into responders and non-responders was clearly demonstrated by the results.[271] Interestingly, in colorectal cancer (CRC) PRMT5 has been discovered to inversely correlate with survival and to be a potential SL target with KRAS mutation.[272] Thus, underlying mechanisms can vary between tumor types and many of them remain unclear so far. It has also been described that inhibition of PRMT5 synergizes with inhibition of type I PRMTs to inhibit oncogenic growth, as does the genetic loss of 5-methylthioadenosine phosphorylase (MTAP).[273] Endogenous regulation of PRMT5 happens mainly through transcriptional activation, microRNAs, the UPS, post-translational modifications, protein-protein-interactions, and the endogenous inhibitor 5-methylthioadenosine (MTA).[259] In PDAC, PRMT5 has been linked to epithelial-mesenchymal-transition (EMT) and glycolysis, both hallmarks of more aggressive subtypes.[187,188] Consistently, a PDAC subtype sensitive to PRMT5 inhibition has been identified in organoid pharmacotyping and own group data of patient-derived 3D models.[189,274] Part of this sensitivity can be explained by the aforementioned deletion of MTAP in the methionine salvage pathway, which occurs frequently in PDAC as co-deletion with CDKN2A and leads to accumulation of MTA.[275,276] The same network is involved in PRMT1i sensitivity.[273,277,278] In MTAP-deficient organoids its restoration decreases PRMT5i sensitivity and presence of higher amount of MTA correlates with increased PRMT5i activity.[274] But truth is also that 40% of the PRMT5i sensitive organoids in this study were MTAP-proficient and thus need to feature another factor that determines responsivity. Mutations in splicing factors, other addictions to the splicing machinery, mutations of the tumor suppressor p53 conveying resistance, the Chloride nucleotide-sensitive channel 1A (CLNS1A) / RIO kinase 1 (RIOK1) expression ratio, and also expression of MYC have been detected to determine PRMT5i sensitivity in different tumor entities, suggesting a tumor or tumor subtype specific connection.[191,277,279,280] In chronic lymphatic leukemia and mantle cell lymphoma, MYC expression seems to be connected to PRMT5i resistance.[281] In medulloblastoma, MYC expression sensitizes the cancer cells to inhibition of PRMT5, consistent with our research in PDAC.[282] In addition, Chaturvedi et al. found PRMT5 and MYC to be co-overexpressed in a subtype of medulloblastoma, which inversely correlated with patient survival, and could prove a direct protein-protein-interaction between them. Furthermore, they showed that the small molecule PRMT5 inhibitor

EPZ015666 is especially effective in MYC-amplified cancer cells.[282] The only difference from our study is that they detected a change in MYC and PRMT5 levels after inhibitor treatment, which we did not.[189] The exact same mechanism can be found in neuroblastoma, where 50% of tumors with poor prognosis have amplified and overexpressed N-MYC. SiRNA depletion of PRMT5 in these cell lines resulted in impaired tumor growth and apoptosis compared to N-MYC negative cells and again, PRMT5 expression strongly correlated with N-MYC expression.[283] A third example in this row is glioblastoma multiforme (GBM), featuring deregulated MYC-activity as well. Here, MYC had first been shown to associate with PRMT5 and thus stimulate symmetric dimethylation of histone H4R3.[284] In a follow-up on that topic, Favia et al. showed that MYC is dimethylated symmetrically by PRMT5 and asymmetrically by PRMT1 in GBM regulating not only stability of MYC but also properties of GBM stem cells depending on the ratio between symmetrical and asymmetrical dimethylation.[285] Recently, as well in gastric cancer PRMT5 was documented to bind directly to MYC working together in repressing MYC target genes and promoting cancer cell growth.[286] Again, expression levels of both proteins were upregulated in the tumor and correlated with a worse clinical outcome.[286] Although evidence is quite clear that PRMT5 and MYC work in concert in many cancer types, sometimes the direction cannot be assessed without doubts. In our analysis for example we used the high MYC expressing cell line PaTu-8988T, which showed sensitivity for PRMT5i in our clonogenic growth assay and a significant loss of fitness upon genetic Prmt5 inhibition elsewhere.[189,287] To the contrary, it has also been identified as the most GSK3203591 resistant cell line out of 20 PDAC lines.[191] This demonstrates that not only different cancer types are responsible for varying results regarding MYC-PRMT5-connection, but maybe also the applied assays. Not solely in PDAC, the interplay between MYC and PRMT5 is detectable on several levels. We could see an induction of PRMT5 upon upregulation of MYC activity in our models and PDACs with high PRMT5 expression enrich for MYC signatures.[189] The Eμ-Myc lymphoma model pointed out that Prmt5 is a direct MYC target and genetic inactivation of PRMT5 in this model induced B cell death more than in wild-type B cells.[280] Vice versa, MYC can be dimethylated by PRMT5 directly at different arginine residues as mentioned earlier for GBM, and thus its stability can be regulated post-translationally.[285] Furthermore, PRMT5 methylates Heterogeneous nuclear ribonucleoprotein A1 (hnRNPA1), an Internal ribosome entry site (IRES)-transacting factor regulating IRES-dependent translation of MYC.[288] And in an aggressive B cell lymphoma type PRMT5 has been shown to repress tumor suppressor miRNAs which down-regulate MYC expression.[289] In sum, MYC deregulated cancer cells seem to depend on PRMT5 and this vulnerability could be therapeutically useful.[290] However, crucial for this aim is a deeper understanding of the cellular mechanisms involved. We saw in our experiments that predominantly MYC high cells underwent apoptosis upon PRMT5 inhibition, even though all cell lines seemed to suffer from increased DNA damage and genetic

instability.[189] One aspect is the involvement of PRMT5 in the splicing machinery, which is particularly important for oncogenesis.[279] PRMT5 methylates proteins that are necessary for mRNA splicing and thus maintains splicing fidelity.[266,277,279,291] In a MYC-driven cancer setting, the total RNA amount is increased, which renders the task of PRMT5 even more important.[280,290] An unbiased genetic screen with human mammary epithelial cells revealed Bud morphology abnormal gene homolog 31 (BUD31), a component of the spliceosome, to be SL with MYC.[155] And blocking the spliceosome led to intron retention and subsequent cell death in MYC-driven breast cancer.[292] This fits as well into the greater picture of splicing being one huge vulnerability in MYC hyperactivated tumor cells as the work of Salvador et al.[293] They treated MYC high breast cancer cells with a Cell division cycle protein 2 homolog (CDC2)-like kinase inhibitor and by doing so induced alternative splicing and cell death.[293] In the same direction hints the fact that ARK5, which is known to promote spliceosome activity, also constitutes a dependency for MYC deregulated cells.[159,294] Another significant aspect to maintain genetic stability is the DNA damage response. PRMT5 also ensures correct splicing of DNA damage repair genes, which has been shown in hematopoietic stem cells but is true for multiple cell types.[295] The inhibition or knockout of PRMT5 caused oxidative DNA damage and resulted in p53-induced apoptosis in this work.[295] It has also been detected that the alternative splicing of histone-modifying enzymes triggered by PRMT5 guarantees DNA damage repair.[296] Additionally, Tyrosyl-DNA phosphodiesterase 1 (TDP1), involved in the repair of replication-coupled camptothecin-induced DNA damage, is methylated by PRMT5.[297] A context potentially independent of the methylation activity of PRMT5 with MEP50 is that the transcription of double strand break (DSB) repair genes upon DNA damage can be activated by PRMT5 in cooperation with pICln, which is rather uncommon.[298] Targeting PRMT5 sensitized several cancer types to radiation and the expression of PRMT5 correlated positively with DSB repair gene products like Radiation sensitive 51 (RAD51).[298] DSB can be repaired either by homologous recombination (HR) or by non-homologous end joining (NHEJ). In addition to the already mentioned study, also others have shown that depletion or inhibition of PRMT5 impairs HR, which leads to accumulation of DNA damage, activation of p53, cell cycle arrest and finally cell death.[296] Furthermore, PRMT5 methylates RuvB-like 1 (RUVBL1), a regulator of DSB HR repair.[299] Fitting to the role of PRMT5, its SL partner MYC is known to enhance DSB and genetic instability. One mechanism behind this is that MYC inhibits the binding of Ku70 to the DNA and DNA end joining, which is necessary for V(D)J recombination and NHEJ repair.[300] Thus, the combination of MYC overexpression and PRMT5 inhibition may lead to accumulation of DSB, reduced ability for repair, and impaired splicing fidelity resulting in pronounced genetic instability and apoptosis in PDAC cells.

To see if this effect could be enhanced even, we tried to scan for synergism with PRMT5 inhibition. Some have been reported in other models so far, like a synergistic effect with

Disruptor of telomeric silencing 1 like (DOT1L) inhibition in Mixed-lineage leukemia (MLL)-rearranged leukemia.[301] In PDAC cells, a recent publication described a synergism between PRMT5i and Gemcitabine using a targeted CRISPR screen in a PDX model.[193] The cytotoxicity was again based on depleted Replication protein A (RPA) levels and impaired NHEJ repair.[193] None of them investigated the level of MYC expression in the context of these synergies, which may be an explanation for no detectable synergistic effects in our work. We used PSN1, a MYC-amplified cell line, in a clonogenic growth assay to screen for PRMT5i synergy. Maybe the SL between MYC overexpression and PRMT5i covers other possible mechanisms and thus excludes the more aggressive phenotype of PDAC from synergistic drug combinations. Additionally, the aforementioned bias using different assays can play a role here. Extensive preclinical research is of course still required for the molecular understanding of all these mechanisms.

A major advantage of PRMT5 as a SL partner with the “undruggable” MYC is that a bundle of PRMT5 inhibitors has already been developed. Some of them are currently being investigated in the clinic, such as the ones used in our studies: GSK591, GSK3326595, and JNJ-64619178.[190-192] The inhibitors from GSK work in a SAM-uncompetitive way targeting the peptide binding site of PRMT5, whereas JNJ-64619178 is SAM-competitive and targets the SAM- and substrate binding domain. In patient-derived xenotransplant models of hematologic malignancies and solid cancers, including PDAC, in vivo efficacy of JNJ-64619178 was reported recently.[302] Currently, four clinical trials investigating PRMT5 inhibitors are ongoing: A phase 1 study with JNJ-64619178 in patients with advanced solid tumor or Non-Hodgkin lymphoma (NHL), a phase 1 study with GSK3326595 also in solid tumor or NHL patients alone or combined with Pembrolizumab, a phase 1/2 study with GSK3326595 in patients with myelodysplastic syndrome or AML alone or combined with 5-azacytidine, and a phase 1 trial with another SAM-competitive inhibitor, PF-06939999, in patients with advanced or metastatic solid tumors alone or combined with Docetaxel.[303] Furthermore, new potent and selective PRMT5 inhibitors are continuously under development.[304,305] In sum, PRMT5 seems a reachable therapeutic target in PDAC and high expression of it marks cancers with deregulated MYC. Thus, a real clinical benefit from our knowledge comes within reach.

In conclusion, we showed in our work on the proteasome inhibitor Bortezomib and PRMT5 inhibition two possibilities to target synthetic lethal vulnerabilities in MYC-driven pancreatic cancer, improving the outlooks for patients suffering from a particularly aggressive subtype of this tumor type (Fig.19).[175,189]

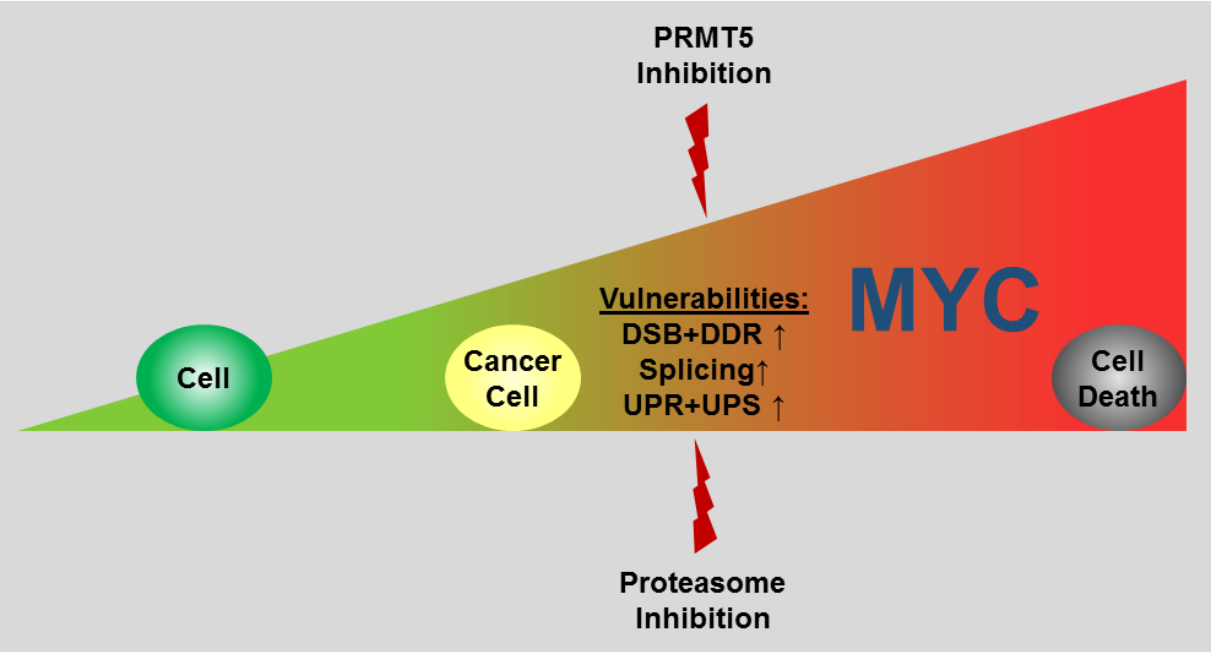

Fig. 19 Graphical abstract
PDAC cells with hyperactive MYC are primed for death due to several cellular vulnerabilities. Perturbance of proteostasis by inhibition of the proteasome triggers NOXA-dependent apoptotic cell death. Inhibition of PRMT5 leads to genetic instability and cell death, probably via reduction of splicing fidelity and ability for DSB repair. Both pharmacologic interventions target synthetic lethal vulnerabilities with MYC overexpression, providing novel therapeutic options for patients with a particularly aggressive subtype of PDAC.

IX. Supplementary Material

Tab.S 1 List of compounds and responses from the FDA-approved drug screen
Complete list of the response to drugs used in the screen. Panc1, PaTu-8988S, DanG, and PSN1 cells were treated with n = 129 compounds in biological and technical triplicates. Drug response as well as the ratio between mean of MYC high and mean of MYC low are displayed.

Drug	Panc1	PaTu-8988S	DanG	PSN1	
	MYC^{low}	MYC^{low}	MYC^{high}	MYC^{high}	Mean MYC^{high} / Mean MYC^{low}
Panobinostat	0,592737	0,4316097	0,128357	0,101244	4,461432123
Cladribine	1,036295	0,8812915	0,378447	0,196484	3,335335254
Idarubicin hydrochloride	0,385309	0,3580649	0,131662	0,106136	3,126073667
Clofarabine	0,690753	0,9303737	0,36315	0,173511	3,020768958
Topotecan hydrochloride	0,633855	0,7889655	0,37664	0,146818	2,718118017
Gemcitabine hydrochloride	0,628533	0,7472625	0,312112	0,218904	2,590869276
Floxuridine	0,76727	0,9213013	0,489905	0,303322	2,128737275
Doxorubicin hydrochloride	0,538108	0,4160912	0,309046	0,140615	2,122040469
Bortezomib	0,174094	0,3174964	0,132343	0,103227	2,086811521
Dactinomycin	0,277875	0,4070966	0,239836	0,091861	2,065052824
Pralatrexate	0,533484	0,8566843	0,330167	0,343941	2,062235104
Daunorubicin hydrochloride	0,320186	0,6879631	0,428118	0,084397	1,967063898
Dasatinib	1,064976	0,8051341	0,324829	0,651647	1,915164076
Methotrexate	0,543753	0,8269723	0,397461	0,327411	1,890991486
Romidepsin	0,614223	0,6397273	0,447201	0,226604	1,860999368
Pemetrexed, Disodium salt, Heptahydrate	1,116051	0,8835727	0,753129	0,341361	1,826991624
Ixabepilone	0,607697	0,4359349	0,198123	0,385184	1,789165199
Epirubicin hydrochloride	0,597648	0,600278	0,443216	0,243513	1,744391794
Paclitaxel	0,593712	0,4850653	0,229946	0,38993	1,740312281
Mitomycin	0,81866	0,7457391	0,547275	0,368628	1,708040398
Trametinib	1,052275	0,3858011	0,515249	0,344398	1,672867182
Belinostat	1,223561	0,9651008	0,610551	0,742512	1,617561069
Plicamycin	0,240645	0,5661695	0,374168	0,145588	1,552296875
Docetaxel	0,600699	0,358746	0,203751	0,425522	1,524688004
Cytarabine hydrochloride	0,790623	0,7922291	0,490557	0,589107	1,466060789
Valrubicin	0,658399	0,6932424	0,613569	0,317822	1,4512062
Vincristine sulfate	0,484299	0,4904168	0,356312	0,368309	1,34513844
Cobimetinib	0,805701	0,4227304	0,574965	0,346726	1,332801963
Cabazitaxel	0,559448	0,4260106	0,348366	0,399078	1,318437226
Vinblastine sulfate	0,46619	0,6971546	0,547977	0,379263	1,254630907
Teniposide	0,709991	0,6541106	0,513022	0,578521	1,249700352
Vorinostat	1,198426	1,0365938	0,813855	0,985923	1,241830561
Mitoxantrone	0,41117	0,360539	0,418033	0,204913	1,23880501
Carfilzomib	0,123085	0,2872714	0,119533	0,217341	1,218130104

Pazopanib hydrochloride	1,1507	1,1699473	0,931946	0,973809	1,217704961
Tamoxifen citrate	1,225822	0,8767898	0,811255	0,937359	1,202445098
Vemurafenib	1,298351	1,0166108	0,909679	1,016283	1,201976341
Bleomycin sulfate	0,92009	0,8969911	0,706642	0,81285	1,195847316
Axitinib	1,055165	1,0017045	0,816527	0,91024	1,191167527
Thioguanine	1,098183	0,8629344	1,015838	0,63837	1,185533008
Vinorelbine tartrate	0,520118	0,5633463	0,497125	0,42531	1,174569397
Sorafenib	1,162171	1,2830505	1,017811	1,074596	1,168616375
Lenvatinib	1,149886	1,0538571	0,899617	0,990869	1,165701528
Ponatinib	0,967681	0,8053608	0,730816	0,803648	1,155479361
Trifluridine	1,151218	1,0878322	0,905379	1,0408	1,150485363
Pomalidomide	1,090629	1,0283482	0,954765	0,921233	1,129520454
Celecoxib	1,150274	1,1248195	0,96115	1,082292	1,113362995
Idelalisib	1,114514	1,0326372	0,985693	0,947134	1,110886312
Anastrozole	1,094064	1,0583861	0,962257	0,975792	1,110627962
Megestrol acetate	1,110645	1,1060051	0,999144	1,004437	1,106344418
Mechlorethamine hydrochloride	1,106987	0,9741389	1,035016	0,847608	1,105438979
Raloxifene	1,097342	1,055331	1,020281	0,927767	1,1050411
Chlorambucil	1,287068	1,0877594	1,087541	1,062375	1,104614114
Omacetaxine mepesuccinate	0,139202	0,5614243	0,44822	0,187793	1,101590466
Carboplatin	1,1176	1,0182414	0,993622	0,955833	1,095609456
Regorafenib	1,106303	0,9268283	0,960654	0,896391	1,094821059
Decitabine	0,966737	0,9534292	0,622724	1,140081	1,089267518
Afatinib	1,070509	0,892516	0,878287	0,933929	1,083218081
Hydroxyurea	1,129012	0,9838368	0,996175	0,954918	1,082905492
Amifostine	1,09446	1,0792695	0,979767	1,028968	1,082138826
Fluorouracil	1,087649	1,0280319	0,925682	1,032076	1,08066543
Mitotane	1,156101	1,0283327	1,045081	0,978455	1,079512906
Crizotinib	1,009358	0,8524901	0,734752	0,99145	1,078580271
Carmustine	1,169459	1,0111272	1,015479	1,015251	1,073794532
Lenalidomide	1,175856	1,0865372	0,962586	1,151652	1,070074789
Arsenic trioxide	1,154364	1,0026565	1,009919	1,009896	1,067929769
Dabrafenib mesylate	1,0477	0,7038174	0,627176	1,014357	1,067000238
Streptozocin	1,062921	1,1350681	1,020049	1,044316	1,064728879
Estramustine phosphate sodium	1,117481	0,9156263	0,923025	0,991505	1,061935398
Aminolevulinic acid hydrochloride	1,27354	1,0125003	1,047228	1,105995	1,061682585
Vismodegib	1,114029	1,0051374	0,978548	1,017618	1,061618157
Methoxsalen	1,107799	1,0322965	1,001781	1,017235	1,059969685
Uridine triacetate	1,110519	0,934566	0,904067	1,026801	1,05915346
Ifosfamide	1,067342	1,0517827	0,998463	1,006323	1,057032755
Pentostatin	1,116898	1,1328357	1,000084	1,128789	1,056772122

Etoposide	0,825738	0,9160592	0,800849	0,858368	1,049769979
Plerixafor	1,015608	1,0299569	0,969355	0,984082	1,047162072
Mercaptopurine	1,153389	1,064621	1,042117	1,076255	1,047035651
Temozolomide	1,100926	0,9987936	1,017078	0,994339	1,043900587
Melphalan hydrochloride	1,116792	0,8871951	0,988473	0,931793	1,043598772
Gefitinib	1,067133	0,9157831	0,935539	0,964965	1,043363337
Busulfan	1,151544	0,9183881	1,019652	0,970382	1,040148863
Exemestane	1,089191	1,0271264	1,056178	0,98645	1,036075461
Altretamine	1,221577	0,9396757	1,063862	1,024276	1,035014345
Triethylenemelamine	0,84804	0,8116295	0,693622	0,910579	1,034577136
Ibrutinib	1,016712	0,8967658	0,900519	0,950386	1,033806651
Temsirolimus	0,799155	0,7438944	0,556973	0,9391	1,031399575
Pipobroman	1,042191	1,0351135	0,913129	1,108665	1,027456309
Cyclophosphamide	1,096337	1,0779427	1,025754	1,092142	1,026622568
Nelarabine	1,036414	1,0449675	0,978402	1,060861	1,020653647
Dacarbazine	1,077374	0,9799451	0,999857	1,032958	1,012054519
Lapatinib	1,211823	1,0117246	1,045359	1,152982	1,011466159
Olaparib	1,033357	0,9618045	0,987475	0,995395	1,006199381
Azacitidine	1,105719	0,8669931	0,898315	1,062428	1,006104312
Sunitinib	1,125673	0,9359795	1,008253	1,043755	1,004700285
Procarbazine hydrochloride	1,046722	0,9620981	0,978071	1,023625	1,003558771
Cisplatin	0,978325	0,9864485	0,971788	0,988198	1,002442154
Thalidomide	1,101689	0,8760751	0,957413	1,015575	1,002420886
Capecitabine	1,103358	0,9785461	0,991254	1,087819	1,001361478
Fludarabine phosphate	1,073507	0,9572477	1,017532	1,011327	1,000934311
Letrozole	0,964071	1,0074587	0,995672	0,981026	0,997385394
Ixazomib citrate	0,245811	0,5349317	0,363314	0,420532	0,996041413
Erismodegib	1,101577	0,8690601	0,903458	1,078405	0,99433599
Erlotinib hydrochloride	1,083135	0,9835468	1,002844	1,077168	0,993591089
Imatinib	1,091015	0,9407156	1,012413	1,032737	0,993438465
Irinotecan hydrochloride	1,056576	0,8007072	0,93322	0,942739	0,990044197
Tretinoin	1,065936	0,9976059	1,080714	1,00587	0,988956574
Dexrazoxane	1,052776	0,9693531	0,969325	1,079505	0,986967628
Uracil mustard	1,001703	1,0043368	1,04548	0,990609	0,98524151
Allopurinol	1,112212	1,0559206	1,027041	1,179255	0,982702291
Vandetanib	1,090495	0,819051	0,931901	1,011438	0,98261128
Bendamustine hydrochloride	1,115963	0,9338939	1,078548	1,01494	0,979158848
Sirolimus	0,787637	0,736924	0,624014	0,944173	0,972180429
Enzalutamide	0,97125	0,9460363	1,008043	0,967643	0,970440678
Nilotinib	1,122425	1,146312	1,264487	1,085551	0,965404678
Thiotepa	0,989979	0,9029347	0,989111	0,976867	0,962835683
Everolimus	0,811472	0,776071	0,680229	0,971491	0,961145951
Lomustine	0,952152	0,9542411	1,005607	0,978821	0,960676527

Oxaliplatin	1,034603	0,8738007	1,006481	0,980128	0,960633421
Cabozantinib	1,032604	0,8079131	0,875607	1,04596	0,95782062
Palbociclib	0,833218	0,7235895	0,736792	0,889579	0,957228421
Fulvestrant	1,030141	0,8667615	1,002599	0,985799	0,953985335
Zoledronic acid	1,148475	0,9349664	1,106178	1,091512	0,94801437
Osimertinib	1,050889	0,7746164	0,93517	0,997295	0,94465117
Alectinib	0,984529	0,765287	0,878473	0,989748	0,936621134
Ceritinib	0,992057	0,6634162	0,938527	0,878684	0,910996414
Bosutinib	1,109097	0,7804824	1,098541	0,977648	0,910118767
Imiquimod	1,099182	0,8491946	1,202601	0,991752	0,887904663
Abiraterone	1,044395	0,846116	1,10875	1,102911	0,854792766

Tab.S 2 List of compounds and responses from the epigenetic drug screen

Complete list of the response to drugs used in the screen. Panc1, PaTu-8988S, HPAC, DanG, PSN1, and PaTu-8988T cells were treated with n = 181 compounds in technical triplicates. Drug area under the dose-response curve (AUC) as well as the ratio between mean of MYC high AUC and mean of MYC low AUC and corresponding p-value of unpaired t-test are displayed.

Drug	**Panc1**	**PaTu-8988S**	**HPAC**	**DanG**	**PSN1**	**PaTu-8988T**	**delta AUC**	**p-value**
	MYC^{low}	**MYC^{low}**	**MYC^{low}**	**MYC^{high}**	**MYC^{high}**	**MYC^{high}**		
Resminostat	252,2	265,3	256,7	194,9	204,3	214	53,66667	0,001333
GSK591	275,8	292,9	283,1	243,4	223,1	221,9	54,46667	0,003121
Givinostat (ITF2357)	182,8	176,5	199,8	113,6	126,1	147,3	57,36667	0,008896
CUDC-101	195,2	212	195,7	175,6	153,9	152,8	40,2	0,012196
M344	247,7	239,8	235,2	201,8	171,4	211,3	46,06667	0,021515
CUDC-907	102,3	83,17	53,53	20,45	24,21	38,66	51,89333	0,027119
AZD1208	297,4	307,8	318	286,7	256,3	272,6	35,86667	0,027751
Mitomycin C	268	268,3	210,2	181,3	115,4	176,2	91,2	0,033456
XL019	332,4	404,7	351,2	290,3	281,2	308,5	69,43333	0,039699
Gemcitabine HCl	215,8	325,8	146,8	78,52	20,07	86,12	167,8967	0,04032
PCI-34051	280	278,2	276,1	275,3	269,4	268	7,2	0,045257
AR-42	210,2	228,8	170,2	121,3	129,1	169	63,26667	0,049709
Cytarabine	194,8	278,6	164,8	136,1	104	130,6	89,16667	0,065766
Pirarubicin	157,6	248,3	142,1	109,3	86,77	97,73	84,73333	0,06603
2-Methoxyestradiol (2-MeOE2)	221,2	315,2	296,7	217,5	177,3	205,7	77,53333	0,067423
JNJ-7706621	262,9	332,6	270,5	253,4	192	205,7	71,63333	0,068136
Ellagic acid	306,3	367,2	348	304,9	301,2	285,8	43,2	0,084291
Ruxolitinib (INCB018424)	314,2	380,4	351,1	298,3	311,5	303,7	44,06667	0,08705
Azacitidine	292,1	276,6	258,3	233,8	200,6	259,7	44,3	0,087734
Resveratrol	282,1	317	318,2	283	275,2	278,6	26,83333	0,08996
Vorinostat (SAHA, MK0683)	229,4	245,4	253,5	220,2	193,1	229,8	28,4	0,095537
OF-1	317,3	348,7	299,7	297,5	275,5	291,6	33,7	0,09938
Pracinostat (SB939)	197,7	150,5	155,8	108,9	130,6	149,4	38,36667	0,113148
CX-6258 HCl	244,5	342,6	238,2	228	183,1	197,6	72,2	0,117557
PFI-1 (PF-6405761)	285,8	321,5	314,9	295,3	270,3	278,8	25,93333	0,120824

AZ 960	236,5	256,4	431,4	194,4	172,2	222,8	111,6333	0,154195
GSK J4 HCl	255,2	303,3	236,1	239,7	157,7	228	56,4	0,157558
Iniparib (BSI-201)	295,4	329,3	208,3	347,6	335,9	337,9	-62,8	0,157954
Mocetinostat (MGCD0103)	207,7	238,1	188,4	179	153,8	200,2	33,73333	0,162425
Trichostatin A (TSA)	152,7	207,8	133,9	93,06	104,1	152,1	48,38	0,166415
EPZ5676	284,5	368,1	335,6	291,8	268	302,5	41,96667	0,186871
TAK-901	224,5	265,7	124,7	137,1	107,5	158,7	70,53333	0,187441
PJ34	271,9	277,9	272,3	264	250	274	11,36667	0,190755
ENMD-2076 L-(+)-Tartaric acid	213	211,1	246,2	176,4	194	219,9	26,66667	0,192108
Blasticidin S HCl	338,8	375,3	244,6	274,9	203,9	270,4	69,83333	0,197224
Roxadustat (FG-4592)	323,9	440,3	399	327,2	338,8	341,3	51,96667	0,204827
Momelotinib (CYT387)	256,3	332	249,8	247,6	205,8	249,2	45,16667	0,206219
PFI-3	296,6	275	275,5	314,2	279,2	317,2	-21,16667	0,208298
SMI-4a	306,8	258,4	216,4	347,6	301,7	278	-48,56667	0,216872
SP2509	252,4	228,8	224,5	222,6	185,1	227,8	23,4	0,217525
Tofacitinib (CP-690550) Citrate	295,6	319,6	300,4	300,3	271	294,1	16,73333	0,220745
Decitabine	271,6	300,7	254	164,2	244	268,9	49,73333	0,221663
Veliparib (ABT-888)	284,8	410,6	362,1	307,3	311,4	272,8	55,33333	0,225228
OTX015	242,4	230,4	222,2	230,8	211,1	161,9	30,4	0,22689
Ricolinostat (ACY-1215)	345,4	333,4	394,1	356,3	305,3	301,9	36,46667	0,227026
TG101209	247,7	243,2	188	194,2	189,8	209,2	28,56667	0,227769
Dacinostat (LAQ824)	79,75	106,4	58,1	26,63	34,09	85,82	32,57	0,234197
NVP-BSK805 2HCl	275,5	288,1	275,4	255,7	240,7	285,3	19,1	0,237554
UPF 1069	343	289,9	269,1	395,8	330,7	311	-45,16667	0,252082
GSK2879552 2HCl	315,7	288,9	312,1	308,9	281,9	260,9	21,66667	0,252882
UNC0379	210,7	313,6	240,8	226,3	190,3	220,8	42,56667	0,260845
Decernotinib (VX-509)	305	298,4	289	322,8	290,5	327,9	-16,26667	0,266141
ORY-1001 (RG-6016) 2HCl	274,8	288,6	289,1	266,9	263,3	287,8	11,5	0,268652
Gandotinib (LY2784544)	249,3	276,2	394,4	254,7	237	255,1	57,7	0,268697
EI1	300,1	293,5	294,7	306,2	263,9	265	17,73333	0,275978
CYC116	261,1	324,8	250,6	223,7	223,3	278,2	37,1	0,276857
Sirtinol	250,5	228,1	313,6	293,6	291,2	301	-31,2	0,292589
Tubastatin A HCl	253,7	276,3	296,9	256,6	257,9	265,9	15,5	0,292883
GSK1324726A (I-BET726)	238,3	239,5	177,8	210,8	177,8	184,7	27,43333	0,293655
Daptomycin	424,3	552	309,1	349,4	333,9	347,7	84,8	0,294311
Entacapone	300,5	327,4	352,8	315,2	296,7	310,8	19,33333	0,296005
BI-7273	293,2	294,1	315	303,2	245,6	287,8	21,9	0,305019
RG2833 (RGFP109)	257,2	287,9	270,1	251,8	221	277,4	21,66667	0,308242
A-366	319,5	369,5	300,7	310,8	285,3	315,3	26,1	0,311605
S-Ruxolitinib (INCB018424)	291	359,6	310,6	299,7	289,9	300	23,86667	0,312484
AZD2461	250,8	338,8	300,9	270,5	254,5	275,8	29,9	0,318695
UNC1215	305	349	341,5	344,1	274,2	294,3	27,63333	0,328063
Valproic acid sodium salt (Sodium valproate)	304,6	351,3	331,2	320,3	315,5	304,2	15,7	0,335143
Daphnetin	276,6	322,6	278,6	275,2	266,8	284,2	17,2	0,33832
Sodium Phenylbutyrate	271,1	315,5	318,2	294,2	272,3	285,2	17,7	0,344827

ENMD-2076	223,9	243,9	184,3	162,2	192,8	219,8	25,76667	0,346224
C646	291,4	314,1	331,2	302,3	265,3	311,1	19,33333	0,347038
Droxinostat	296,2	339	311,7	310,9	295	298,8	14,06667	0,353
4SC-202	215,4	233,4	216	173,6	122,9	252,3	38,66667	0,367618
Panobinostat (LBH589)	68,37	146,3	58,58	37,97	29,46	99,12	35,56667	0,371609
SGC 0946	306,8	401,8	363,6	346,1	264,9	345,4	38,6	0,373624
MI-3 (Menin-MLL Inhibitor)	260,6	277,4	288,4	287,4	254,6	228	18,8	0,378108
MS023	270,9	312,2	298,8	295,4	244,5	285	19	0,389958
MG149	302,3	280,9	306,1	324,7	286,2	319,6	-13,73333	0,39417
WHI-P154	289,1	325,4	280	245,5	305,1	281,3	20,86667	0,400244
EPZ015666(GSK3235025)	326,8	309,2	285,6	320,5	277,9	266,4	18,93333	0,404372
AMG-900	275,9	397,7	101,4	132,7	118,3	259,8	88,06667	0,415408
NVP-TNKS656	311,6	271,1	261	330	299,6	274,6	-20,16667	0,416238
AG-490 (Tyrphostin B42)	290,1	295,8	323,9	342	316	296,6	-14,93333	0,424194
ML324	267,4	360,4	290,1	290	254,1	292,6	27,06667	0,426749
IOX2	297	363	345,5	327,9	309,4	314,9	17,76667	0,43478
Mizoribine	291,8	456,5	271,2	301,1	274	290,7	51,23333	0,435369
Carboplatin	300,8	502,9	306,1	339,4	282	311,5	58,96667	0,438088
AZD1480	230,5	264	266,3	245,4	267,2	296	-15,93333	0,441518
MK-5108 (VX-689)	190,5	224,9	248,7	187,1	214,3	213,9	16,26667	0,443307
Tacedinaline (CI994)	246,3	223,7	300,7	226,7	224,4	256,1	21,16667	0,445304
Scriptaid	254,2	228,3	177,3	209,1	175	211,4	21,43333	0,447455
Fedratinib (SAR302503, TG101348)	251,7	348,4	168,8	213,6	221,7	205,6	42,66667	0,458845
Nexturastat A	260,5	273,8	277,9	252	231,9	287	13,76667	0,461849
SGI-1776 free base	249	222,9	381,4	251,6	240,6	241,4	39,9	0,462814
Tranylcypromine (2-PCPA) HCl	285,2	324,4	362,4	317,5	288,5	308,2	19,26667	0,46484
TMP269	279,1	307,1	277,3	291,6	260,5	472,2	-53,6	0,466657
Belinostat (PXD101)	182,6	253,1	138,1	126,2	136,9	209,2	33,83333	0,469883
(+)-JQ1	202,3	201,3	217,2	224,7	195,1	142,9	19,36667	0,472779
GSK1070916	244	322,2	76,27	121,7	112,6	220,8	62,45667	0,480616
MLN8054	246	299,9	150,5	284,3	231,2	289,2	-36,1	0,489288
Mirin	279	326,2	332,5	330,9	265,2	285	18,86667	0,504539
Clevudine	300,3	358,2	353,9	335,1	315,6	318,8	14,3	0,505637
SGC-CBP30	283,5	317,4	283,1	294,7	263,2	292,9	11,06667	0,50904
AG-14361	251,3	274	484,7	295,6	276,8	276,2	53,8	0,510585
BIX 01294	267,1	220,9	170,1	293,7	227,4	216,1	-26,36667	0,515668
GSK2801	291,8	278,1	316,1	359,2	297	284	-18,06667	0,52126
CPI-203	210,5	190,1	189,9	210,5	191,5	146,3	14,06667	0,525116
Norfloxacin	310,1	263	288,8	324,9	287,3	286,6	-12,3	0,544316
Ofloxacin	280,9	251	279,2	291,2	269,3	273,9	-7,766667	0,54529
Hesperadin	146,6	122,3	42,98	71,3	70,41	104,4	21,92333	0,545419
ZM 39923 HCl	321,8	322,1	380	356,2	319,5	298,2	16,66667	0,552253
Apabetalone (RVX-208)	289,9	394,4	294,6	314,2	278	317	23,23333	0,557154
EPZ004777	293,9	288,8	308,3	287	264,1	311,6	9,433333	0,561204
I-BET-762	251,1	224,6	253,4	260,3	233,1	198	12,56667	0,568714

ME0328	288,5	285,9	321,8	283,5	277,5	308	9,066667	0,574557
SGI-1027	205,7	237,2	191,9	298,1	189,6	212	-21,63333	0,577086
Anacardic Acid	281,4	283,8	296,1	305,5	220	287,8	16	0,577884
Nedaplatin	264,2	410,1	307,5	355	229,5	298	33,1	0,589193
Tubastatin A	285,1	313,7	341,3	326	276,1	301,3	12,23333	0,602975
Lomeguatrib	320,3	366,4	376,5	381,3	298,5	334,4	16,33333	0,610013
GSK503	312,3	324,9	291,3	299	279,8	323,7	8,666667	0,61779
Entinostat (MS-275)	289,8	268,5	247,5	231,2	198,7	316,2	19,9	0,620105
Niraparib (MK-4827) tosylate	275,4	361,9	257,1	316,4	240	275,6	20,8	0,62323
Remodelin	318,8	359,8	280,1	340,6	294,4	276,8	15,63333	0,628216
ZM 447439	263,2	314,2	135,9	243,4	237,3	327,6	-31,66667	0,628327
Aurora A Inhibitor I	214,1	292,5	310,5	230,3	268,1	270,3	16,13333	0,643817
CPI-360	296,8	339,5	264,6	303,6	269,9	292,7	11,56667	0,653143
CEP-33779	271,9	249,3	306,9	267,1	288	301,2	-9,4	0,654566
BRD4770	284,1	283,8	293,4	306,4	246,4	283,3	8,4	0,660789
RG108	252,3	283,1	259,7	265,4	260,6	285,6	-5,5	0,671383
WP1066	214,4	196,5	255,8	223,6	220,4	249	-8,766667	0,680148
AT9283	172,8	236,1	91,58	265,9	145,6	162,9	-24,64	0,683757
SRT1720 HCl	222,4	265,9	201,9	271,2	213,3	236,7	-10,33333	0,7036
PHA-680632	249,6	307,7	172,8	235,6	199,7	244,5	16,76667	0,706188
Oclacitinib-maleate	331,7	246,5	298,3	334	223,3	271,7	15,83333	0,715819
Abexinostat (PCI-24781)	176,6	215,1	142,9	150,5	163,9	192,3	9,3	0,720596
APTSTAT3-9R	242,9	354,4	274,7	338,2	286	288	-13,4	0,737576
INO-1001 (3-Aminobenzamide)	262,5	304,1	282,4	306,7	280,9	277	-5,2	0,749539
Pacritinib (SB1518)	229	233,4	244,6	286,1	200,9	191	9,666667	0,76744
SNS-314	202,5	283,2	118,9	139,9	172,4	240,5	17,26667	0,772952
Rucaparib (AG-014699,PF-01367338) phosphate	264,4	336,3	226	313,3	253,9	293,5	-11,33333	0,773128
Tozasertib (VX-680, MK-0457)	258,1	278,5	176,1	252,1	219,7	273	-10,7	0,774596
HLCL-61 HCL	332,8	233,7	296,4	336,7	238	251,7	12,16667	0,787995
UNC0631	211,6	227,6	243,1	247,1	201,7	219,8	4,566667	0,789815
Barasertib (AZD1152-HQPA)	238	281,5	135,2	253,6	193,4	248,2	-13,5	0,790123
I-BRD9	338,2	342,6	439,9	416,6	361,7	304,5	12,63333	0,798711
Quercetin	268,3	328,3	287,9	285,6	282,1	301,6	5,066667	0,799382
AZ6102	254,7	293,3	194,7	253,2	208,8	254,4	8,766667	0,799942
SGC707	315,1	323,4	367,6	362,3	331	291,7	7,033333	0,801094
JIB-04	162	151,3	159,5	209,1	87,71	147,8	9,396667	0,802659
GSK-LSD1 2HCl	322,1	368,4	348,5	325,5	286,8	399,1	9,2	0,808626
IOX1	285,7	279,3	275,9	298,2	270,7	278,6	-2,2	0,812087
Olaparib (AZD2281, Ku-0059436)	269,8	283,2	303,9	292,8	272,8	282,6	2,9	0,812968
OG-L002	318,6	284,4	308,2	343,8	287,6	293,7	-4,633333	0,832109
Procainamide HCl	286	333,3	334,4	328,4	301,1	312,4	3,933333	0,836032
MI-2 (Menin-MLL Inhibitor)	286,1	275,4	298,7	328,4	274,8	239,7	5,766667	0,839304
MC1568	299,9	254,5	289,6	293,2	280,9	278,5	-2,866667	0,852687
MS436	274,4	281,5	274,2	294,7	250,9	293,1	-2,866667	0,853321

Bromosporine	226,1	231,6	253,9	269,3	231,8	220,1	-3,2	0,860674
Quisinostat (JNJ-26481585) 2HCl	57,52	85,32	42,78	91,02	35,33	48,17	3,7	0,868411
Selisistat (EX 527)	287,5	267,4	273,5	289,1	268,1	266,3	1,633333	0,870927
MM-102	280,1	266	281,9	280,5	269,5	281,1	-1,033333	0,877359
Danusertib (PHA-739358)	201,9	253,8	112	231,2	168,7	188,6	-6,933333	0,885862
Filgotinib (GLPG0634)	295,3	271,8	296,2	317,6	267,6	284,9	-2,266667	0,898562
RGFP966	285,2	265	301,6	331,8	274,1	256,1	-3,4	0,899058
PFI-2 HCl	265,6	347,6	282,6	292,3	268,2	347,5	-4,066667	0,911291
UNC669	313,4	289,4	325,7	324,5	299,3	309,3	-1,533333	0,911345
PF-CBP1 HCl	299,8	229,6	289,1	308,9	226,6	272,8	3,4	0,921265
Zebularine	306,7	292,2	355,2	349,4	296,9	300,3	2,5	0,926635
Procarbazine HCl	295,4	398,8	329	381,1	322,2	309,2	3,566667	0,929063
EPZ011989	288,1	312,2	255,1	271,9	257	320,5	2	0,940852
Baricitinib (LY3009104, INCB028050)	257,1	329,8	272,2	274,1	285,7	303,2	-1,3	0,958903
ITSA-1 (ITSA1)	308,4	225,7	282,3	313,7	227,1	270,4	1,733333	0,962812
Alisertib (MLN8237)	199,1	252	153,7	202	185	215	0,933333	0,976438
PJ34 HCl	277,5	356,4	277,1	293,3	265,2	349,1	1,133333	0,976458
CPI-169	334,5	312,2	302,2	346,5	287	316,7	-0,433333	0,983463
GSK J1	286,4	352,6	308,2	285,7	277,8	385,1	-0,466667	0,991171
KW-2449	288,6	267,9	315,8	284	263,2	324,4	0,233333	0,99229
3-Deazaneplano	229,3	128	221,8	276,8	167,9	133,2	0,4	0,994461
Tofacitinib (CP-690550,Tasocitinib)	315,7	282,7	276,5	308,1	273,6	292,9	0,1	0,995234

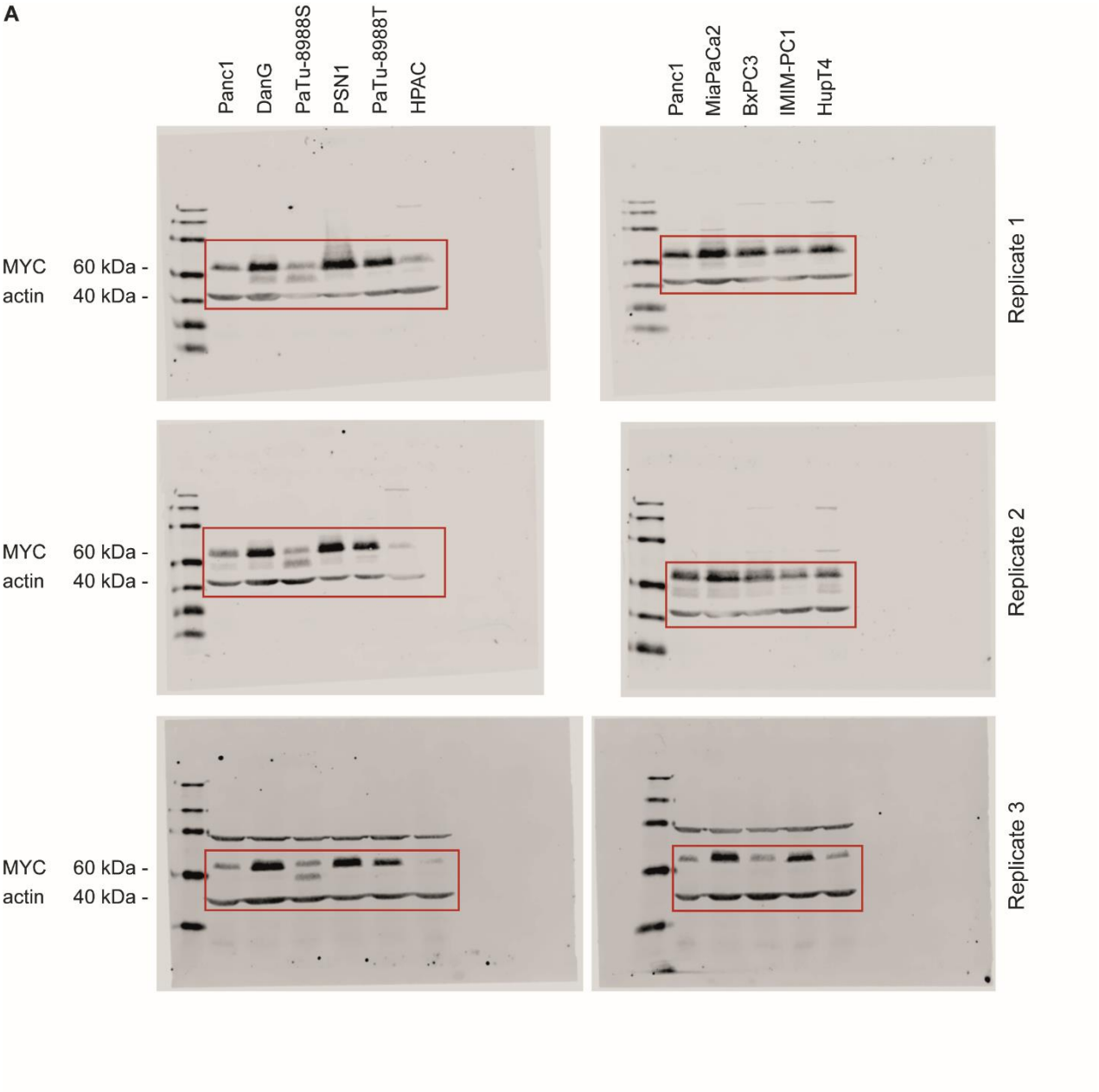
A
Panc1
DanG
PaTu-8988S
PSN1
PaTu-8988T
HPAC
Panc1
MiaPaCa2
BxPC3
IMIM-PC1
HupT4
MYC 60 kDa -
actin 40 kDa -
Replicate 1
MYC 60 kDa -
actin 40 kDa -
Replicate 2
MYC 60 kDa -
actin 40 kDa -
Replicate 3

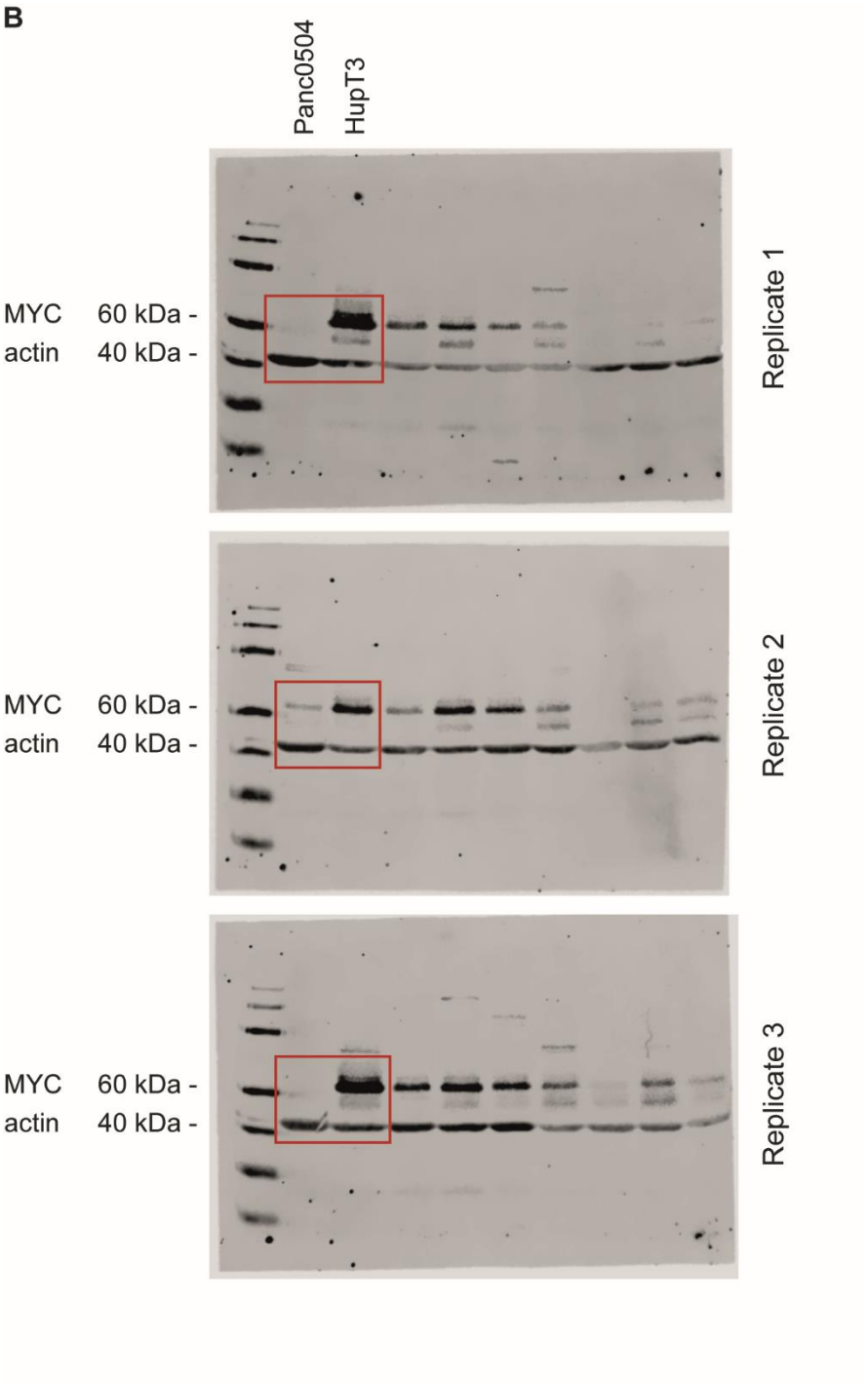

Fig. S 1 Uncropped western blots of three replicates of Fig. 2A
All three biological replicates described in Fig. 2A depicting MYC protein expression in human PDAC cell lines with Panc1, DanG, PaTu-988S, PSN1, PaTu8988T, HPAC, MiaPaCa2, BxPC3, IMIM-PC1, and HupT4 shown in **A)** and Panc0504, and HupT3 shown in **B).**

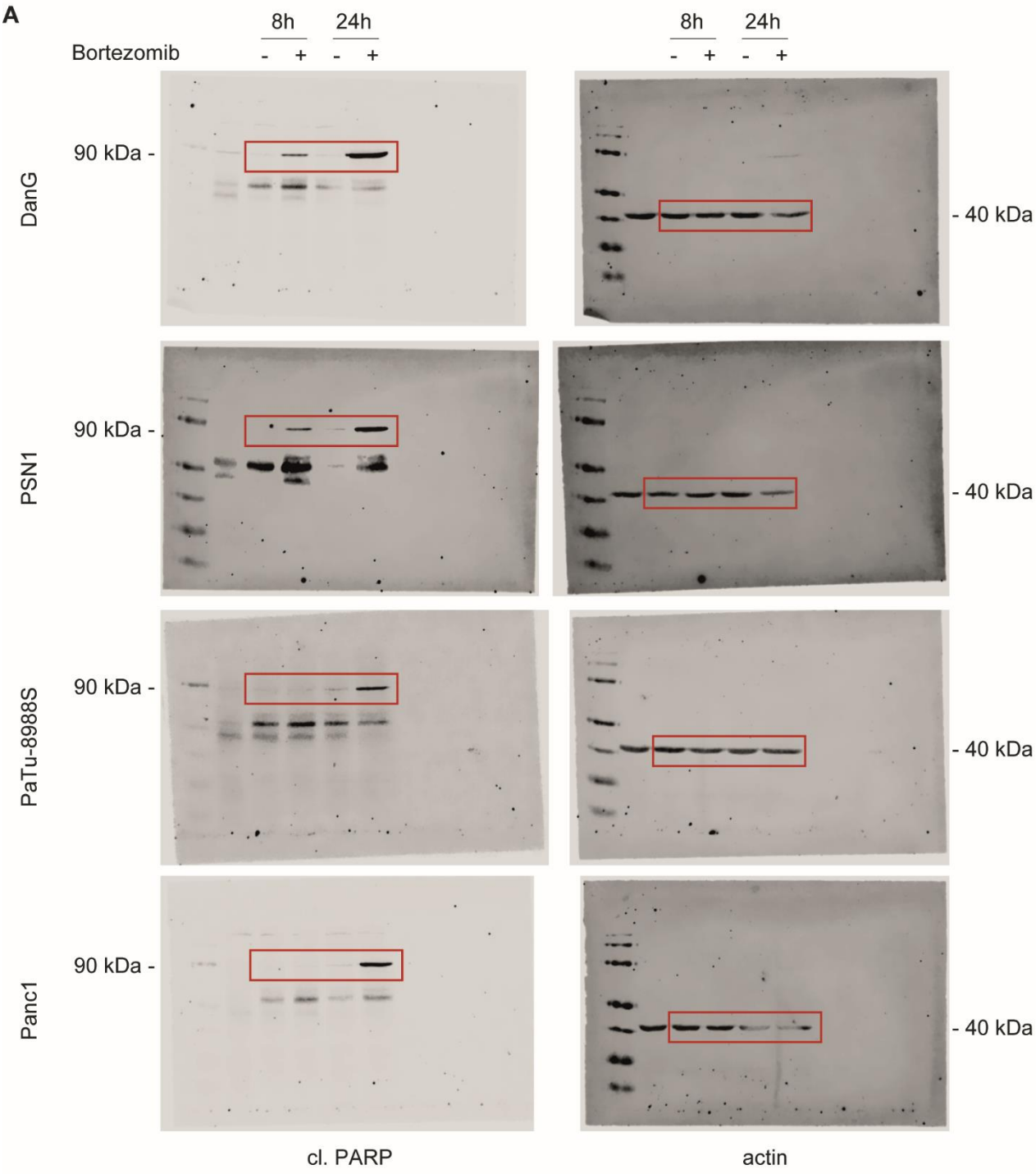
A
8h
24h
8h
24h
Bortezomib
- + - +
- + - +
DanG
PSN1
PaTu-8988S
Panc1
90 kDa -
- 40 kDa
cl. PARP
actin

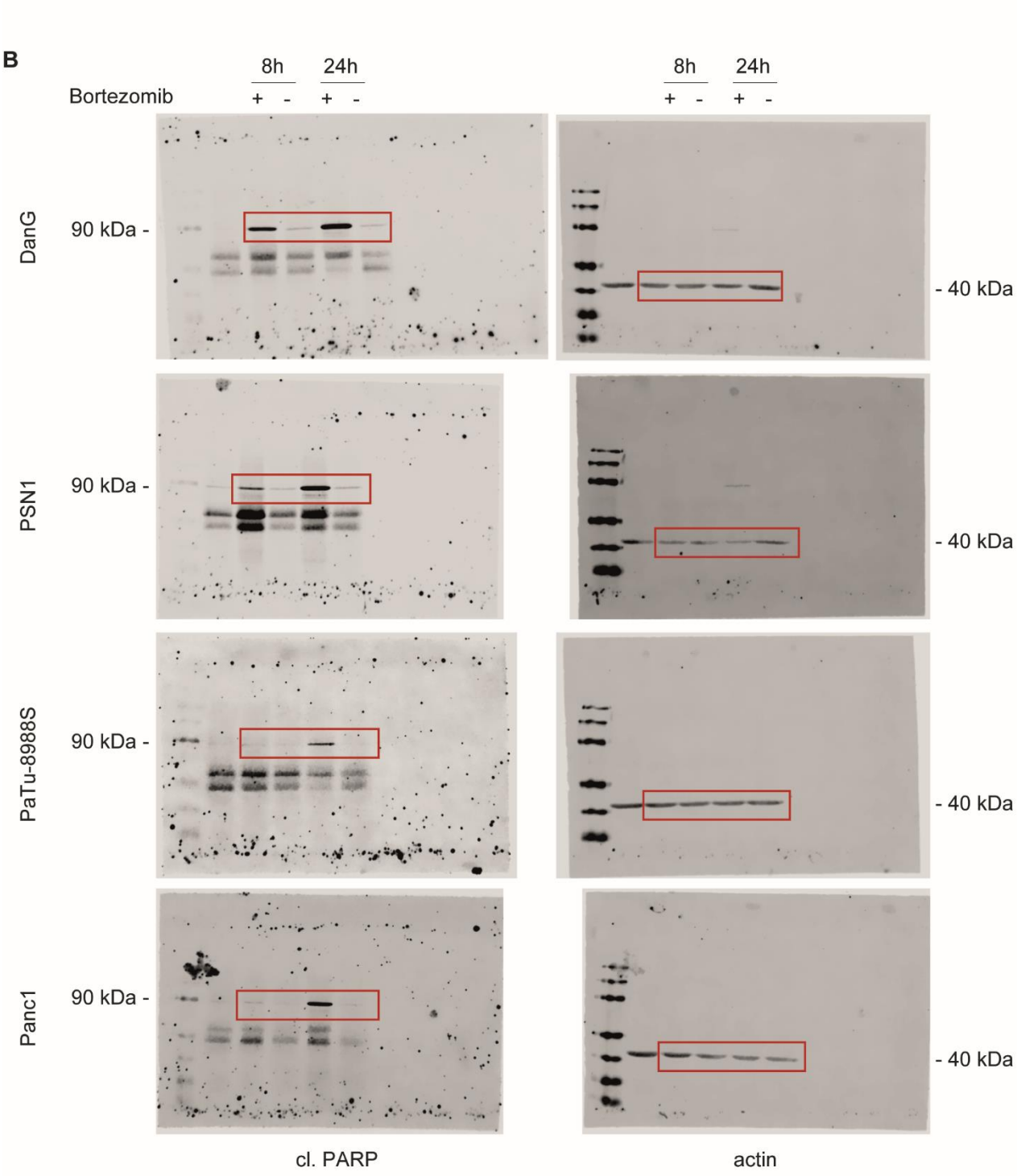
B
8h
24h
8h
24h
Bortezomib
+ - + -
+ - + -
DanG
PSN1
PaTu-8988S
Panc1
90 kDa -
- 40 kDa
cl. PARP
actin

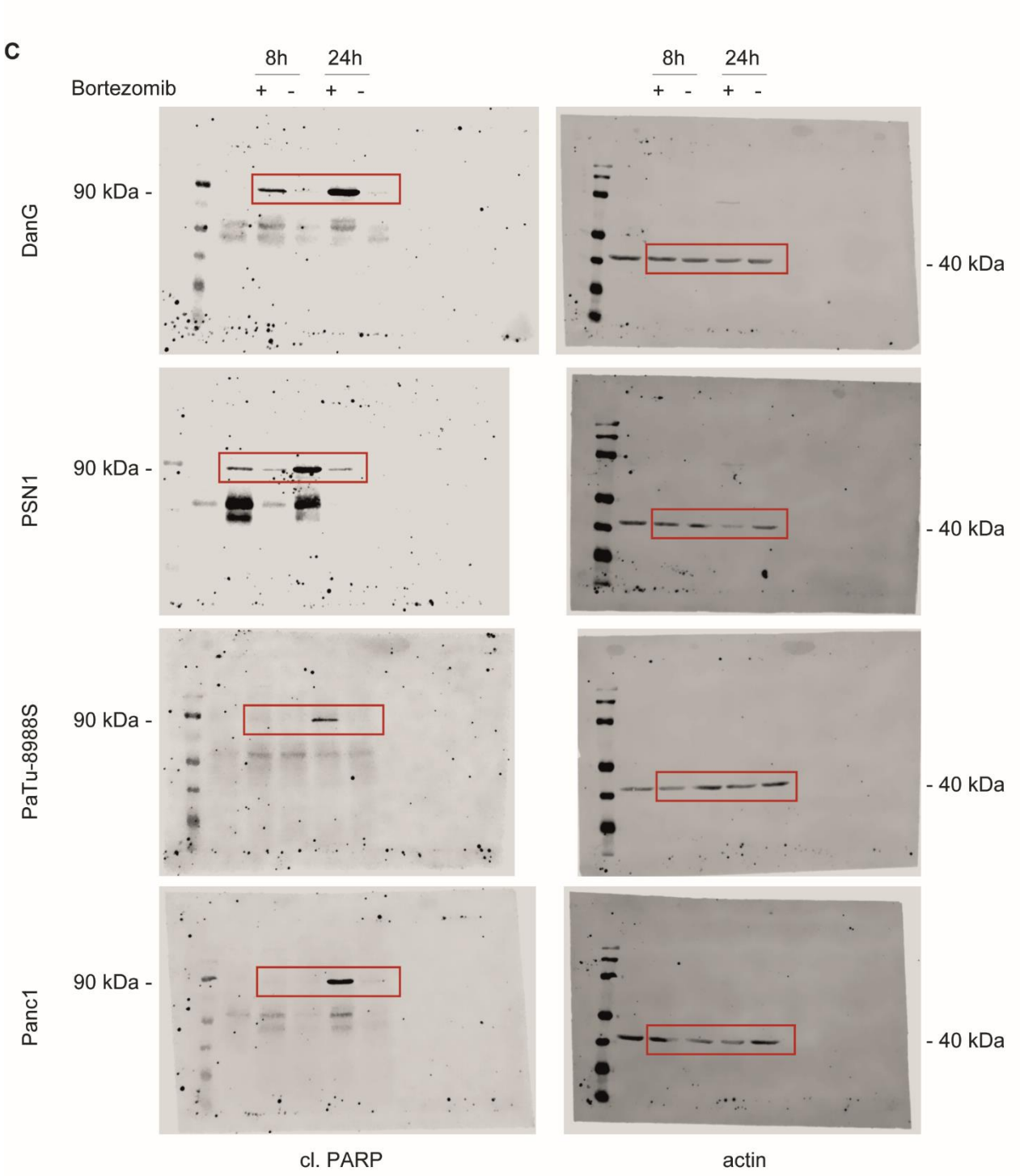

Fig. S 2 Uncropped western blots of three replicates of Fig. 7A
Biological replicate 1 (A), replicate 2 (B), and replicate 3 (C) of experiment described in Fig. 7A depicting cleaved PARP protein expression after Bortezomib treatment in human PDAC cell lines.

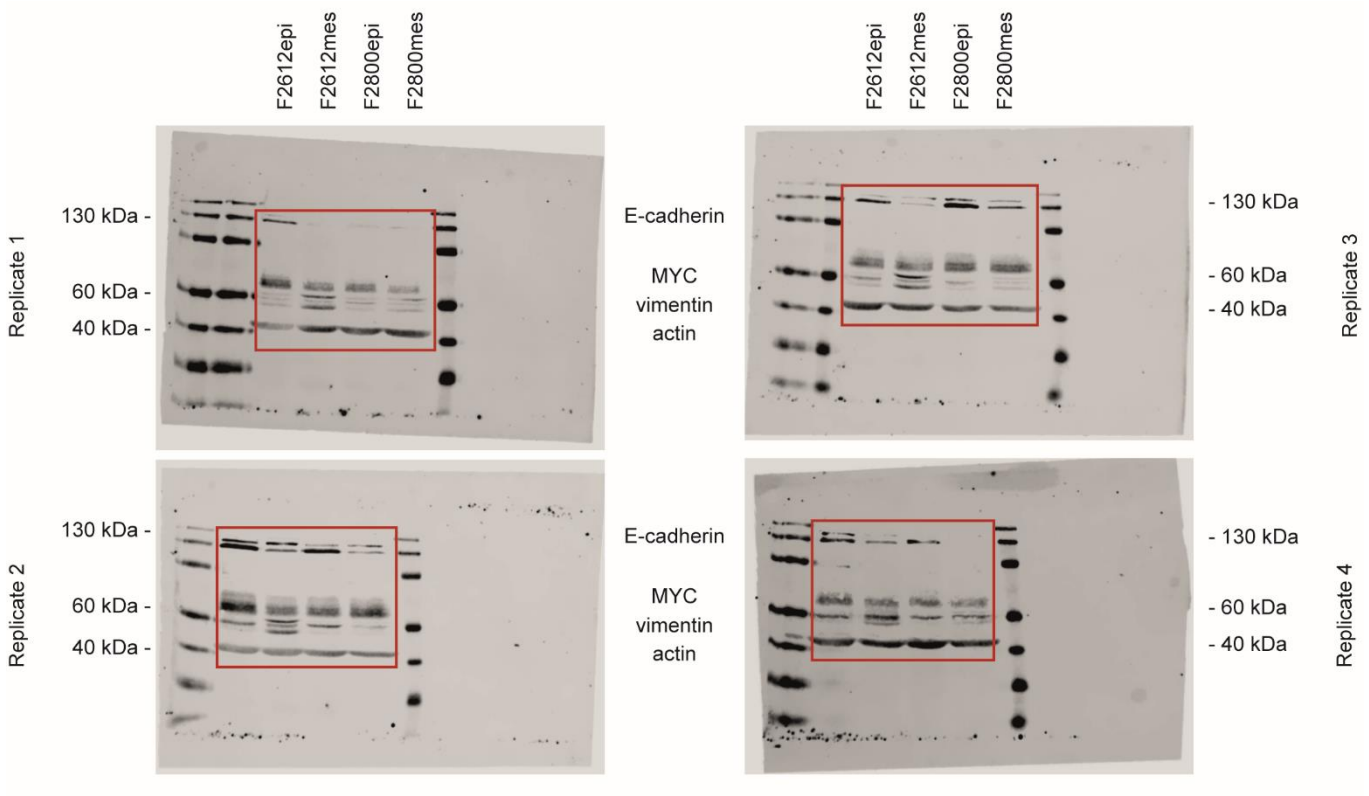

Fig. S 3 Uncropped western blots of four replicates of Fig. 9B
All four biological replicates described in Fig. 9B depicting E-cadherin, vimentin, and MYC protein expression in epithelial and mesenchymal fractions of murine PDAC cell lines.

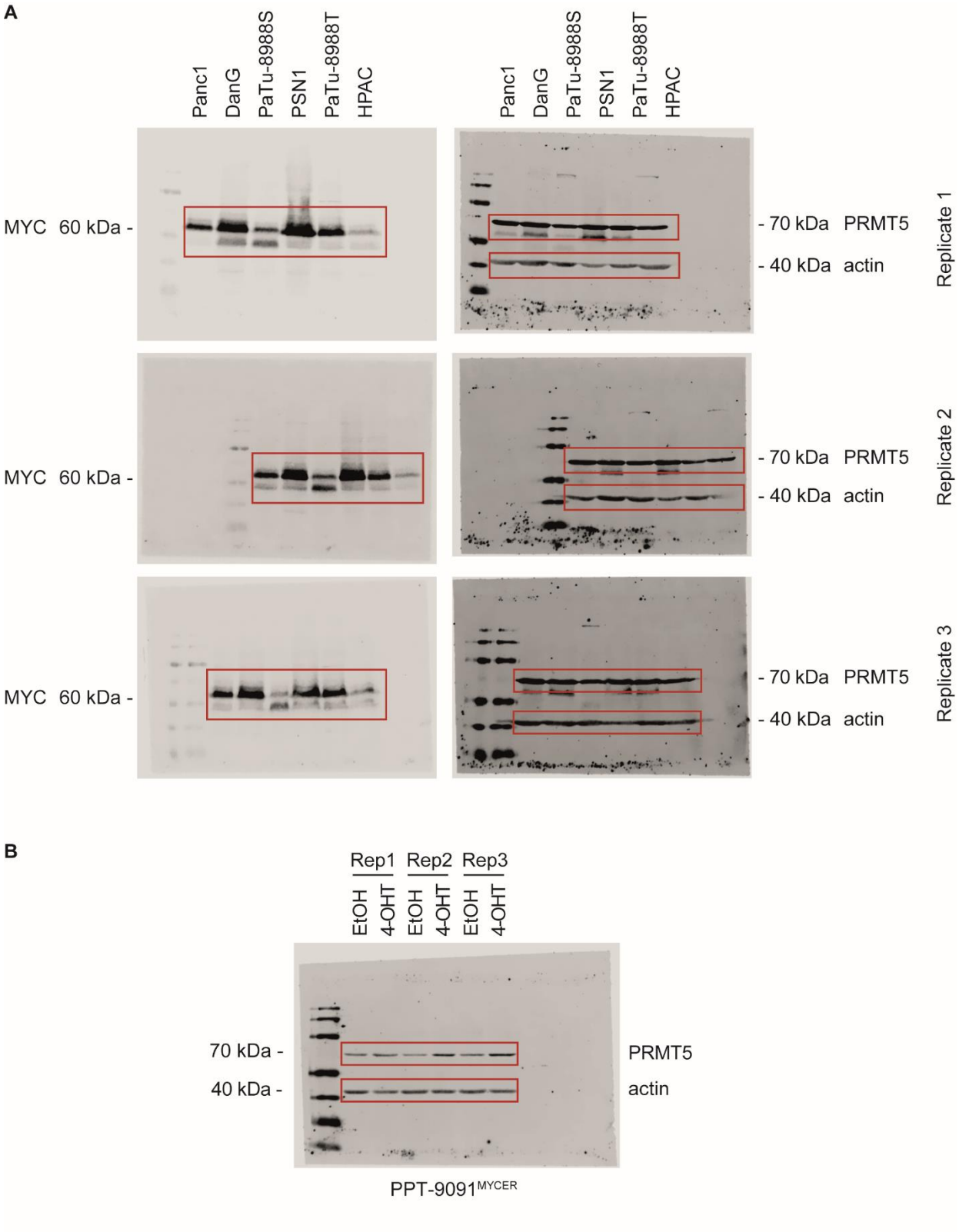

Fig. S 4 Uncropped western blots of three replicates in Fig. 11
A) All three biological replicates described in Fig. 11A depicting PRMT5 and MYC protein expression in human PDAC cell lines. **B)** All three biological replicates described in Fig. 11D depicting PRMT5 protein expression in PPT-9091 MYC-ER cell line treated with EtOH or 4-OHT.

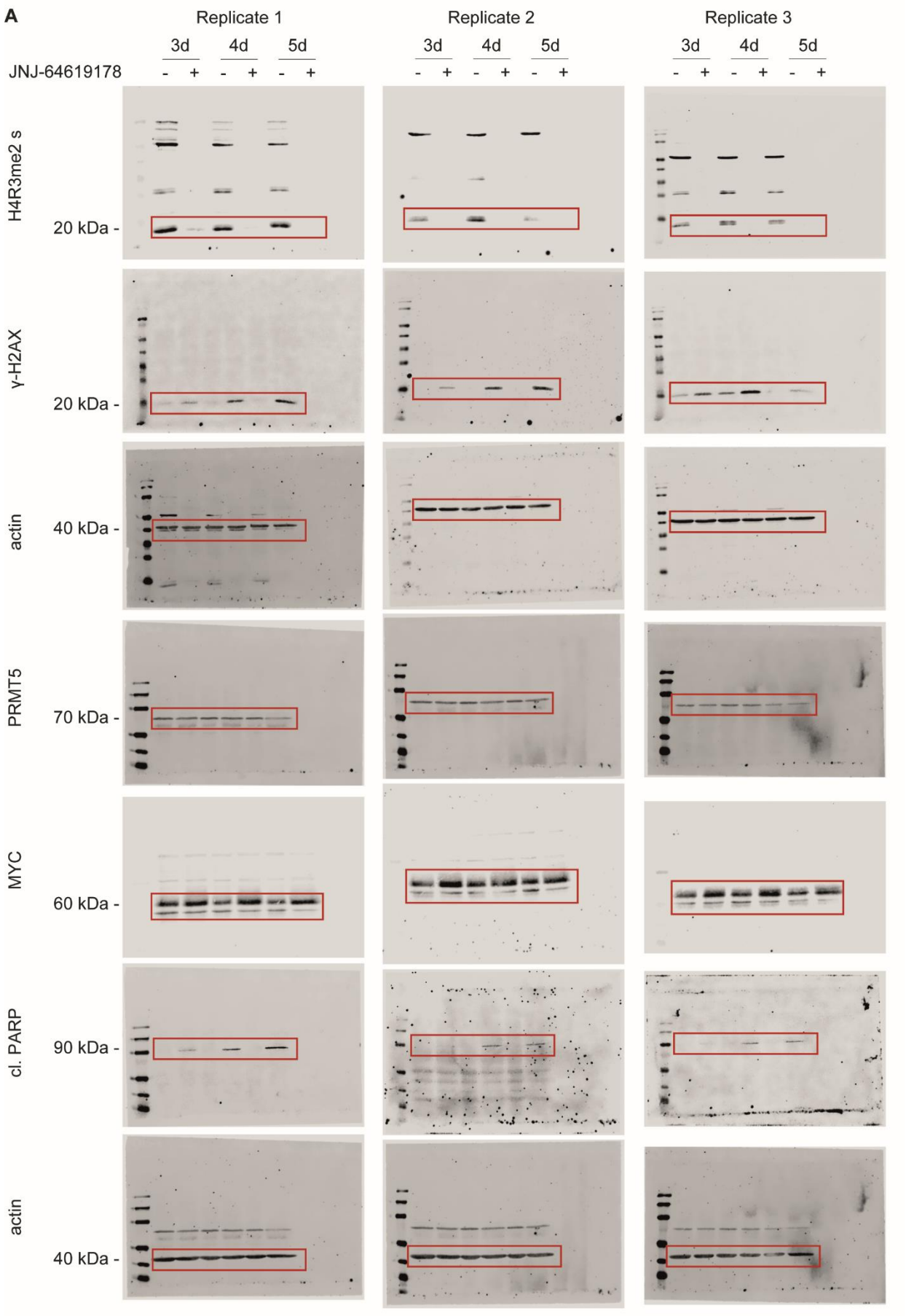
A
Replicate 1
Replicate 2
Replicate 3
3d
4d
5d
JNJ-64619178
- + - + - +
H4R3me2 s
20 kDa -
γ-H2AX
20 kDa -
actin
40 kDa -
PRMT5
70 kDa -
MYC
60 kDa -
cl. PARP
90 kDa -
actin
40 kDa -

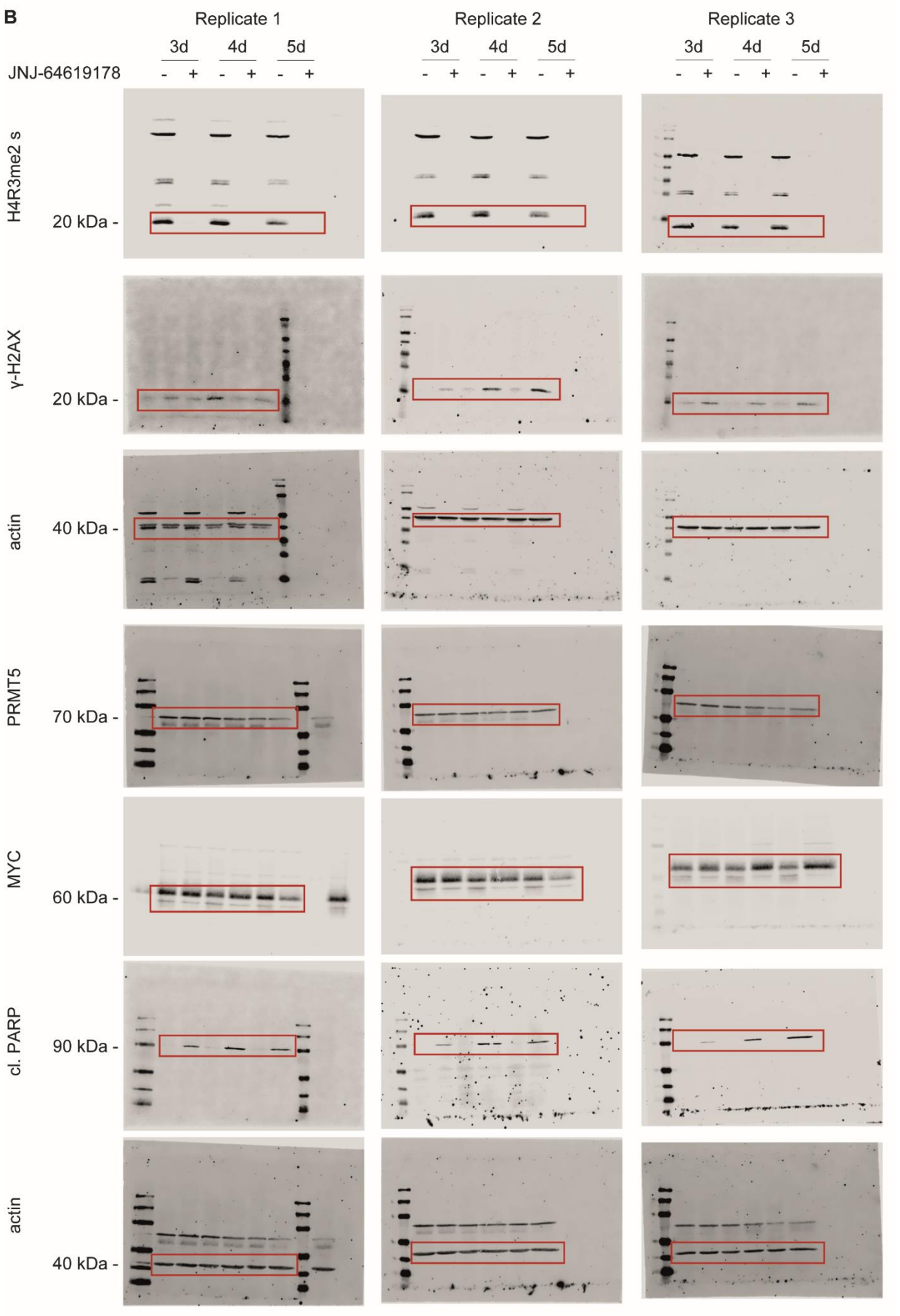
B
Replicate 1
Replicate 2
Replicate 3
3d
4d
5d
JNJ-64619178
- + - + - +
H4R3me2 s
20 kDa -
γ-H2AX
20 kDa -
actin
40 kDa -
PRMT5
70 kDa -
MYC
60 kDa -
cl. PARP
90 kDa -
actin
40 kDa -

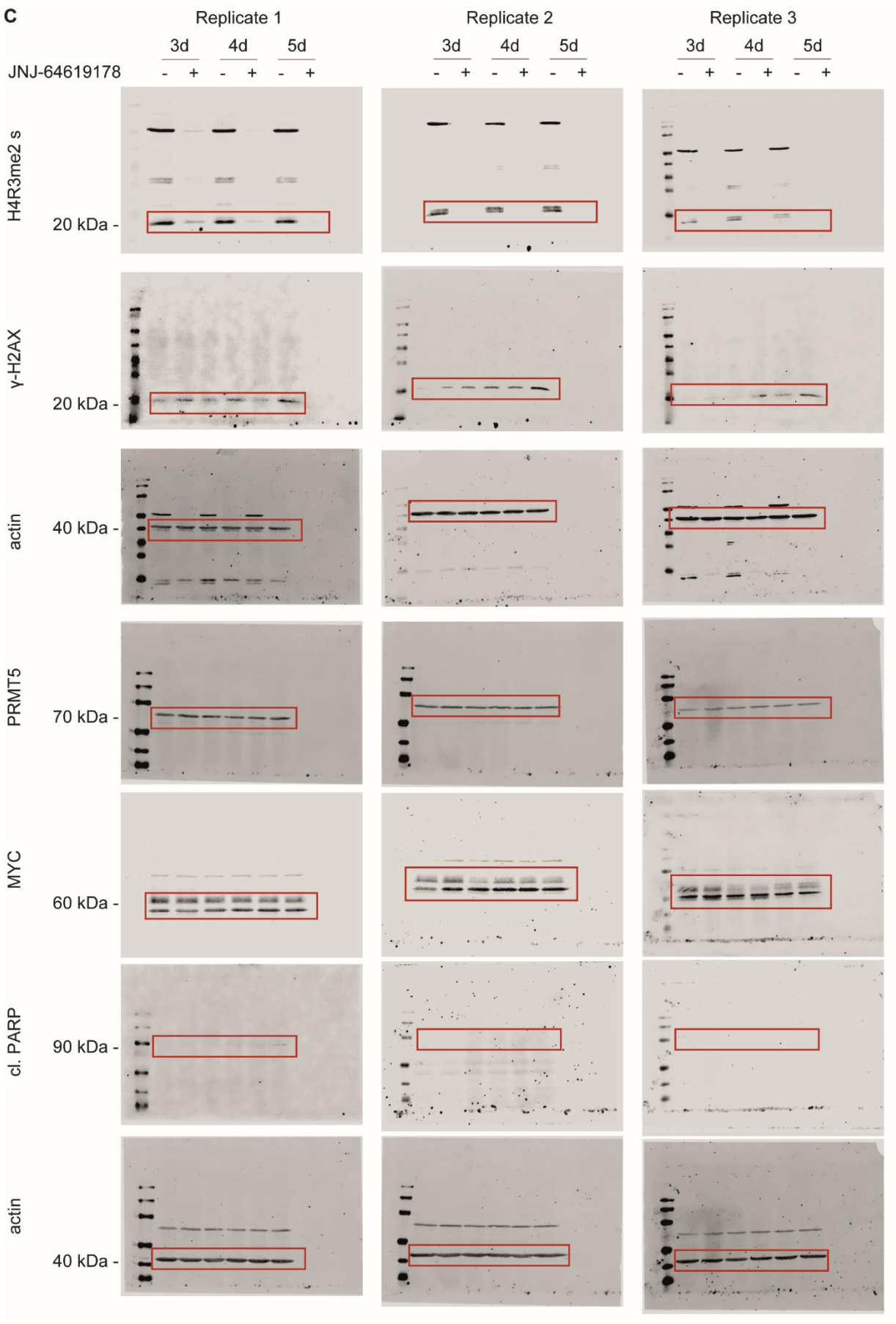
C
Replicate 1
Replicate 2
Replicate 3
3d
4d
5d
JNJ-64619178
- + - + - +
H4R3me2 s
20 kDa -
γ-H2AX
20 kDa -
actin
40 kDa -
PRMT5
70 kDa -
MYC
60 kDa -
cl. PARP
90 kDa -
actin
40 kDa -

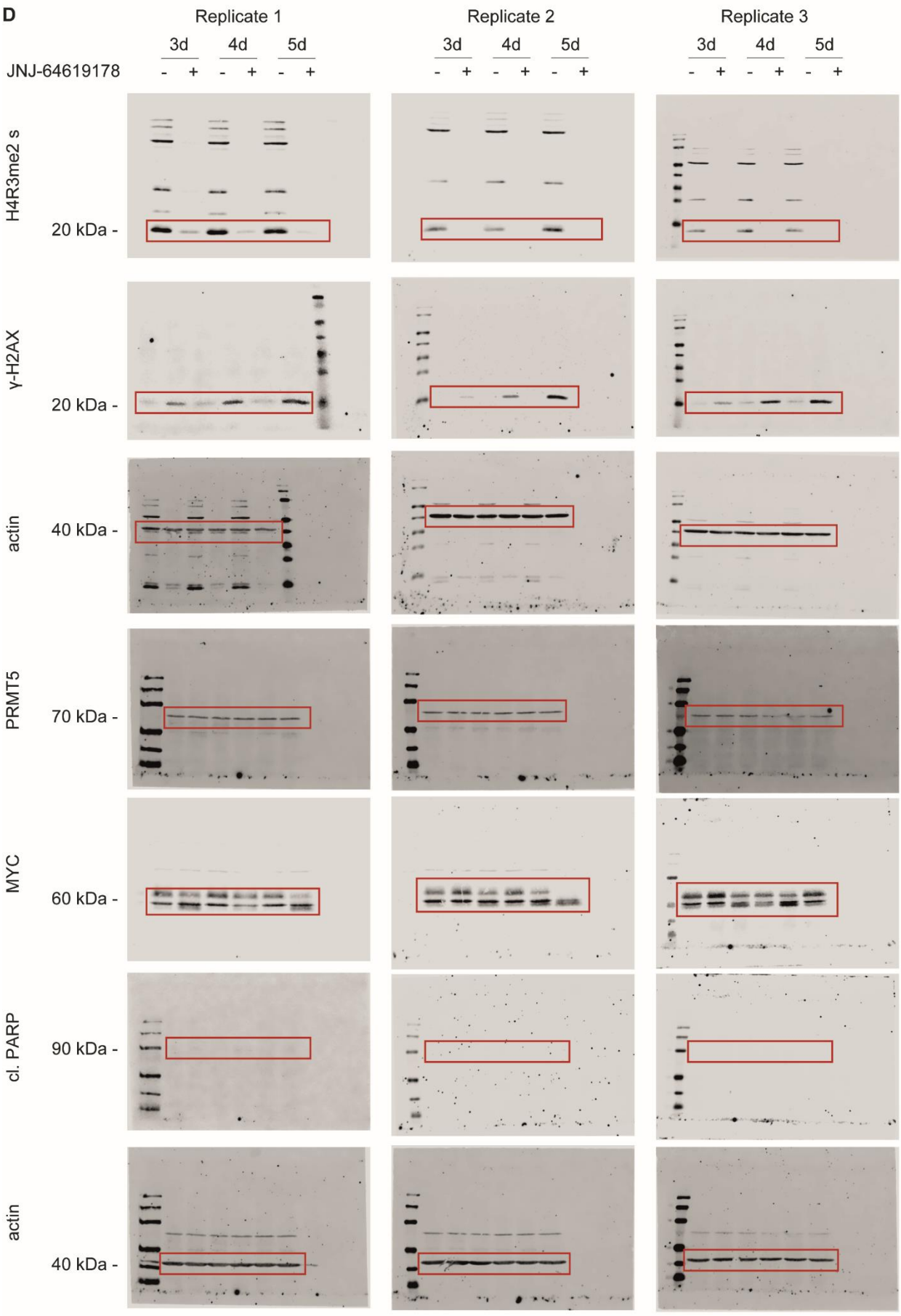
D
Replicate 1
Replicate 2
Replicate 3
3d
4d
5d
JNJ-64619178
- + - + - +
H4R3me2 s
20 kDa -
γ-H2AX
20 kDa -
actin
40 kDa -
PRMT5
70 kDa -
MYC
60 kDa -
cl. PARP
90 kDa -
actin
40 kDa -

Fig. S 5 Uncropped western blots of three replicates of Fig. 17
All three biological replicates described in Fig. 17 depicting H4R3me2 s, γ-H2AX, PRMT5, MYC, and cleaved PARP protein expression in four human PDAC cell lines: **A)** DanG, **B)** PSN1, **C)** Panc1, and **D)** PaTu-8988S.

X. Abbreviations

°C	Degree celsius
4-OHT	4-hydroxytamoxifen
5-FU	5-fluorouracil
ACCORD	Actions concertées dans les cancers colorectaux et digestifs
ADEX	Aberrantly differentiated endocrine exocrine subtype
ADP	Adenosine diphosphate
ALLIANCE	Alliance for clinical trials in oncology study
AML	Acute myeloid leukemia
AMPK	5' adenosine monophosphate-activated protein kinase
APS	Ammonium persulphate
ARF	ADP ribosylation factor
ARK5 (=NUAK1)	AMPK-related protein kinase 5
ASR	Age-standardized mortality rates using the world standard population
ATF6	Activating transcription factor 6
ATP	Adenosine triphosphate
AUC	Area under the curve
BAX	Bcl-2-associated X
Bcl-2	B-cell lymphoma 2
Bcl-xL	B-cell lymphoma-extra large
BET	Bromodomain and extra terminal domain
BH3-only	Bcl-2 homology domain 3 only proteins
bHLH-LZ	Basic helix loop helix leucine zipper
BIM	Bcl-2-interacting mediator of cell death
bp	Base pair
BRAF	V-Raf murine sarcoma viral oncogene homolog B
BRCA	Breast cancer gene
BRD	Bromodomain-containing protein
BSA	Bovine serum albumin
BUD31	Bud morphology abnormal gene homolog 31
CAD	Carbamoyl-phosphate synthetase 2, aspartate transcarbamylase, and dihydroorotase
CARM1	Coactivator-associated arginine methyltransferase 1
CCLE	Cancer Cell Line Encyclopedia
CDC2	Cell division cycle protein 2 homolog
CDK	Cyclin-dependent kinase
CDKN2A	Cyclin-dependent kinase inhibitor 2A
cDNA	Complementary deoxyribonucleic acid
CLNS1A	Chloride nucleotide-sensitive channel 1A
CNV	Copy number variation
CRC	Colorectal cancer
CRISPR	Clustered regularly interspaced short palindromic repeats
CSNK1e	Casein kinase 1 epsilon
CTF13	Centromere DNA-binding protein complex CBF3 subunit C
CTG	CellTiter-Glo assay
CTLA-4	cytotoxic T-lymphocyte-associated Protein 4
DLBCL	Diffuse large B-cell lymphoma
DMEM	Dulbecco`s Modified Eagle`s Medium
DMSO	Dimethyl sulfoxide

DNA	Deoxyribonucleic acid
DoRothEA	Discriminant Regulon Expression Analysis
DOT1L	Disruptor of telomeric silencing 1 like
DSB	Double strand break
E2F1	E2F transcription factor 1
EDTA	Ethylenediaminetetraacetic acid
EGFR	Epidermal growth factor receptor
EGR1	Early growth response 1
EMT	Epithelial-mesenchymal-transition
ER	Endoplasmic reticulum
ERAD	ER-associated degradation
ERCC3	Excision repair cross-complementation group 3
ERK	extracellular-signal-regulated kinase
ESPAC	European Study Group for Pancreatic Cancer
EtOH	Ethanol
FBW7	F-box and WD repeat domain-containing 7
FCS	Fetal calf serum
FDA	Food and drug administration
FDR	False Discovery Rate
Fig	Figure
FOLFIRINOX	Folinic acid, fluorouracil, Irinotecan, Oxaliplatin
GAPDH	Glyceraldehyde 3-phosphate dehydrogenase
GBM	Glioblastoma multiforme
GI PRODIGE	Gastrointestinal *Partenariat de Recherche en Oncologie Digestive* (trial)
GNAS	Guanine nucleotide binding protein, alpha stimulating activity polypeptide
GRP78	78-kDa glucose regulated protein
GSEA	Gene Set Enrichment Analysis
GSK	GlaxoSmithKline
GSK3β	Glycogen synthase kinase 3 beta
HCC	Hepatocellular carcinoma
HDAC	Histone de-acetylase
HFF	Human foreskin fibroblasts
HIF-1α	Hypoxia-inducible factor 1-alpha
HMEC	Human mammary epithelial cell
hnRNP A1	Heterogeneous nuclear ribonucleoprotein A1
HR	Homologous recombination
HUWE1	HECT, UBA and WWE domain containing E3 ubiquitin protein ligase 1
IBP72	ICln-binding protein of 72 kD
IPMN	Intraductal papillary mucinous neoplasm
IRE1	Inositol-requiring enzyme 1
IRES	Internal ribosome entry site
JAK2	Janus kinase 2
JBP1	JAK-binding protein 1
JNJ	Johnson & Johnson
JSAP	Japanese Study Group of Adjuvant Therapy for Pancreatic Cancer
kb	Kilo bases
kDa	Kilo Dalton
KDM6A	Lysine Demethylase 6A
ko	Knock-out

KRAS	Kirsten rat sarcoma viral oncogene homolog
MAX	MYC-associated protein X
MB	MYC boxes
MCL-1	Myeloid cell leukemia 1
MCN	Mucinous cystic neoplasm
MEP50	Methylosome protein 50
MEK	Mitogen-activated protein kinase kinase
MIZ-1	Myc interacting zinc finger protein 1
ml	Milliliter
MLL	Mixed-lineage leukemia
mm	Millimeter
MM	Multiple myeloma
mM	Millimolar
mOS	Median overall survival
MPACT	Metastatic pancreatic adenocarcinoma clinical trial
mRNA	Messenger ribonucleic acid
MTA	5-Methylthioadenosine
MTAP	5-Methylthioadenosine phosphorylase
mTORC	Mechanistic target of rapamycin kinase complex
MTT	3-(4,5-dimethylthiazol-2-yl)-2,5-diphenyltetrazolium bromide
MW	Molecular weight
MYC	Myelocytomatosis oncogene
MYC-ER	MYC-estrogen-receptor fusion transgene
NEMO	NF-kappa-B essential modulator
NFκB	Nuclear factor 'kappa-light-chain-enhancer' of activated B-cells
NHEJ	Non-homologous end joining
NHL	Non-hodgkin lymphoma
nM	Nanomolar
nm	Nanometer
NOTCH	Neurogenic locus notch homolog protein
NOXA (=PMAIP1)	Phorbol-12-myristate-13-acetate-induced protein 1
NRF2	Nuclear factor erythroid 2-related factor 2
NSCLC	Non-small cell lung cancer
ODC	Ornithine decarboxylase
ORC6	Origin recognition complex subunit 6
p14/16/19	Protein 14/16/19
p53	Transformation related protein 53 (Mus musculus)
PALB2	Partner and localizer of BRCA2
PanIN	Pancreatic intraepithelial neoplasm
PARP	Poly (ADP-ribose) polymerase
PBS	Phosphate buffered saline
PCR	Polymerase chain reaction
PD-1	Programmed cell death protein 1
PDAC	Pancreatic ductal adenocarcinoma
PDO	Patient-derived organoid
PDX	Patient-derived xenograft
PERK	Protein kinase R-like endoplasmic reticulum kinase
PEST	Polypeptide sequence rich in proline (P), glutamic acid (E), serine (S), and threonine (T)

PET	Positron emission tomography
PI	Propidium iodide
PI3K	Phosphoinositide 3 kinase
PIM	Proviral integration of Moloney virus (kinase family)
PNET	Pancreatic neuroendocrine tumor
PP2A	Protein phosphatase 2A
PREOPANC	Preoperative chemoradiotherapy versus immediate surgery for resectable and borderline resectable pancreatic cancer
PRMT	Protein arginine methyltransferase
PROTAC	Proteolysis targeting chimera
qRT-PCR	Real-Time Quantitative Reverse Transcription Polymerase Chain Reaction
RAD51	Radiation sensitive 51
RB	Retinoblastoma
Rel.	Relative
RIOK	RIO kinase 1
RNA	Ribonucleic acid
RNAi	RNA interference
RNF-43	Ring finger protein 43
ROS	Reactive oxygen species
RPA	Replication protein A
rpm	Revolutions per minute
RPMI	Roswell Park Memorial Institute (medium)
RT	Room temperature
RUVBL1	RuvB-like 1
SAE	SUMO-activating enzyme
SAHA (=Vorinostat)	Suberanilohydroxamic acid
SAM	S-adenosyl methionine
SCF	Skp, Cullin, F-box containing complex
SD	Standard deviation
SDL	Synthetic dosage lethality
SDS	Sodium dodecyl sulphate
SEER	Surveillance, Epidemiology, and End Results (Program)
SEM	Standard error of mean
shRNA	Short hairpin RNA
siRNA	Small interfering RNA
SL	Synthetic lethality
SLAMseq	Thiol (SH)-linked alkylation for the metabolic sequencing of RNA
SMAD4	Mothers against decapentaplegic homolog 4
SMARCB1	SWI/SNF-related matrix-associated actin-dependent regulator of chromatin subfamily B member 1
SNP	Single nucleotide polymorphism
SUMO	Small ubiquitin-like modifier
TAD	Transactivation domain
TAE	Tris acetate EDTA
TBS	Tris buffered saline
TCGA	The Cancer Genome Atlas
TDP1	Tyrosyl-DNA phosphodiesterase 1
TEMED	N,N,N',N'-Tetramethylethylenediamine

TGF-β	Transforming growth factor beta
TIM barrel	Triose-phosphate isomerase barrel
TP53	Tumor protein 53 (Homo sapiens)
TRRAP	Transformation/Transcription Domain Associated Protein
Tris	Tris(hydroxymethyl)-aminomethane
UAE	Ubiquitin-activating enzyme
UPR	Unfolded protein response
UPS	Ubiquitin proteasome system
USP28	Ubiquitin specific peptidase 28
V	Volt
VCP	Valosin-containing protein
v/v	Volume per volume
w/v	Weight per volume
Wnt	Wingless-related integration site
wt	Wild type
XBP1	X-box binding protein 1
XIAP	X-linked inhibitor of apoptosis protein
ZIP	Zero interaction potency
µl	Microliter
µM	Micromolar
µm	Micrometer

XI. Figures

Fig. 1 Concept of synthetic lethality ... 18
Fig. 2 MYC protein expression and morphology of human PDAC cell lines ... 42
Fig. 3 Growth curves of human PDAC cell lines used for screening ... 43
Fig. 4 Unbiased FDA-approved anticancer drug screen in human PDAC cell lines with differential MYC expression ... 45
Fig. 5 Validation of FDA-approved anticancer drug screen ... 47
Fig. 6 Proteasome inhibitor sensitivity in MYC genetic gain-of-function ... 48
Fig. 7 Priming of PDAC cells with MYC overexpression for proteasome inhibitor-induced apoptosis ... 49
Fig. 8 UEA-inhibitor sensitivity in human PDAC cell lines and MYC genetic gain-of-function ... 51
Fig. 9 Unbiased epigenetic drug screen in epithelial and mesenchymal fractions of murine PDAC cell lines ... 54
Fig. 10 Unbiased epigenetic drug screen in human PDAC cell lines with differential MYC expression ... 55
Fig. 11 Connection between MYC and PRMT5 in PDAC ... 56
Fig. 12 Dose response of human PDAC lines with different MYC status to PRMT5 inhibitors ... 57
Fig. 13 Clonogenic growth assays of human PDAC lines with different MYC status treated with PRMT5 inhibitors ... 58
Fig. 14 Clonogenic growth in human PDAC lines with different MYC levels after treatment with PRMT5 inhibitors ... 59
Fig. 15 Sensitivity for PRMT5 inhibitors in a murine model with MYC activation ... 60
Fig. 16 Apoptosis and cell cycle measurement in PDAC cells after PRMT5 inhibitor treatment ... 63
Fig. 17 Protein expression of human PDAC cell lines after PRMT5 inhibition ... 63
Fig. 18 PRMT5 inhibition in primary human PDAC cell lines ... 66
Fig. 19 Graphical abstract ... 76

Fig. S 1 Uncropped western blots of three replicates of Fig. 2A ... 86
Fig. S 2 Uncropped western blots of three replicates of Fig. 7A ... 89
Fig. S 3 Uncropped western blots of four replicates of Fig. 9B ... 90
Fig. S 4 Uncropped western blots of three replicates in Fig. 11 ... 91
Fig. S 5 Uncropped western blots of three replicates of Fig. 17 ... 96

XII. Tables

Tab. 1 Doubling Times of human PDAC cell lines ... 44
Tab. 2 ZIP scores of various inhibitors with PRMT5i ... 64

Tab.S 1 List of compounds and responses from the FDA-approved drug screen ... 77
Tab.S 2 List of compounds and responses from the epigenetic drug screen ... 80

XIII. References

1 seer.cancer.gov. <https://seer.cancer.gov/statfacts/html/pancreas.html> (accessed on 26.10.2020).

2 Rahib, L. *et al.* Projecting cancer incidence and deaths to 2030: the unexpected burden of thyroid, liver, and pancreas cancers in the United States. *Cancer research* **74**, 2913-2921, doi:10.1158/0008-5472.CAN-14-0155 (2014).

3 Malvezzi, M. *et al.* European cancer mortality predictions for the year 2019 with focus on breast cancer. *Ann Oncol* **30**, 781-787, doi:10.1093/annonc/mdz051 (2019).

4 Ilic, M. & Ilic, I. Epidemiology of pancreatic cancer. *World J Gastroenterol* **22**, 9694-9705, doi:10.3748/wjg.v22.i44.9694 (2016).

5 McGuigan, A. *et al.* Pancreatic cancer: A review of clinical diagnosis, epidemiology, treatment and outcomes. *World J Gastroenterol* **24**, 4846-4861, doi:10.3748/wjg.v24.i43.4846 (2018).

6 Spanknebel, K. & Conlon, K. C. Advances in the surgical management of pancreatic cancer. *Cancer J* **7**, 312-323 (2001).

7 Clinicaltrials.gov. <https://www.clinicaltrials.gov/ct2/results?cond=Pancreatic+Cancer&term=&cntry=&state=&city=&dist=> (accessed on 26.10.2020).

8 Vincent, A., Herman, J., Schulick, R., Hruban, R. H. & Goggins, M. Pancreatic cancer. *Lancet* **378**, 607-620, doi:10.1016/s0140-6736(10)62307-0 (2011).

9 Bond-Smith, G., Banga, N., Hammond, T. M. & Imber, C. J. Pancreatic adenocarcinoma. *Bmj* **344**, e2476, doi:10.1136/bmj.e2476 (2012).

10 Pishvaian, M. J. & Brody, J. R. Therapeutic Implications of Molecular Subtyping for Pancreatic Cancer. *Oncology (Williston Park)* **31**, 159-166, 168 (2017).

11 Distler, M., Aust, D., Weitz, J., Pilarsky, C. & Grützmann, R. Precursor lesions for sporadic pancreatic cancer: PanIN, IPMN, and MCN. *Biomed Res Int* **2014**, 474905, doi:10.1155/2014/474905 (2014).

12 Hruban, R. H. *et al.* Pancreatic intraepithelial neoplasia: a new nomenclature and classification system for pancreatic duct lesions. *Am J Surg Pathol* **25**, 579-586, doi:10.1097/00000478-200105000-00003 (2001).

13 Wu, J. *et al.* Recurrent GNAS mutations define an unexpected pathway for pancreatic cyst development. *Sci Transl Med* **3**, 92ra66, doi:10.1126/scitranslmed.3002543 (2011).

14 Kanda, M. *et al.* Presence of somatic mutations in most early-stage pancreatic intraepithelial neoplasia. *Gastroenterology* **142**, 730-733.e739, doi:10.1053/j.gastro.2011.12.042 (2012).

15 Zamboni, G., Hirabayashi, K., Castelli, P. & Lennon, A. M. Precancerous lesions of the pancreas. *Best Pract Res Clin Gastroenterol* **27**, 299-322, doi:10.1016/j.bpg.2013.04.001 (2013).

16 Caldas, C. *et al.* Frequent somatic mutations and homozygous deletions of the p16 (MTS1) gene in pancreatic adenocarcinoma. *Nature genetics* **8**, 27-32, doi:10.1038/ng0994-27 (1994).

17 Caldas, C. & Kern, S. E. K-ras mutation and pancreatic adenocarcinoma. *Int J Pancreatol* **18**, 1-6, doi:10.1007/bf02825415 (1995).

18 Rozenblum, E. *et al.* Tumor-suppressive pathways in pancreatic carcinoma. *Cancer research* **57**, 1731-1734 (1997).

19 Mueller, S. *et al.* Evolutionary routes and KRAS dosage define pancreatic cancer phenotypes. *Nature* **554**, 62-68, doi:10.1038/nature25459 (2018).

20 Zhou, B. *et al.* Early detection of pancreatic cancer: Where are we now and where are we going? *Int J Cancer* **141**, 231-241, doi:10.1002/ijc.30670 (2017).

21 Roth, M. T., Cardin, D. B. & Berlin, J. D. Recent advances in the treatment of pancreatic cancer. *F1000Res* **9**, doi:10.12688/f1000research.21981.1 (2020).

22 Neoptolemos, J. P. *et al.* Comparison of adjuvant gemcitabine and capecitabine with gemcitabine monotherapy in patients with resected pancreatic cancer (ESPAC-4): a multicentre, open-label, randomised, phase 3 trial. *Lancet* **389**, 1011-1024, doi:10.1016/s0140-6736(16)32409-6 (2017).

23 Conroy, T. *et al.* FOLFIRINOX or Gemcitabine as Adjuvant Therapy for Pancreatic Cancer. *N Engl J Med* **379**, 2395-2406, doi:10.1056/NEJMoa1809775 (2018).
24 Conroy, T. *et al.* FOLFIRINOX versus gemcitabine for metastatic pancreatic cancer. *N Engl J Med* **364**, 1817-1825, doi:10.1056/NEJMoa1011923 (2011).
25 Von Hoff, D. D. *et al.* Increased survival in pancreatic cancer with nab-paclitaxel plus gemcitabine. *N Engl J Med* **369**, 1691-1703, doi:10.1056/NEJMoa1304369 (2013).
26 Katz, M. H. G. *et al.* Alliance for clinical trials in oncology (ALLIANCE) trial A021501: preoperative extended chemotherapy vs. chemotherapy plus hypofractionated radiation therapy for borderline resectable adenocarcinoma of the head of the pancreas. *BMC Cancer* **17**, 505, doi:10.1186/s12885-017-3441-z (2017).
27 Versteijne, E. *et al.* Preoperative Chemoradiotherapy Versus Immediate Surgery for Resectable and Borderline Resectable Pancreatic Cancer: Results of the Dutch Randomized Phase III PREOPANC Trial. *J Clin Oncol* **38**, 1763-1773, doi:10.1200/jco.19.02274 (2020).
28 Henriksen, A., Dyhl-Polk, A., Chen, I. & Nielsen, D. Checkpoint inhibitors in pancreatic cancer. *Cancer Treat Rev* **78**, 17-30, doi:10.1016/j.ctrv.2019.06.005 (2019).
29 Upadhrasta, S. & Zheng, L. Strategies in Developing Immunotherapy for Pancreatic Cancer: Recognizing and Correcting Multiple Immune "Defects" in the Tumor Microenvironment. *J Clin Med* **8**, doi:10.3390/jcm8091472 (2019).
30 Rouanet, M. *et al.* Gene Therapy for Pancreatic Cancer: Specificity, Issues and Hopes. *Int J Mol Sci* **18**, doi:10.3390/ijms18061231 (2017).
31 Motoi, F. *et al.* Randomized phase II/III trial of neoadjuvant chemotherapy with gemcitabine and S-1 versus upfront surgery for resectable pancreatic cancer (Prep-02/JSAP05). *Jpn J Clin Oncol* **49**, 190-194, doi:10.1093/jjco/hyy190 (2019).
32 Ghaneh, P. *et al.* ESPAC-5F: Four-arm, prospective, multicenter, international randomized phase II trial of immediate surgery compared with neoadjuvant gemcitabine plus capecitabine (GEMCAP) or FOLFIRINOX or chemoradiotherapy (CRT) in patients with borderline resectable pancreatic cancer. *Journal of Clinical Oncology* **38**, 4505-4505, doi:10.1200/JCO.2020.38.15_suppl.4505 (2020).
33 Katz, M. H. *et al.* Preoperative Modified FOLFIRINOX Treatment Followed by Capecitabine-Based Chemoradiation for Borderline Resectable Pancreatic Cancer: Alliance for Clinical Trials in Oncology Trial A021101. *JAMA Surg* **151**, e161137, doi:10.1001/jamasurg.2016.1137 (2016).
34 Golan, T. *et al.* Overall survival and clinical characteristics of pancreatic cancer in BRCA mutation carriers. *Br J Cancer* **111**, 1132-1138, doi:10.1038/bjc.2014.418 (2014).
35 Golan, T. *et al.* Maintenance Olaparib for Germline BRCA-Mutated Metastatic Pancreatic Cancer. *N Engl J Med* **381**, 317-327, doi:10.1056/NEJMoa1903387 (2019).
36 O'Reilly, E. M. *et al.* Phase IB trial of cisplatin (C), gemcitabine (G), and veliparib (V) in patients with known or potential BRCA or PALB2-mutated pancreas adenocarcinoma (PC). *Journal of Clinical Oncology* **32**, 4023-4023, doi:10.1200/jco.2014.32.15_suppl.4023 (2014).
37 Lowery, M. A. *et al.* Phase II trial of veliparib in patients with previously treated BRCA-mutated pancreas ductal adenocarcinoma. *Eur J Cancer* **89**, 19-26, doi:10.1016/j.ejca.2017.11.004 (2018).
38 Jones, S. *et al.* Core signaling pathways in human pancreatic cancers revealed by global genomic analyses. *Science* **321**, 1801-1806, doi:10.1126/science.1164368 (2008).
39 Collisson, E. A. *et al.* Subtypes of pancreatic ductal adenocarcinoma and their differing responses to therapy. *Nature medicine* **17**, 500-503, doi:10.1038/nm.2344 (2011).
40 Badea, L., Herlea, V., Dima, S. O., Dumitrascu, T. & Popescu, I. Combined gene expression analysis of whole-tissue and microdissected pancreatic ductal adenocarcinoma identifies genes specifically overexpressed in tumor epithelia. *Hepatogastroenterology* **55**, 2016-2027 (2008).
41 Biankin, A. V. *et al.* Pancreatic cancer genomes reveal aberrations in axon guidance pathway genes. *Nature* **491**, 399-405, doi:10.1038/nature11547 (2012).

42 Waddell, N. *et al.* Whole genomes redefine the mutational landscape of pancreatic cancer. *Nature* **518**, 495-501, doi:10.1038/nature14169 (2015).
43 Moffitt, R. A. *et al.* Virtual microdissection identifies distinct tumor- and stroma-specific subtypes of pancreatic ductal adenocarcinoma. *Nature genetics* **47**, 1168-1178, doi:10.1038/ng.3398 (2015).
44 Witkiewicz, A. K. *et al.* Whole-exome sequencing of pancreatic cancer defines genetic diversity and therapeutic targets. *Nature communications* **6**, 6744, doi:10.1038/ncomms7744 (2015).
45 Bailey, P. *et al.* Genomic analyses identify molecular subtypes of pancreatic cancer. *Nature* **531**, 47-52, doi:10.1038/nature16965 (2016).
46 Chan-Seng-Yue, M. *et al.* Transcription phenotypes of pancreatic cancer are driven by genomic events during tumor evolution. *Nature genetics* **52**, 231-240, doi:10.1038/s41588-019-0566-9 (2020).
47 Topham, J. T. *et al.* Subtype-Discordant Pancreatic Ductal Adenocarcinoma Tumors Show Intermediate Clinical and Molecular Characteristics. *Clinical cancer research : an official journal of the American Association for Cancer Research* **27**, 150-157, doi:10.1158/1078-0432.ccr-20-2831 (2021).
48 Garnett, M. J. *et al.* Systematic identification of genomic markers of drug sensitivity in cancer cells. *Nature* **483**, 570-575, doi:10.1038/nature11005 (2012).
49 Garnett, M. J. & McDermott, U. The evolving role of cancer cell line-based screens to define the impact of cancer genomes on drug response. *Curr Opin Genet Dev* **24**, 114-119, doi:10.1016/j.gde.2013.12.002 (2014).
50 Barretina, J. *et al.* The Cancer Cell Line Encyclopedia enables predictive modelling of anticancer drug sensitivity. *Nature* **483**, 603-607, doi:10.1038/nature11003 (2012).
51 Tiriac, H. *et al.* Organoid Profiling Identifies Common Responders to Chemotherapy in Pancreatic Cancer. *Cancer discovery* **8**, 1112-1129, doi:10.1158/2159-8290.cd-18-0349 (2018).
52 Iorio, F. *et al.* A Landscape of Pharmacogenomic Interactions in Cancer. *Cell* **166**, 740-754, doi:10.1016/j.cell.2016.06.017 (2016).
53 Schlaeger, C. *et al.* Etiology-dependent molecular mechanisms in human hepatocarcinogenesis. *Hepatology* **47**, 511-520, doi:10.1002/hep.22033 (2008).
54 Lin, C. P., Liu, C. R., Lee, C. N., Chan, T. S. & Liu, H. E. Targeting c-Myc as a novel approach for hepatocellular carcinoma. *World J Hepatol* **2**, 16-20, doi:10.4254/wjh.v2.i1.16 (2010).
55 Zhang, T., Li, N., Sun, C., Jin, Y. & Sheng, X. MYC and the unfolded protein response in cancer: synthetic lethal partners in crime? *EMBO Mol Med* **12**, e11845, doi:10.15252/emmm.201911845 (2020).
56 Ciriello, G. *et al.* Emerging landscape of oncogenic signatures across human cancers. *Nature genetics* **45**, 1127-1133, doi:10.1038/ng.2762 (2013).
57 Schleger, C., Verbeke, C., Hildenbrand, R., Zentgraf, H. & Bleyl, U. c-MYC activation in primary and metastatic ductal adenocarcinoma of the pancreas: incidence, mechanisms, and clinical significance. *Mod Pathol* **15**, 462-469, doi:10.1038/modpathol.3880547 (2002).
58 Wirth, M. & Schneider, G. MYC: A Stratification Marker for Pancreatic Cancer Therapy. *Trends Cancer* **2**, 1-3, doi:10.1016/j.trecan.2015.12.002 (2016).
59 Karasinska, J. M. *et al.* Altered Gene Expression along the Glycolysis-Cholesterol Synthesis Axis Is Associated with Outcome in Pancreatic Cancer. *Clinical cancer research : an official journal of the American Association for Cancer Research* **26**, 135-146, doi:10.1158/1078-0432.ccr-19-1543 (2020).
60 Sodir, N. M. *et al.* MYC Instructs and Maintains Pancreatic Adenocarcinoma Phenotype. *Cancer discovery* **10**, 588-607, doi:10.1158/2159-8290.cd-19-0435 (2020).
61 Muthalagu, N. *et al.* Repression of the Type I Interferon Pathway Underlies MYC- and KRAS-Dependent Evasion of NK and B Cells in Pancreatic Ductal Adenocarcinoma. *Cancer discovery* **10**, 872-887, doi:10.1158/2159-8290.cd-19-0620 (2020).

62 Bhattacharyya, S. *et al.* Acidic fibroblast growth factor underlies microenvironmental regulation of MYC in pancreatic cancer. *The Journal of experimental medicine* **217**, doi:10.1084/jem.20191805 (2020).
63 Holland, J. P. *et al.* Annotating MYC status with 89Zr-transferrin imaging. *Nature medicine* **18**, 1586-1591, doi:10.1038/nm.2935 (2012).
64 Dang, C. V. MYC on the path to cancer. *Cell* **149**, 22-35, doi:10.1016/j.cell.2012.03.003 (2012).
65 Malynn, B. A. *et al.* N-myc can functionally replace c-myc in murine development, cellular growth, and differentiation. *Genes Dev* **14**, 1390-1399 (2000).
66 Brodeur, G. M., Seeger, R. C., Schwab, M., Varmus, H. E. & Bishop, J. M. Amplification of N-myc in untreated human neuroblastomas correlates with advanced disease stage. *Science* **224**, 1121-1124, doi:10.1126/science.6719137 (1984).
67 Nau, M. M. *et al.* L-myc, a new myc-related gene amplified and expressed in human small cell lung cancer. *Nature* **318**, 69-73, doi:10.1038/318069a0 (1985).
68 Duesberg, P. H. & Vogt, P. K. Avian acute leukemia viruses MC29 and MH2 share specific RNA sequences: evidence for a second class of transforming genes. *Proc Natl Acad Sci U S A* **76**, 1633-1637, doi:10.1073/pnas.76.4.1633 (1979).
69 Vennstrom, B., Sheiness, D., Zabielski, J. & Bishop, J. M. Isolation and characterization of c-myc, a cellular homolog of the oncogene (v-myc) of avian myelocytomatosis virus strain 29. *J Virol* **42**, 773-779, doi:10.1128/jvi.42.3.773-779.1982 (1982).
70 Dalla-Favera, R. *et al.* Human c-myc onc gene is located on the region of chromosome 8 that is translocated in Burkitt lymphoma cells. *Proc Natl Acad Sci U S A* **79**, 7824-7827, doi:10.1073/pnas.79.24.7824 (1982).
71 Blackwood, E. M. & Eisenman, R. N. Max: a helix-loop-helix zipper protein that forms a sequence-specific DNA-binding complex with Myc. *Science* **251**, 1211-1217, doi:10.1126/science.2006410 (1991).
72 Schneider, A., Peukert, K., Eilers, M. & Hänel, F. Association of Myc with the zinc-finger protein Miz-1 defines a novel pathway for gene regulation by Myc. *Curr Top Microbiol Immunol* **224**, 137-146, doi:10.1007/978-3-642-60801-8_14 (1997).
73 Wiese, K. E. *et al.* The role of MIZ-1 in MYC-dependent tumorigenesis. *Cold Spring Harb Perspect Med* **3**, a014290, doi:10.1101/cshperspect.a014290 (2013).
74 Beaulieu, M. E., Castillo, F. & Soucek, L. Structural and Biophysical Insights into the Function of the Intrinsically Disordered Myc Oncoprotein. *Cells* **9**, doi:10.3390/cells9041038 (2020).
75 Boxer, L. M. & Dang, C. V. Translocations involving c-myc and c-myc function. *Oncogene* **20**, 5595-5610, doi:10.1038/sj.onc.1204595 (2001).
76 Grandori, C. *et al.* c-Myc binds to human ribosomal DNA and stimulates transcription of rRNA genes by RNA polymerase I. *Nat Cell Biol* **7**, 311-318, doi:10.1038/ncb1224 (2005).
77 Gomez-Roman, N., Grandori, C., Eisenman, R. N. & White, R. J. Direct activation of RNA polymerase III transcription by c-Myc. *Nature* **421**, 290-294, doi:10.1038/nature01327 (2003).
78 Adhikary, S. & Eilers, M. Transcriptional regulation and transformation by Myc proteins. *Nat Rev Mol Cell Biol* **6**, 635-645, doi:10.1038/nrm1703 (2005).
79 Fletcher, S. & Prochownik, E. V. Small-molecule inhibitors of the Myc oncoprotein. *Biochim Biophys Acta* **1849**, 525-543, doi:10.1016/j.bbagrm.2014.03.005 (2015).
80 Hsieh, A. L. & Dang, C. V. MYC, Metabolic Synthetic Lethality, and Cancer. *Recent Results Cancer Res* **207**, 73-91, doi:10.1007/978-3-319-42118-6_4 (2016).
81 Wolf, E., Lin, C. Y., Eilers, M. & Levens, D. L. Taming of the beast: shaping Myc-dependent amplification. *Trends Cell Biol* **25**, 241-248, doi:10.1016/j.tcb.2014.10.006 (2015).
82 Lin, C. Y. *et al.* Transcriptional amplification in tumor cells with elevated c-Myc. *Cell* **151**, 56-67, doi:10.1016/j.cell.2012.08.026 (2012).
83 Baluapuri, A., Wolf, E. & Eilers, M. Target gene-independent functions of MYC oncoproteins. *Nat Rev Mol Cell Biol* **21**, 255-267, doi:10.1038/s41580-020-0215-2 (2020).

84 Johnston, L. A., Prober, D. A., Edgar, B. A., Eisenman, R. N. & Gallant, P. Drosophila myc regulates cellular growth during development. *Cell* **98**, 779-790, doi:10.1016/s0092-8674(00)81512-3 (1999).
85 Land, H., Parada, L. F. & Weinberg, R. A. Tumorigenic conversion of primary embryo fibroblasts requires at least two cooperating oncogenes. *Nature* **304**, 596-602, doi:10.1038/304596a0 (1983).
86 Iritani, B. M. & Eisenman, R. N. c-Myc enhances protein synthesis and cell size during B lymphocyte development. *Proc Natl Acad Sci U S A* **96**, 13180-13185, doi:10.1073/pnas.96.23.13180 (1999).
87 Baudino, T. A. *et al.* c-Myc is essential for vasculogenesis and angiogenesis during development and tumor progression. *Genes Dev* **16**, 2530-2543, doi:10.1101/gad.1024602 (2002).
88 Stine, Z. E., Walton, Z. E., Altman, B. J., Hsieh, A. L. & Dang, C. V. MYC, Metabolism, and Cancer. *Cancer discovery* **5**, 1024-1039, doi:10.1158/2159-8290.cd-15-0507 (2015).
89 Freytag, S. O. & Geddes, T. J. Reciprocal regulation of adipogenesis by Myc and C/EBP alpha. *Science* **256**, 379-382, doi:10.1126/science.256.5055.379 (1992).
90 Felsher, D. W. & Bishop, J. M. Transient excess of MYC activity can elicit genomic instability and tumorigenesis. *Proc Natl Acad Sci U S A* **96**, 3940-3944, doi:10.1073/pnas.96.7.3940 (1999).
91 Mateyak, M. K., Obaya, A. J., Adachi, S. & Sedivy, J. M. Phenotypes of c-Myc-deficient rat fibroblasts isolated by targeted homologous recombination. *Cell Growth Differ* **8**, 1039-1048 (1997).
92 Herold, S. *et al.* Negative regulation of the mammalian UV response by Myc through association with Miz-1. *Mol Cell* **10**, 509-521, doi:10.1016/s1097-2765(02)00633-0 (2002).
93 Pelengaris, S., Khan, M. & Evan, G. I. Suppression of Myc-induced apoptosis in beta cells exposes multiple oncogenic properties of Myc and triggers carcinogenic progression. *Cell* **109**, 321-334, doi:10.1016/s0092-8674(02)00738-9 (2002).
94 Adams, J. M. *et al.* The c-myc oncogene driven by immunoglobulin enhancers induces lymphoid malignancy in transgenic mice. *Nature* **318**, 533-538, doi:10.1038/318533a0 (1985).
95 Jain, M. *et al.* Sustained loss of a neoplastic phenotype by brief inactivation of MYC. *Science* **297**, 102-104, doi:10.1126/science.1071489 (2002).
96 Gurel, B. *et al.* Nuclear MYC protein overexpression is an early alteration in human prostate carcinogenesis. *Mod Pathol* **21**, 1156-1167, doi:10.1038/modpathol.2008.111 (2008).
97 Palaskas, N. *et al.* 18F-fluorodeoxy-glucose positron emission tomography marks MYC-overexpressing human basal-like breast cancers. *Cancer research* **71**, 5164-5174, doi:10.1158/0008-5472.can-10-4633 (2011).
98 Mazur, P. K. *et al.* Notch2 is required for progression of pancreatic intraepithelial neoplasia and development of pancreatic ductal adenocarcinoma. *Proc Natl Acad Sci U S A* **107**, 13438-13443, doi:10.1073/pnas.1002423107 (2010).
99 Schild, C. *et al.* PI3K signaling maintains c-myc expression to regulate transcription of E2F1 in pancreatic cancer cells. *Mol Carcinog* **48**, 1149-1158, doi:10.1002/mc.20569 (2009).
100 Gysin, S., Paquette, J. & McMahon, M. Analysis of mRNA profiles after MEK1/2 inhibition in human pancreatic cancer cell lines reveals pathways involved in drug sensitivity. *Mol Cancer Res* **10**, 1607-1619, doi:10.1158/1541-7786.mcr-12-0188 (2012).
101 Grippo, P. J. & Sandgren, E. P. Acinar-to-ductal metaplasia accompanies c-myc-induced exocrine pancreatic cancer progression in transgenic rodents. *Int J Cancer* **131**, 1243-1248, doi:10.1002/ijc.27322 (2012).
102 Diersch, S. *et al.* Kras(G12D) induces EGFR-MYC cross signaling in murine primary pancreatic ductal epithelial cells. *Oncogene* **35**, 3880-3886, doi:10.1038/onc.2015.437 (2016).
103 Hessmann, E., Schneider, G., Ellenrieder, V. & Siveke, J. T. MYC in pancreatic cancer: novel mechanistic insights and their translation into therapeutic strategies. *Oncogene* **35**, 1609-1618, doi:10.1038/onc.2015.216 (2016).

104 Evan, G. I. *et al.* Induction of apoptosis in fibroblasts by c-myc protein. *Cell* **69**, 119-128, doi:10.1016/0092-8674(92)90123-t (1992).
105 Zindy, F. *et al.* Myc signaling via the ARF tumor suppressor regulates p53-dependent apoptosis and immortalization. *Genes Dev* **12**, 2424-2433, doi:10.1101/gad.12.15.2424 (1998).
106 Juin, P., Hueber, A. O., Littlewood, T. & Evan, G. c-Myc-induced sensitization to apoptosis is mediated through cytochrome c release. *Genes Dev* **13**, 1367-1381, doi:10.1101/gad.13.11.1367 (1999).
107 Mitchell, K. O. *et al.* Bax is a transcriptional target and mediator of c-myc-induced apoptosis. *Cancer research* **60**, 6318-6325 (2000).
108 Egle, A., Harris, A. W., Bouillet, P. & Cory, S. Bim is a suppressor of Myc-induced mouse B cell leukemia. *Proc Natl Acad Sci U S A* **101**, 6164-6169, doi:10.1073/pnas.0401471101 (2004).
109 Eischen, C. M., Woo, D., Roussel, M. F. & Cleveland, J. L. Apoptosis triggered by Myc-induced suppression of Bcl-X(L) or Bcl-2 is bypassed during lymphomagenesis. *Mol Cell Biol* **21**, 5063-5070, doi:10.1128/mcb.21.15.5063-5070.2001 (2001).
110 Strasser, A., Harris, A. W., Bath, M. L. & Cory, S. Novel primitive lymphoid tumours induced in transgenic mice by cooperation between myc and bcl-2. *Nature* **348**, 331-333, doi:10.1038/348331a0 (1990).
111 Vafa, O. *et al.* c-Myc can induce DNA damage, increase reactive oxygen species, and mitigate p53 function: a mechanism for oncogene-induced genetic instability. *Mol Cell* **9**, 1031-1044, doi:10.1016/s1097-2765(02)00520-8 (2002).
112 Wirth, M., Mahboobi, S., Krämer, O. H. & Schneider, G. Concepts to Target MYC in Pancreatic Cancer. *Molecular cancer therapeutics* **15**, 1792-1798, doi:10.1158/1535-7163.mct-16-0050 (2016).
113 Allen-Petersen, B. L. & Sears, R. C. Mission Possible: Advances in MYC Therapeutic Targeting in Cancer. *BioDrugs* **33**, 539-553, doi:10.1007/s40259-019-00370-5 (2019).
114 Soucek, L. *et al.* Omomyc, a potential Myc dominant negative, enhances Myc-induced apoptosis. *Cancer research* **62**, 3507-3510 (2002).
115 Soucek, L. *et al.* Modelling Myc inhibition as a cancer therapy. *Nature* **455**, 679-683, doi:10.1038/nature07260 (2008).
116 Massó-Vallés, D. & Soucek, L. Blocking Myc to Treat Cancer: Reflecting on Two Decades of Omomyc. *Cells* **9**, doi:10.3390/cells9040883 (2020).
117 Kiessling, A., Sperl, B., Hollis, A., Eick, D. & Berg, T. Selective inhibition of c-Myc/Max dimerization and DNA binding by small molecules. *Chem Biol* **13**, 745-751, doi:10.1016/j.chembiol.2006.05.011 (2006).
118 Stellas, D. *et al.* Therapeutic effects of an anti-Myc drug on mouse pancreatic cancer. *J Natl Cancer Inst* **106**, doi:10.1093/jnci/dju320 (2014).
119 Yin, X., Giap, C., Lazo, J. S. & Prochownik, E. V. Low molecular weight inhibitors of Myc-Max interaction and function. *Oncogene* **22**, 6151-6159, doi:10.1038/sj.onc.1206641 (2003).
120 Zhang, M., Fan, H. Y. & Li, S. C. Inhibition of c-Myc by 10058-F4 induces growth arrest and chemosensitivity in pancreatic ductal adenocarcinoma. *Biomed Pharmacother* **73**, 123-128, doi:10.1016/j.biopha.2015.05.019 (2015).
121 Guo, J. *et al.* Efficacy, pharmacokinetics, tisssue distribution, and metabolism of the Myc-Max disruptor, 10058-F4 [Z,E]-5-[4-ethylbenzylidine]-2-thioxothiazolidin-4-one, in mice. *Cancer Chemother Pharmacol* **63**, 615-625, doi:10.1007/s00280-008-0774-y (2009).
122 Zuber, J. *et al.* RNAi screen identifies Brd4 as a therapeutic target in acute myeloid leukaemia. *Nature* **478**, 524-528, doi:10.1038/nature10334 (2011).
123 Nicodeme, E. *et al.* Suppression of inflammation by a synthetic histone mimic. *Nature* **468**, 1119-1123, doi:10.1038/nature09589 (2010).
124 Filippakopoulos, P. *et al.* Selective inhibition of BET bromodomains. *Nature* **468**, 1067-1073, doi:10.1038/nature09504 (2010).
125 Delmore, J. E. *et al.* BET bromodomain inhibition as a therapeutic strategy to target c-Myc. *Cell* **146**, 904-917, doi:10.1016/j.cell.2011.08.017 (2011).

126 Sahai, V. *et al.* BET bromodomain inhibitors block growth of pancreatic cancer cells in three-dimensional collagen. *Molecular cancer therapeutics* **13**, 1907-1917, doi:10.1158/1535-7163.mct-13-0925 (2014).
127 Garcia, P. L. *et al.* The BET bromodomain inhibitor JQ1 suppresses growth of pancreatic ductal adenocarcinoma in patient-derived xenograft models. *Oncogene* **35**, 833-845, doi:10.1038/onc.2015.126 (2016).
128 Muhar, M. *et al.* SLAM-seq defines direct gene-regulatory functions of the BRD4-MYC axis. *Science* **360**, 800-805, doi:10.1126/science.aao2793 (2018).
129 Bian, B. *et al.* Gene expression profiling of patient-derived pancreatic cancer xenografts predicts sensitivity to the BET bromodomain inhibitor JQ1: implications for individualized medicine efforts. *EMBO Mol Med* **9**, 482-497, doi:10.15252/emmm.201606975 (2017).
130 Bian, B. *et al.* Pancreatic Cancer Organoids for Determining Sensitivity to Bromodomain and Extra-Terminal Inhibitors (BETi). *Front Oncol* **9**, 475, doi:10.3389/fonc.2019.00475 (2019).
131 Farrell, A. S. & Sears, R. C. MYC degradation. *Cold Spring Harb Perspect Med* **4**, doi:10.1101/cshperspect.a014365 (2014).
132 Conacci-Sorrell, M., Ngouenet, C. & Eisenman, R. N. Myc-nick: a cytoplasmic cleavage product of Myc that promotes alpha-tubulin acetylation and cell differentiation. *Cell* **142**, 480-493, doi:10.1016/j.cell.2010.06.037 (2010).
133 Gregory, M. A., Qi, Y. & Hann, S. R. Phosphorylation by glycogen synthase kinase-3 controls c-myc proteolysis and subnuclear localization. *J Biol Chem* **278**, 51606-51612, doi:10.1074/jbc.M310722200 (2003).
134 Wang, L. *et al.* CIP2A expression is associated with altered expression of epithelial-mesenchymal transition markers and predictive of poor prognosis in pancreatic ductal adenocarcinoma. *Tumour Biol* **34**, 2309-2313, doi:10.1007/s13277-013-0775-2 (2013).
135 Popov, N. *et al.* The ubiquitin-specific protease USP28 is required for MYC stability. *Nat Cell Biol* **9**, 765-774, doi:10.1038/ncb1601 (2007).
136 Winter, G. E. *et al.* DRUG DEVELOPMENT. Phthalimide conjugation as a strategy for in vivo target protein degradation. *Science* **348**, 1376-1381, doi:10.1126/science.aab1433 (2015).
137 Toure, M. & Crews, C. M. Small-Molecule PROTACS: New Approaches to Protein Degradation. *Angew Chem Int Ed Engl* **55**, 1966-1973, doi:10.1002/anie.201507978 (2016).
138 Adhikary, S. *et al.* The ubiquitin ligase HectH9 regulates transcriptional activation by Myc and is essential for tumor cell proliferation. *Cell* **123**, 409-421, doi:10.1016/j.cell.2005.08.016 (2005).
139 Peter, S. *et al.* Tumor cell-specific inhibition of MYC function using small molecule inhibitors of the HUWE1 ubiquitin ligase. *EMBO Mol Med* **6**, 1525-1541, doi:10.15252/emmm.201403927 (2014).
140 Crawford, L. J. *et al.* The E3 ligase HUWE1 inhibition as a therapeutic strategy to target MYC in multiple myeloma. *Oncogene* **39**, 5001-5014, doi:10.1038/s41388-020-1345-x (2020).
141 O'Neil, N. J., Bailey, M. L. & Hieter, P. Synthetic lethality and cancer. *Nat Rev Genet* **18**, 613-623, doi:10.1038/nrg.2017.47 (2017).
142 Huang, A., Garraway, L. A., Ashworth, A. & Weber, B. Synthetic lethality as an engine for cancer drug target discovery. *Nat Rev Drug Discov* **19**, 23-38, doi:10.1038/s41573-019-0046-z (2020).
143 Hartwell, L. H., Szankasi, P., Roberts, C. J., Murray, A. W. & Friend, S. H. Integrating genetic approaches into the discovery of anticancer drugs. *Science* **278**, 1064-1068, doi:10.1126/science.278.5340.1064 (1997).
144 Yan, H., Gibson, S. & Tye, B. K. Mcm2 and Mcm3, two proteins important for ARS activity, are related in structure and function. *Genes Dev* **5**, 944-957, doi:10.1101/gad.5.6.944 (1991).
145 Kroll, E. S., Hyland, K. M., Hieter, P. & Li, J. J. Establishing genetic interactions by a synthetic dosage lethality phenotype. *Genetics* **143**, 95-102 (1996).
146 Tong, A. H. *et al.* Global mapping of the yeast genetic interaction network. *Science* **303**, 808-813, doi:10.1126/science.1091317 (2004).

147 Farmer, H. *et al.* Targeting the DNA repair defect in BRCA mutant cells as a therapeutic strategy. *Nature* **434**, 917-921, doi:10.1038/nature03445 (2005).
148 Fong, P. C. *et al.* Inhibition of poly(ADP-ribose) polymerase in tumors from BRCA mutation carriers. *N Engl J Med* **361**, 123-134, doi:10.1056/NEJMoa0900212 (2009).
149 Costanzo, M. *et al.* A global genetic interaction network maps a wiring diagram of cellular function. *Science* **353**, doi:10.1126/science.aaf1420 (2016).
150 Srivas, R. *et al.* A Network of Conserved Synthetic Lethal Interactions for Exploration of Precision Cancer Therapy. *Mol Cell* **63**, 514-525, doi:10.1016/j.molcel.2016.06.022 (2016).
151 Rottmann, S., Wang, Y., Nasoff, M., Deveraux, Q. L. & Quon, K. C. A TRAIL receptor-dependent synthetic lethal relationship between MYC activation and GSK3beta/FBW7 loss of function. *Proc Natl Acad Sci U S A* **102**, 15195-15200, doi:10.1073/pnas.0505114102 (2005).
152 Mo, H. & Henriksson, M. Identification of small molecules that induce apoptosis in a Myc-dependent manner and inhibit Myc-driven transformation. *Proc Natl Acad Sci U S A* **103**, 6344-6349, doi:10.1073/pnas.0601418103 (2006).
153 Goga, A., Yang, D., Tward, A. D., Morgan, D. O. & Bishop, J. M. Inhibition of CDK1 as a potential therapy for tumors over-expressing MYC. *Nature medicine* **13**, 820-827, doi:10.1038/nm1606 (2007).
154 Frenzel, A., Zirath, H., Vita, M., Albihn, A. & Henriksson, M. A. Identification of cytotoxic drugs that selectively target tumor cells with MYC overexpression. *PLoS One* **6**, e27988, doi:10.1371/journal.pone.0027988 (2011).
155 Kessler, J. D. *et al.* A SUMOylation-dependent transcriptional subprogram is required for Myc-driven tumorigenesis. *Science* **335**, 348-353, doi:10.1126/science.1212728 (2012).
156 Eilers, M., Picard, D., Yamamoto, K. R. & Bishop, J. M. Chimaeras of myc oncoprotein and steroid receptors cause hormone-dependent transformation of cells. *Nature* **340**, 66-68, doi:10.1038/340066a0 (1989).
157 Biederstädt, A. *et al.* SUMO pathway inhibition targets an aggressive pancreatic cancer subtype. *Gut* **69**, 1472-1482, doi:10.1136/gutjnl-2018-317856 (2020).
158 Toyoshima, M. *et al.* Functional genomics identifies therapeutic targets for MYC-driven cancer. *Proc Natl Acad Sci U S A* **109**, 9545-9550, doi:10.1073/pnas.1121119109 (2012).
159 Liu, L. *et al.* Deregulated MYC expression induces dependence upon AMPK-related kinase 5. *Nature* **483**, 608-612, doi:10.1038/nature10927 (2012).
160 Cermelli, S., Jang, I. S., Bernard, B. & Grandori, C. Synthetic lethal screens as a means to understand and treat MYC-driven cancers. *Cold Spring Harb Perspect Med* **4**, doi:10.1101/cshperspect.a014209 (2014).
161 Topham, C. *et al.* MYC Is a Major Determinant of Mitotic Cell Fate. *Cancer cell* **28**, 129-140, doi:10.1016/j.ccell.2015.06.001 (2015).
162 Beglyarova, N. *et al.* Screening of Conditionally Reprogrammed Patient-Derived Carcinoma Cells Identifies ERCC3-MYC Interactions as a Target in Pancreatic Cancer. *Clinical cancer research : an official journal of the American Association for Cancer Research* **22**, 6153-6163, doi:10.1158/1078-0432.ccr-16-0149 (2016).
163 Zhao, N. *et al.* Pharmacological targeting of MYC-regulated IRE1/XBP1 pathway suppresses MYC-driven breast cancer. *J Clin Invest* **128**, 1283-1299, doi:10.1172/jci95873 (2018).
164 Xie, H. *et al.* IRE1α RNase-dependent lipid homeostasis promotes survival in Myc-transformed cancers. *J Clin Invest* **128**, 1300-1316, doi:10.1172/jci95864 (2018).
165 Sheng, X. *et al.* IRE1α-XBP1s pathway promotes prostate cancer by activating c-MYC signaling. *Nature communications* **10**, 323, doi:10.1038/s41467-018-08152-3 (2019).
166 Walter, P. & Ron, D. The unfolded protein response: from stress pathway to homeostatic regulation. *Science* **334**, 1081-1086, doi:10.1126/science.1209038 (2011).
167 Nguyen, H. G. *et al.* Development of a stress response therapy targeting aggressive prostate cancer. *Sci Transl Med* **10**, doi:10.1126/scitranslmed.aar2036 (2018).
168 Hart, L. S. *et al.* ER stress-mediated autophagy promotes Myc-dependent transformation and tumor growth. *J Clin Invest* **122**, 4621-4634, doi:10.1172/jci62973 (2012).

169 Genovese, G. *et al.* Synthetic vulnerabilities of mesenchymal subpopulations in pancreatic cancer. *Nature* **542**, 362-366, doi:10.1038/nature21064 (2017).
170 Best, S. *et al.* Targeting ubiquitin-activating enzyme induces ER stress-mediated apoptosis in B-cell lymphoma cells. *Blood Adv* **3**, 51-62, doi:10.1182/bloodadvances.2018026880 (2019).
171 Lomberk, G., Dusetti, N., Iovanna, J. & Urrutia, R. Emerging epigenomic landscapes of pancreatic cancer in the era of precision medicine. *Nature communications* **10**, 3875, doi:10.1038/s41467-019-11812-7 (2019).
172 Mazur, P. K. *et al.* Combined inhibition of BET family proteins and histone deacetylases as a potential epigenetics-based therapy for pancreatic ductal adenocarcinoma. *Nature medicine* **21**, 1163-1171, doi:10.1038/nm.3952 (2015).
173 database, c. <https://web.expasy.org/cellosaurus/> (accessed on 13.11.2020).
174 Conradt, L. *et al.* Disclosure of erlotinib as a multikinase inhibitor in pancreatic ductal adenocarcinoma. *Neoplasia* **13**, 1026-1034, doi:10.1593/neo.111016 (2011).
175 Lankes, K. *et al.* Targeting the ubiquitin-proteasome system in a pancreatic cancer subtype with hyperactive MYC. *Mol Oncol* **14**, 3048-3064, doi:10.1002/1878-0261.12835 (2020).
176 Metsalu, T. & Vilo, J. ClustVis: a web tool for visualizing clustering of multivariate data using Principal Component Analysis and heatmap. *Nucleic acids research* **43**, W566-570, doi:10.1093/nar/gkv468 (2015).
177 SynergyFinder2.0. <https://doi.org/10.1093/nar/gkaa216> (accessed October 2020).
178 von Burstin, J. *et al.* E-cadherin regulates metastasis of pancreatic cancer in vivo and is suppressed by a SNAIL/HDAC1/HDAC2 repressor complex. *Gastroenterology* **137**, 361-371, 371.e361-365, doi:10.1053/j.gastro.2009.04.004 (2009).
179 Ossewaarde, J. M., de Vries, A., Bestebroer, T. & Angulo, A. F. Application of a Mycoplasma group-specific PCR for monitoring decontamination of Mycoplasma-infected Chlamydia sp. strains. *Appl Environ Microbiol* **62**, 328-331, doi:10.1128/aem.62.2.328-331.1996 (1996).
180 Christensen, C. L. *et al.* Targeting transcriptional addictions in small cell lung cancer with a covalent CDK7 inhibitor. *Cancer cell* **26**, 909-922, doi:10.1016/j.ccell.2014.10.019 (2014).
181 thermofisher.com. <https://www.thermofisher.com/de/de/home/brands/thermo-scientific/molecular-biology/molecular-biology-learning-center/molecular-biology-resource-library/thermo-scientific-web-tools/qpcr-efficiency-calculator.html> (accessed October 2020).
182 Garcia-Alonso, L., Holland, C. H., Ibrahim, M. M., Turei, D. & Saez-Rodriguez, J. Benchmark and integration of resources for the estimation of human transcription factor activities. *Genome Res* **29**, 1363-1375, doi:10.1101/gr.240663.118 (2019).
183 Wirth, M. *et al.* MYC and EGR1 synergize to trigger tumor cell death by controlling NOXA and BIM transcription upon treatment with the proteasome inhibitor bortezomib. *Nucleic acids research* **42**, 10433-10447, doi:10.1093/nar/gku763 (2014).
184 Daemen, A. *et al.* Metabolite profiling stratifies pancreatic ductal adenocarcinomas into subtypes with distinct sensitivities to metabolic inhibitors. *Proc Natl Acad Sci U S A* **112**, E4410-4417, doi:10.1073/pnas.1501605112 (2015).
185 Krauß, L. *et al.* HDAC2 Facilitates Pancreatic Cancer Metastasis. *Cancer research* **82**, 695-707, doi:10.1158/0008-5472.can-20-3209 (2022).
186 Guccione, E. & Richard, S. The regulation, functions and clinical relevance of arginine methylation. *Nat Rev Mol Cell Biol* **20**, 642-657, doi:10.1038/s41580-019-0155-x (2019).
187 Qin, Y. *et al.* PRMT5 enhances tumorigenicity and glycolysis in pancreatic cancer via the FBW7/cMyc axis. *Cell Commun Signal* **17**, 30, doi:10.1186/s12964-019-0344-4 (2019).
188 Ge, L. *et al.* PRMT5 promotes epithelial-mesenchymal transition via EGFR-β-catenin axis in pancreatic cancer cells. *J Cell Mol Med* **24**, 1969-1979, doi:10.1111/jcmm.14894 (2020).
189 Orben, F. *et al.* Epigenetic drug screening defines a PRMT5 inhibitor-sensitive pancreatic cancer subtype. *JCI Insight* **7**, doi:10.1172/jci.insight.151353 (2022).

190 Duncan, K. W. *et al.* Structure and Property Guided Design in the Identification of PRMT5 Tool Compound EPZ015666. *ACS Med Chem Lett* **7**, 162-166, doi:10.1021/acsmedchemlett.5b00380 (2016).
191 Gerhart, S. V. *et al.* Activation of the p53-MDM4 regulatory axis defines the anti-tumour response to PRMT5 inhibition through its role in regulating cellular splicing. *Sci Rep* **8**, 9711, doi:10.1038/s41598-018-28002-y (2018).
192 Brehmer, D. *et al.* Abstract DDT02-04: A novel PRMT5 inhibitor with potent in vitro and in vivo activity in preclinical lung cancer models. *Cancer research* **77**, DDT02-04, doi:10.1158/1538-7445.AM2017-DDT02-04 (2017).
193 Wei, X. *et al.* Targeted CRISPR screening identifies PRMT5 as synthetic lethality combinatorial target with gemcitabine in pancreatic cancer cells. *Proc Natl Acad Sci U S A*, doi:10.1073/pnas.2009899117 (2020).
194 Yadav, B., Wennerberg, K., Aittokallio, T. & Tang, J. Searching for Drug Synergy in Complex Dose-Response Landscapes Using an Interaction Potency Model. *Computational and structural biotechnology journal* **13**, 504-513, doi:10.1016/j.csbj.2015.09.001 (2015).
195 Sottile, F., Gnemmi, I., Cantilena, S., D'Acunto, W. C. & Sala, A. A chemical screen identifies the chemotherapeutic drug topotecan as a specific inhibitor of the B-MYB/MYCN axis in neuroblastoma. *Oncotarget* **3**, 535-545, doi:10.18632/oncotarget.498 (2012).
196 Ecker, J. *et al.* Targeting class I histone deacetylase 2 in MYC amplified group 3 medulloblastoma. *Acta Neuropathol Commun* **3**, 22, doi:10.1186/s40478-015-0201-7 (2015).
197 Nebbioso, A. *et al.* c-Myc Modulation and Acetylation Is a Key HDAC Inhibitor Target in Cancer. *Clinical cancer research : an official journal of the American Association for Cancer Research* **23**, 2542-2555, doi:10.1158/1078-0432.ccr-15-2388 (2017).
198 Wang, J. *et al.* FDA-approved drug screen identifies proteasome as a synthetic lethal target in MYC-driven neuroblastoma. *Oncogene* **38**, 6737-6751, doi:10.1038/s41388-019-0912-5 (2019).
199 Farrell, A. S. *et al.* MYC regulates ductal-neuroendocrine lineage plasticity in pancreatic ductal adenocarcinoma associated with poor outcome and chemoresistance. *Nature communications* **8**, 1728, doi:10.1038/s41467-017-01967-6 (2017).
200 Parasido, E. *et al.* The Sustained Induction of c-MYC Drives Nab-Paclitaxel Resistance in Primary Pancreatic Ductal Carcinoma Cells. *Mol Cancer Res* **17**, 1815-1827, doi:10.1158/1541-7786.mcr-19-0191 (2019).
201 Liu, Y. *et al.* UAE1 inhibition mediates the unfolded protein response, DNA damage and caspase-dependent cell death in pancreatic cancer. *Transl Oncol* **13**, 100834, doi:10.1016/j.tranon.2020.100834 (2020).
202 Fraunhoffer, N. A. *et al.* Evidencing a Pancreatic Ductal Adenocarcinoma Subpopulation Sensitive to the Proteasome Inhibitor Carfilzomib. *Clinical cancer research : an official journal of the American Association for Cancer Research* **26**, 5506-5519, doi:10.1158/1078-0432.ccr-20-1232 (2020).
203 Wolpaw, A. J. & Dang, C. V. MYC-induced metabolic stress and tumorigenesis. *Biochim Biophys Acta Rev Cancer* **1870**, 43-50, doi:10.1016/j.bbcan.2018.05.003 (2018).
204 Madden, E., Logue, S. E., Healy, S. J., Manie, S. & Samali, A. The role of the unfolded protein response in cancer progression: From oncogenesis to chemoresistance. *Biol Cell* **111**, 1-17, doi:10.1111/boc.201800050 (2019).
205 Vekaria, P. H., Home, T., Weir, S., Schoenen, F. J. & Rao, R. Targeting p97 to Disrupt Protein Homeostasis in Cancer. *Front Oncol* **6**, 181, doi:10.3389/fonc.2016.00181 (2016).
206 Magnaghi, P. *et al.* Covalent and allosteric inhibitors of the ATPase VCP/p97 induce cancer cell death. *Nat Chem Biol* **9**, 548-556, doi:10.1038/nchembio.1313 (2013).
207 Chng, W. J. *et al.* Clinical and biological implications of MYC activation: a common difference between MGUS and newly diagnosed multiple myeloma. *Leukemia* **25**, 1026-1035, doi:10.1038/leu.2011.53 (2011).

208 Di Bacco, A. *et al.* c-MYC expression and maturity phenotypes are associated with outcome benefit from addition of ixazomib to lenalidomide-dexamethasone in myeloma. *Eur J Haematol* **105**, 35-46, doi:10.1111/ejh.13405 (2020).
209 Chang, C. W. *et al.* ROS-independent ER stress-mediated NRF2 activation promotes warburg effect to maintain stemness-associated properties of cancer-initiating cells. *Cell Death Dis* **9**, 194, doi:10.1038/s41419-017-0250-x (2018).
210 Chio, I. I. C. *et al.* NRF2 Promotes Tumor Maintenance by Modulating mRNA Translation in Pancreatic Cancer. *Cell* **166**, 963-976, doi:10.1016/j.cell.2016.06.056 (2016).
211 Chunduri, N. K. & Storchová, Z. The diverse consequences of aneuploidy. *Nat Cell Biol* **21**, 54-62, doi:10.1038/s41556-018-0243-8 (2019).
212 Chen, S. *et al.* Genome-wide siRNA screen for modulators of cell death induced by proteasome inhibitor bortezomib. *Cancer research* **70**, 4318-4326, doi:10.1158/0008-5472.can-09-4428 (2010).
213 Sloss, C. M. *et al.* Proteasome inhibition activates epidermal growth factor receptor (EGFR) and EGFR-independent mitogenic kinase signaling pathways in pancreatic cancer cells. *Clinical cancer research : an official journal of the American Association for Cancer Research* **14**, 5116-5123, doi:10.1158/1078-0432.ccr-07-4506 (2008).
214 Hideshima, T. *et al.* Bortezomib induces canonical nuclear factor-kappaB activation in multiple myeloma cells. *Blood* **114**, 1046-1052, doi:10.1182/blood-2009-01-199604 (2009).
215 Mitsiades, N. *et al.* Molecular sequelae of proteasome inhibition in human multiple myeloma cells. *Proc Natl Acad Sci U S A* **99**, 14374-14379, doi:10.1073/pnas.202445099 (2002).
216 Nawrocki, S. T., Sweeney-Gotsch, B., Takamori, R. & McConkey, D. J. The proteasome inhibitor bortezomib enhances the activity of docetaxel in orthotopic human pancreatic tumor xenografts. *Molecular cancer therapeutics* **3**, 59-70 (2004).
217 Kawaguchi, K. *et al.* MEK inhibitors cobimetinib and trametinib, regressed a gemcitabine-resistant pancreatic-cancer patient-derived orthotopic xenograft (PDOX). *Oncotarget* **8**, 47490-47496, doi:10.18632/oncotarget.17667 (2017).
218 Alberts, S. R. *et al.* PS-341 and gemcitabine in patients with metastatic pancreatic adenocarcinoma: a North Central Cancer Treatment Group (NCCTG) randomized phase II study. *Ann Oncol* **16**, 1654-1661, doi:10.1093/annonc/mdi324 (2005).
219 Chen, D., Frezza, M., Schmitt, S., Kanwar, J. & Dou, Q. P. Bortezomib as the first proteasome inhibitor anticancer drug: current status and future perspectives. *Curr Cancer Drug Targets* **11**, 239-253, doi:10.2174/156800911794519752 (2011).
220 Coux, O., Tanaka, K. & Goldberg, A. L. Structure and functions of the 20S and 26S proteasomes. *Annu Rev Biochem* **65**, 801-847, doi:10.1146/annurev.bi.65.070196.004101 (1996).
221 Crawford, L. J. *et al.* Comparative selectivity and specificity of the proteasome inhibitors BzLLLCOCHO, PS-341, and MG-132. *Cancer research* **66**, 6379-6386, doi:10.1158/0008-5472.can-06-0605 (2006).
222 Qin, J. Z. *et al.* Proteasome inhibitors trigger NOXA-mediated apoptosis in melanoma and myeloma cells. *Cancer research* **65**, 6282-6293, doi:10.1158/0008-5472.can-05-0676 (2005).
223 Nikiforov, M. A. *et al.* Tumor cell-selective regulation of NOXA by c-MYC in response to proteasome inhibition. *Proc Natl Acad Sci U S A* **104**, 19488-19493, doi:10.1073/pnas.0708380104 (2007).
224 Kane, R. C., Bross, P. F., Farrell, A. T. & Pazdur, R. Velcade: U.S. FDA approval for the treatment of multiple myeloma progressing on prior therapy. *Oncologist* **8**, 508-513, doi:10.1634/theoncologist.8-6-508 (2003).
225 Hideshima, T. *et al.* The proteasome inhibitor PS-341 inhibits growth, induces apoptosis, and overcomes drug resistance in human multiple myeloma cells. *Cancer research* **61**, 3071-3076 (2001).
226 Orlowski, R. Z. *et al.* Tumor growth inhibition induced in a murine model of human Burkitt's lymphoma by a proteasome inhibitor. *Cancer research* **58**, 4342-4348 (1998).

227 Shah, S. A. *et al.* 26S proteasome inhibition induces apoptosis and limits growth of human pancreatic cancer. *J Cell Biochem* **82**, 110-122, doi:10.1002/jcb.1150 (2001).
228 Bold, R. J., Virudachalam, S. & McConkey, D. J. Chemosensitization of pancreatic cancer by inhibition of the 26S proteasome. *J Surg Res* **100**, 11-17, doi:10.1006/jsre.2001.6194 (2001).
229 Orlowski, R. Z. *et al.* Phase I trial of the proteasome inhibitor PS-341 in patients with refractory hematologic malignancies. *J Clin Oncol* **20**, 4420-4427, doi:10.1200/jco.2002.01.133 (2002).
230 Fisher, R. I. *et al.* Multicenter phase II study of bortezomib in patients with relapsed or refractory mantle cell lymphoma. *J Clin Oncol* **24**, 4867-4874, doi:10.1200/jco.2006.07.9665 (2006).
231 Richardson, P. G. *et al.* A phase 2 study of bortezomib in relapsed, refractory myeloma. *N Engl J Med* **348**, 2609-2617, doi:10.1056/NEJMoa030288 (2003).
232 Aghajanian, C. *et al.* A phase I trial of the novel proteasome inhibitor PS341 in advanced solid tumor malignancies. *Clinical cancer research : an official journal of the American Association for Cancer Research* **8**, 2505-2511 (2002).
233 Huang, Z. *et al.* Efficacy of therapy with bortezomib in solid tumors: a review based on 32 clinical trials. *Future Oncol* **10**, 1795-1807, doi:10.2217/fon.14.30 (2014).
234 Richardson, P. G. *et al.* Bortezomib or high-dose dexamethasone for relapsed multiple myeloma. *N Engl J Med* **352**, 2487-2498, doi:10.1056/NEJMoa043445 (2005).
235 San Miguel, J. F. *et al.* Bortezomib plus melphalan and prednisone for initial treatment of multiple myeloma. *N Engl J Med* **359**, 906-917, doi:10.1056/NEJMoa0801479 (2008).
236 Kumatori, A. *et al.* Abnormally high expression of proteasomes in human leukemic cells. *Proc Natl Acad Sci U S A* **87**, 7071-7075, doi:10.1073/pnas.87.18.7071 (1990).
237 Drexler, H. C., Risau, W. & Konerding, M. A. Inhibition of proteasome function induces programmed cell death in proliferating endothelial cells. *Faseb j* **14**, 65-77, doi:10.1096/fasebj.14.1.65 (2000).
238 Oikawa, T. *et al.* The proteasome is involved in angiogenesis. *Biochem Biophys Res Commun* **246**, 243-248, doi:10.1006/bbrc.1998.8604 (1998).
239 Russo, S. M. *et al.* Enhancement of radiosensitivity by proteasome inhibition: implications for a role of NF-kappaB. *Int J Radiat Oncol Biol Phys* **50**, 183-193, doi:10.1016/s0360-3016(01)01446-8 (2001).
240 Kondagunta, G. V. *et al.* Phase II trial of bortezomib for patients with advanced renal cell carcinoma. *J Clin Oncol* **22**, 3720-3725, doi:10.1200/jco.2004.10.155 (2004).
241 Fanucchi, M. P. *et al.* Randomized phase II study of bortezomib alone and bortezomib in combination with docetaxel in previously treated advanced non-small-cell lung cancer. *J Clin Oncol* **24**, 5025-5033, doi:10.1200/jco.2006.06.1853 (2006).
242 Perrone, G. *et al.* Ascorbic acid inhibits antitumor activity of bortezomib in vivo. *Leukemia* **23**, 1679-1686, doi:10.1038/leu.2009.83 (2009).
243 Liu, F. T. *et al.* Dietary flavonoids inhibit the anticancer effects of the proteasome inhibitor bortezomib. *Blood* **112**, 3835-3846, doi:10.1182/blood-2008-04-150227 (2008).
244 Manasanch, E. E. & Orlowski, R. Z. Proteasome inhibitors in cancer therapy. *Nat Rev Clin Oncol* **14**, 417-433, doi:10.1038/nrclinonc.2016.206 (2017).
245 O'Connor, O. A. *et al.* A phase 1 dose escalation study of the safety and pharmacokinetics of the novel proteasome inhibitor carfilzomib (PR-171) in patients with hematologic malignancies. *Clinical cancer research : an official journal of the American Association for Cancer Research* **15**, 7085-7091, doi:10.1158/1078-0432.ccr-09-0822 (2009).
246 Hari, P. *et al.* Oprozomib in patients with newly diagnosed multiple myeloma. *Blood Cancer J* **9**, 66, doi:10.1038/s41408-019-0232-6 (2019).
247 Gupta, N. *et al.* Model-Informed Drug Development for Ixazomib, an Oral Proteasome Inhibitor. *Clin Pharmacol Ther* **105**, 376-387, doi:10.1002/cpt.1047 (2019).
248 Feling, R. H. *et al.* Salinosporamide A: a highly cytotoxic proteasome inhibitor from a novel microbial source, a marine bacterium of the new genus salinospora. *Angew Chem Int Ed Engl* **42**, 355-357, doi:10.1002/anie.200390115 (2003).

249 Clinicaltrials.gov. <https://clinicaltrials.gov/ct2/show/NCT03345095> (accessed on 27.10.2020).
250 Millward, M. *et al.* Phase 1 clinical trial of the novel proteasome inhibitor marizomib with the histone deacetylase inhibitor vorinostat in patients with melanoma, pancreatic and lung cancer based on in vitro assessments of the combination. *Invest New Drugs* **30**, 2303-2317, doi:10.1007/s10637-011-9766-6 (2012).
251 Deshantri, A. K. *et al.* Development and characterization of liposomal formulation of bortezomib. *Int J Pharm X* **1**, 100011, doi:10.1016/j.ijpx.2019.100011 (2019).
252 Nawrocki, S. T. *et al.* Myc regulates aggresome formation, the induction of Noxa, and apoptosis in response to the combination of bortezomib and SAHA. *Blood* **112**, 2917-2926, doi:10.1182/blood-2007-12-130823 (2008).
253 Coffino, P. Antizyme, a mediator of ubiquitin-independent proteasomal degradation. *Biochimie* **83**, 319-323, doi:10.1016/s0300-9084(01)01252-4 (2001).
254 Murai, N., Murakami, Y., Tajima, A. & Matsufuji, S. Novel ubiquitin-independent nucleolar c-Myc degradation pathway mediated by antizyme 2. *Sci Rep* **8**, 3005, doi:10.1038/s41598-018-21189-0 (2018).
255 Wang, Y., Hu, W. & Yuan, Y. Protein Arginine Methyltransferase 5 (PRMT5) as an Anticancer Target and Its Inhibitor Discovery. *J Med Chem* **61**, 9429-9441, doi:10.1021/acs.jmedchem.8b00598 (2018).
256 Shailesh, H., Zakaria, Z. Z., Baiocchi, R. & Sif, S. Protein arginine methyltransferase 5 (PRMT5) dysregulation in cancer. *Oncotarget* **9**, 36705-36718, doi:10.18632/oncotarget.26404 (2018).
257 Reitz, R. C., Lands, W. E., Christie, W. W. & Holman, R. T. Effects of ethylenic bond position upon acyltransferase activity with isomeric cis,cis-octadecadienoyl coenzyme A thiol esters. *J Biol Chem* **243**, 2241-2246 (1968).
258 Lin, W. J., Gary, J. D., Yang, M. C., Clarke, S. & Herschman, H. R. The mammalian immediate-early TIS21 protein and the leukemia-associated BTG1 protein interact with a protein-arginine N-methyltransferase. *J Biol Chem* **271**, 15034-15044, doi:10.1074/jbc.271.25.15034 (1996).
259 Kim, H. & Ronai, Z. A. PRMT5 function and targeting in cancer. *Cell Stress* **4**, 199-215, doi:10.15698/cst2020.08.228 (2020).
260 Jarrold, J. & Davies, C. C. PRMTs and Arginine Methylation: Cancer's Best-Kept Secret? *Trends Mol Med* **25**, 993-1009, doi:10.1016/j.molmed.2019.05.007 (2019).
261 Krapivinsky, G., Pu, W., Wickman, K., Krapivinsky, L. & Clapham, D. E. pICln binds to a mammalian homolog of a yeast protein involved in regulation of cell morphology. *J Biol Chem* **273**, 10811-10814, doi:10.1074/jbc.273.18.10811 (1998).
262 Pollack, B. P. *et al.* The human homologue of the yeast proteins Skb1 and Hsl7p interacts with Jak kinases and contains protein methyltransferase activity. *J Biol Chem* **274**, 31531-31542, doi:10.1074/jbc.274.44.31531 (1999).
263 Branscombe, T. L. *et al.* PRMT5 (Janus kinase-binding protein 1) catalyzes the formation of symmetric dimethylarginine residues in proteins. *J Biol Chem* **276**, 32971-32976, doi:10.1074/jbc.M105412200 (2001).
264 Antonysamy, S. *et al.* Crystal structure of the human PRMT5:MEP50 complex. *Proc Natl Acad Sci U S A* **109**, 17960-17965, doi:10.1073/pnas.1209814109 (2012).
265 Tee, W. W. *et al.* Prmt5 is essential for early mouse development and acts in the cytoplasm to maintain ES cell pluripotency. *Genes Dev* **24**, 2772-2777, doi:10.1101/gad.606110 (2010).
266 Bezzi, M. *et al.* Regulation of constitutive and alternative splicing by PRMT5 reveals a role for Mdm4 pre-mRNA in sensing defects in the spliceosomal machinery. *Genes Dev* **27**, 1903-1916, doi:10.1101/gad.219899.113 (2013).
267 Jing, P. *et al.* Protein arginine methyltransferase 5 promotes lung cancer metastasis via the epigenetic regulation of miR-99 family/FGFR3 signaling. *Cancer Lett* **427**, 38-48, doi:10.1016/j.canlet.2018.04.019 (2018).
268 Gullà, A. *et al.* Protein arginine methyltransferase 5 has prognostic relevance and is a druggable target in multiple myeloma. *Leukemia* **32**, 996-1002, doi:10.1038/leu.2017.334 (2018).

269 Zhang, B. *et al.* Targeting protein arginine methyltransferase 5 inhibits human hepatocellular carcinoma growth via the downregulation of beta-catenin. *J Transl Med* **13**, 349, doi:10.1186/s12967-015-0721-8 (2015).
270 Giuliani, V. *et al.* PRMT1-dependent regulation of RNA metabolism and DNA damage response sustains pancreatic ductal adenocarcinoma. *Nature communications* **12**, 4626, doi:10.1038/s41467-021-24798-y (2021).
271 Repenning, A. *et al.* PRMT1 promotes the tumor suppressor function of p14(ARF) and is indicative for pancreatic cancer prognosis. *The EMBO journal* **40**, e106777, doi:10.15252/embj.2020106777 (2021).
272 Shifteh, D. *et al.* Protein Arginine Methyltransferase 5 as a Therapeutic Target for KRAS Mutated Colorectal Cancer. *Cancers (Basel)* **12**, doi:10.3390/cancers12082091 (2020).
273 Fedoriw, A. *et al.* Anti-tumor Activity of the Type I PRMT Inhibitor, GSK3368715, Synergizes with PRMT5 Inhibition through MTAP Loss. *Cancer cell* **36**, 100-114.e125, doi:10.1016/j.ccell.2019.05.014 (2019).
274 Driehuis, E. *et al.* Pancreatic cancer organoids recapitulate disease and allow personalized drug screening. *Proc Natl Acad Sci U S A* **116**, 26580-26590, doi:10.1073/pnas.1911273116 (2019).
275 Kryukov, G. V. *et al.* MTAP deletion confers enhanced dependency on the PRMT5 arginine methyltransferase in cancer cells. *Science* **351**, 1214-1218, doi:10.1126/science.aad5214 (2016).
276 Mavrakis, K. J. *et al.* Disordered methionine metabolism in MTAP/CDKN2A-deleted cancers leads to dependence on PRMT5. *Science* **351**, 1208-1213, doi:10.1126/science.aad5944 (2016).
277 Fong, J. Y. *et al.* Therapeutic Targeting of RNA Splicing Catalysis through Inhibition of Protein Arginine Methylation. *Cancer cell* **36**, 194-209.e199, doi:10.1016/j.ccell.2019.07.003 (2019).
278 Gao, G. *et al.* PRMT1 loss sensitizes cells to PRMT5 inhibition. *Nucleic acids research* **47**, 5038-5048, doi:10.1093/nar/gkz200 (2019).
279 Braun, C. J. *et al.* Coordinated Splicing of Regulatory Detained Introns within Oncogenic Transcripts Creates an Exploitable Vulnerability in Malignant Glioma. *Cancer cell* **32**, 411-426.e411, doi:10.1016/j.ccell.2017.08.018 (2017).
280 Koh, C. M. *et al.* MYC regulates the core pre-mRNA splicing machinery as an essential step in lymphomagenesis. *Nature* **523**, 96-100, doi:10.1038/nature14351 (2015).
281 Schnormeier, A. K., Pommerenke, C., Kaufmann, M., Drexler, H. G. & Koeppel, M. Genomic deregulation of PRMT5 supports growth and stress tolerance in chronic lymphocytic leukemia. *Sci Rep* **10**, 9775, doi:10.1038/s41598-020-66224-1 (2020).
282 Chaturvedi, N. K. *et al.* Role of protein arginine methyltransferase 5 in group 3 (MYC-driven) Medulloblastoma. *BMC Cancer* **19**, 1056, doi:10.1186/s12885-019-6291-z (2019).
283 Park, J. H. *et al.* Protein arginine methyltransferase 5 is a key regulator of the MYCN oncoprotein in neuroblastoma cells. *Mol Oncol* **9**, 617-627, doi:10.1016/j.molonc.2014.10.015 (2015).
284 Mongiardi, M. P. *et al.* Myc and Omomyc functionally associate with the Protein Arginine Methyltransferase 5 (PRMT5) in glioblastoma cells. *Sci Rep* **5**, 15494, doi:10.1038/srep15494 (2015).
285 Favia, A. *et al.* The Protein Arginine Methyltransferases 1 and 5 affect Myc properties in glioblastoma stem cells. *Sci Rep* **9**, 15925, doi:10.1038/s41598-019-52291-6 (2019).
286 Liu, M. *et al.* PRMT5-dependent transcriptional repression of c-Myc target genes promotes gastric cancer progression. *Theranostics* **10**, 4437-4452, doi:10.7150/thno.42047 (2020).
287 Behan, F. M. *et al.* Prioritization of cancer therapeutic targets using CRISPR-Cas9 screens. *Nature* **568**, 511-516, doi:10.1038/s41586-019-1103-9 (2019).
288 Gao, G., Dhar, S. & Bedford, M. T. PRMT5 regulates IRES-dependent translation via methylation of hnRNP A1. *Nucleic acids research* **45**, 4359-4369, doi:10.1093/nar/gkw1367 (2017).

289 Karkhanis, V. *et al.* Protein arginine methyltransferase 5 represses tumor suppressor miRNAs that down-regulate CYCLIN D1 and c-MYC expression in aggressive B-cell lymphoma. *J Biol Chem* **295**, 1165-1180, doi:10.1074/jbc.RA119.008742 (2020).
290 Koh, C. M., Sabò, A. & Guccione, E. Targeting MYC in cancer therapy: RNA processing offers new opportunities. *Bioessays* **38**, 266-275, doi:10.1002/bies.201500134 (2016).
291 Radzisheuskaya, A. *et al.* PRMT5 methylome profiling uncovers a direct link to splicing regulation in acute myeloid leukemia. *Nat Struct Mol Biol* **26**, 999-1012, doi:10.1038/s41594-019-0313-z (2019).
292 Hsu, T. Y. *et al.* The spliceosome is a therapeutic vulnerability in MYC-driven cancer. *Nature* **525**, 384-388, doi:10.1038/nature14985 (2015).
293 Salvador, F. & Gomis, R. R. CLK2 blockade modulates alternative splicing compromising MYC-driven breast tumors. *EMBO Mol Med* **10**, doi:10.15252/emmm.201809213 (2018).
294 Cossa, G. *et al.* Localized Inhibition of Protein Phosphatase 1 by NUAK1 Promotes Spliceosome Activity and Reveals a MYC-Sensitive Feedback Control of Transcription. *Mol Cell* **77**, 1322-1339.e1311, doi:10.1016/j.molcel.2020.01.008 (2020).
295 Tan, D. Q. *et al.* PRMT5 Modulates Splicing for Genome Integrity and Preserves Proteostasis of Hematopoietic Stem Cells. *Cell Rep* **26**, 2316-2328.e2316, doi:10.1016/j.celrep.2019.02.001 (2019).
296 Hamard, P. J. *et al.* PRMT5 Regulates DNA Repair by Controlling the Alternative Splicing of Histone-Modifying Enzymes. *Cell Rep* **24**, 2643-2657, doi:10.1016/j.celrep.2018.08.002 (2018).
297 Rehman, I. *et al.* PRMT5-mediated arginine methylation of TDP1 for the repair of topoisomerase I covalent complexes. *Nucleic acids research* **46**, 5601-5617, doi:10.1093/nar/gky291 (2018).
298 Owens, J. L. *et al.* PRMT5 Cooperates with pICln to Function as a Master Epigenetic Activator of DNA Double-Strand Break Repair Genes. *iScience* **23**, 100750, doi:10.1016/j.isci.2019.100750 (2020).
299 Clarke, T. L. *et al.* PRMT5-Dependent Methylation of the TIP60 Coactivator RUVBL1 Is a Key Regulator of Homologous Recombination. *Mol Cell* **65**, 900-916.e907, doi:10.1016/j.molcel.2017.01.019 (2017).
300 Li, Z. *et al.* c-Myc suppression of DNA double-strand break repair. *Neoplasia* **14**, 1190-1202, doi:10.1593/neo.121258 (2012).
301 Secker, K. A. *et al.* Inhibition of DOT1L and PRMT5 promote synergistic anti-tumor activity in a human MLL leukemia model induced by CRISPR/Cas9. *Oncogene* **38**, 7181-7195, doi:10.1038/s41388-019-0937-9 (2019).
302 Brehmer, D. *et al.* Discovery and Pharmacological Characterization of JNJ-64619178, a Novel Small-Molecule Inhibitor of PRMT5 with Potent Antitumor Activity. *Molecular cancer therapeutics* **20**, 2317-2328, doi:10.1158/1535-7163.mct-21-0367 (2021).
303 Clinicaltrials.gov. <https://www.clinicaltrials.gov/ct2/results?cond=&term=Prmt5&cntry=&state=&city=&dist=> (accessed on 22.10.2020).
304 Lin, H. *et al.* Discovery of Potent and Selective Covalent Protein Arginine Methyltransferase 5 (PRMT5) Inhibitors. *ACS Med Chem Lett* **10**, 1033-1038, doi:10.1021/acsmedchemlett.9b00074 (2019).
305 Tao, H., Yan, X., Zhu, K. & Zhang, H. Discovery of Novel PRMT5 Inhibitors by Virtual Screening and Biological Evaluations. *Chem Pharm Bull (Tokyo)* **67**, 382-388, doi:10.1248/cpb.c18-00980 (2019).

XIV. Acknowledgement

First of all, I thank my first supervisor **Prof. Dr. Günter Schneider** for giving me the opportunity to conduct my doctoral thesis in his group and for his great advice during the work. I also thank him for his support in the successful publication of my work.

I thank **Prof. Dr. Matthias Feige** for agreeing to be second supervisor of my thesis and for providing counseling whenever needed.

I also thank **Prof. Dr. Maximilian Reichert** for agreeing to be my mentor during the thesis and for providing constant counseling.

I like to thank the **DKFZ** and the **MRI** for financing my doctoral work, the **TUM graduate school** for supporting my thesis and **Prof. Dr. Roland Schmid** for his permission to work in the Department of II. Med. Clinic.

Additionally, I thank our former post-doc **PD Dr. Matthias Wirth** working now at the Charité in Berlin for the successful collaboration and his support for publishing part of my work. Likewise, I thank **all co-authors** on the publications I had the chance to contribute to and I thank **Dr. Markus Tschurtschenthaler** for providing his greatly appreciated advice.

I also like to mention the **administrative staff** at DKFZ, MRI and TUM graduate school, who always lent a sympathetic ear to me.

Especially, I want to thank **all my great colleagues** in AG Schneider, AG Geisler, AG Saur, AG Reichert, AG Rad and all the other groups of II. Med. and the whole MRI. All these people, also a lot of former group members, created a great working atmosphere, were always helpful and supportive and accompanied me also through tough times. Again, many, many thanks to you all, I wouldn`t have made it to the end without you.

Finally, I want to thank **my mother Martina** for loving and supporting me throughout my life and also during the years of my doctoral thesis. She made all my achievements possible. As well, I thank the rest of my family and my friends for always being around.